

2024

MOLECULAR SIMULATION STUDIES OF THE SALT EFFECT ON AQUEOUS SOLUTIONS

Hiroyuki KATSUTO

*Research Institute for Interdisciplinary Science, Okayama University, Okayama
700-8530, Japan*

Contents

1	General Introduction	3
I	BACKGROUND	3
II	HOFMEISTER SERIES	4
III	THE KIRKWOOD-BUFF INTEGRAL OF SOLUTIONS	8
IV	OUTLINE OF THESIS	14
2	Development and Validation of Charge Scaling Force Field of Ions: Solution Density, Solubility of Hydrophobic Solute, and Partial Molar Volume of Salt	16
I	INTRODUCTION	17
II	THEORETICAL BACKGROUND	19
A	Charge Scaling Force Field of Point Charge Ions	19
B	Charge Scaling Force Field of Hydronium Ion And Hydroxide Ion	21
C	Setschenow Coefficient K_s	22
D	Partial Molar Volume of Electrolytes	23
III	COMPUTATIONAL DETAILS	25
IV	RESULT AND DISCUSSION	27
A	Point Charge Ions	27
B	Hydronium Ion And Hydroxide Ion	29
C	Setschenow Coefficient	32
D	Partial Molar Volume of Electrolytes	33
V	CONCLUSIONS	34
3	Microscopic Origins of Ion Size Dependences of Gas Solubility in Aqueous Electrolyte Solutions: Reversed Order of Sodium and Lithium Ions	37
I	INTRODUCTION	38

II	THEORETICAL BACKGROUND	40
III	COMPUTATIONAL DETAILS	43
IV	RESULTS AND DISCUSSION	46
V	CONCLUSIONS	75
4	Correlation between the Salting-out/Salting-in Effect and the Osmotic Second Virial Coefficient in Aqueous Electrolyte Solutions	78
I	INTRODUCTION	79
II	THEORETICAL BACKGROUND	81
A	Osmotic Second Virial Coefficient B	81
B	Density Second Derivatives of the Free Energy Density	82
C	Partial Molecular Volume	83
D	Composition Susceptibility of the Electrolyte Solvent	84
E	Setschenow Coefficient K_s	86
F	Salt-Enhanced-Association Coefficient C_I	87
III	COMPUTATIONAL DETAILS	88
IV	RESULT AND DISCUSSION	91
V	CONCLUSIONS	94

Chapter 1

General Introduction

I BACKGROUND

Water is one of the most familiar substances for us and is an indispensable chemical compound for the vital activity of living organisms and heat circulation on the earth. The earth's surface is 70% covered by water. Of that, approximately 97% is salt water and only 3% is fresh water. In other words, most of the water on our planet contains electrolytes. Furthermore, water is the most abundant substance in living organisms, accounting for 70 ~ 80%, most of which contains electrolytes. Understanding the physical properties of aqueous electrolyte solutions is itself an important topic in physical chemistry and contributes to the development of a wide range of sciences and technologies such as biochemistry, pharmacology, colloid chemistry, oceanography, and industrial sciences.

Water molecules have a strong ability to form hydrogen bonds with each other and with other polar molecules. Hydrogen bonding is one of the key factors that give water its unique or less common properties, e.g., the temperature of maximum density in its liquid state and the higher melting and boiling points and the higher viscosity compared to those of other low molecular weight compounds. Another important property of water is the ability to dissolve a wide variety of electrolytes as well as polar and amphiphilic molecules. The addition of electrolytes to water changes a variety of physical properties such as the solubility of gases, the cloud point of protein and polymer solutions, the viscosity, and the surface tension. The important fact is that the magnitude of the effect depends on ionic species of cations and that of anions: the salt effect is ion specific. Ion specificity refers to salt effects that cannot be explained by standard theories of electrolyte solutions[1, 2, 3]. That is, the magnitude (and the direction)

of a given salt effect is different for different electrolytes even if the valence of ions and the salt concentration are the same for different solutions. A striking consequence of the ion specific effect is that replacing one specific ion with another in a living organism leads to malfunction or death. Since Hofmeister’s pioneering work in the late 19th century, there have been extensive experimental and theoretical studies on the ion specific effect for various physical properties of aqueous solutions [4, 5, 6, 7, 8, 9, 3, 10, 11].

II HOFMEISTER SERIES

Many studies have been conducted to date on the ion-specificity of numerous physical properties of aqueous electrolyte solutions, e.g., the salt activity coefficient[6, 9], solution density[12, 13], surface tension[14, 15, 16], solute solubility[17, 18, 19], viscosity[20, 21], and protein cloud point[22, 23]. Among various ion specific effects, the Hofmeister series, a series of ions ordered by the strength of salting out proteins proposed by Hofmeister in 1888[24], is one of the most significant and representative examples. In this section, therefore, we shall describe the history of studies on the Hofmeister series, or the Hofmeister effect, from birth to the present.

Franz Hofmeister[24] quantified the specific effects of salt on the egg white protein precipitation. The anion order on a common cation and the cation order on a common anion in terms of the efficiency in precipitating proteins, i.e., the strength of the salting-out, were reported by Hofmeister (in Figure 1.1).

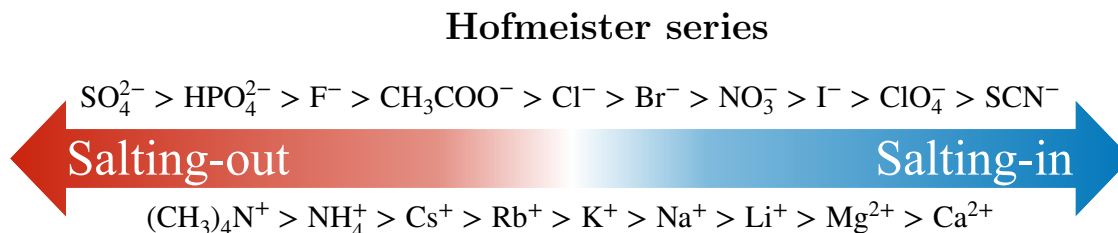


Figure 1.1: The ordering of anions and cations according to the original Hofmeister series. The left side shows the stronger salting-out effect and the right side shows the stronger salting-in effect on proteins in water.

It was significant to understand the mechanism of the order of the Hofmeister series because it was thought that the series is common not only for the solubility of protein, but also for conformational changes in biopolymers such as DNA, for micelle formations of surfactants, and even for properties of systems without protein such as the surface tension of salt solutions. Although it is now known that the ion series depends on the subject physical quantity, the

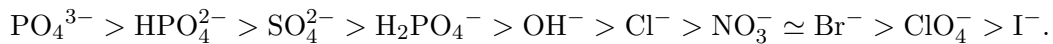
study of the Hofmeister series has been conducted because of the many similarities with the ion series for the other physical quantities. In this section, we shall convey the importance of the Hofmeister series by introducing some ion species dependences of physical quantities.

Viscosity.

Jones and Dole[20] pointed out that in the salt concentration range of $5.0 \times 10^{-3} \sim 1$ M at a given temperature, the ratio of the viscosity η of aqueous solution to η_0 of pure water can be fitted to

$$\frac{\eta}{\eta_0} = 1 + ac^{1/2} + bc, \quad (1.1)$$

where c is the concentration of the salt, a and b are parameters given for each salt species, with the term containing b being particularly dominant at high concentrations. At constant salt concentration (0.4 M), the ranking of the viscosity, or more specifically b -coefficient, for sodium salts is[21, 25, 8]

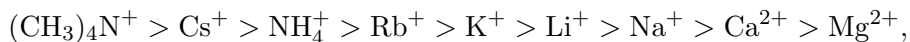


Partial Molar Volume of Salt.

The partial molar volume \bar{V}_s of salt is the solution volume change when one mole of salt is added to the solution, which is defined by $\bar{V}_s = (\partial V / \partial n_s)_{T,p,\{N_i\}_{i \neq s}}$ with n_s the amount of salt substance, V the system volume, and N_i the particle number of species i . When salt species $X_{\nu_+} - Y_{\nu_-}$ dissociates into $\nu_+ X^{z_+}$ and $\nu_- Y^{z_-}$ (z_i is the ion valence), it is known that the partial molar volume of electrolyte at the infinite dilution is additive, i.e., $\bar{V}_s = \nu_+ \bar{V}_+ + \nu_- \bar{V}_-$ due to the disappearance of ion-ion interactions[26, 27]; \bar{V}_+ and \bar{V}_- are the partial molar volumes of cation and anion, respectively, whose magnitudes depend on the ion species. It has been carried out in earlier experimental studies[28, 29, 30, 31] that many partial molar volumes \bar{V}_s of electrolytes are measured and individual partial molar volumes \bar{V}_\pm of ions (cation or anion) are guessed. Only Takenaka and Arakata[32] directly and experimentally measured individual partial molar volumes of a variety of simple monovalent ions at infinite dilution with high precision using the method proposed by Zana and Yeager[33, 34]. The order of anions according to the magnitude of \bar{V}_- at infinite dilution at 298 K is[29, 26, 32]



and that of cations is

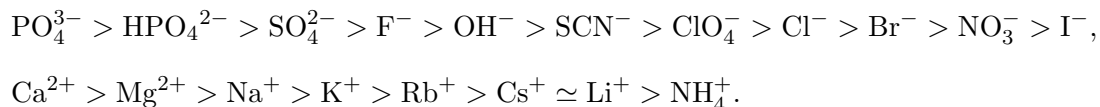


where the ranks of Li^+ and Na^+ depend on the temperature and are reversed at higher temperatures.

Solubility of Solute and Interfacial Tension.

The Hofmeister series in the present notation sequences ions concerning their ability to precipitate proteins and colloids, as shown in Figure 1.1. For the halide in the anion series, the smaller the anion size, the stronger the salting effect ($\text{F}^- > \text{Cl}^- > \text{Br}^- > \text{I}^-$), while, for the alkali metal ions in the cation series, the larger the cation size, the stronger the salting effect ($\text{Cs}^+ > \text{Rb}^+ > \text{K}^+ > \text{Na}^+ > \text{Li}^+$). The asymmetry of those orders is because the Hofmeister series is arranged concerning a spherical protein with a net negative charge. In fact, the ionic ranking of the salting-out effect depends on the properties of the solute: it has been reported[35, 36, 37, 38, 39, 22] that the order follows Figure 1.1 for the solubility of negatively charged proteins, but the order of both cations and anions is reversed for the solubility of positively charged proteins. Furthermore, those series are maintained not only for proteins but also for colloids[40, 1, 41, 3].

The regularity of the salt addition effect on the solubility of solutes with no net charge in aqueous solutions has also been studied extensively[42, 43, 44, 45, 46, 18]. Bergen and Long[47] evaluated measures of salt effects on the solubility of solutes such as benzoic acid, benzene, and benzylamine in aqueous solution from the Setschenow coefficient K_s (defined by eq. 3.1 in Chapter 3) and examined the ionic species dependence of K_s for acidic, neutral, and basic solutes: the positive value of K_s indicates salting-out and negative that indicates and salting-in. For neutral solutes, e.g., hydrocarbons and noble gases, each order of anions and cations for the strength of the salting out is[46]



The cation order of K_s for the three acidic solutes, benzoic acid, phthalic acid, and salicylic

acid, in aqueous solutions of the common anion Cl^- and alkali metal ions are[47]

$$\text{Li}^+ > \text{Na}^+ > \text{K}^+ > \text{Rb}^+ > \text{Cs}^+.$$

Similarly, for the basic solute, aniline, the order of alkali metal ions is

$$\text{Na}^+ > \text{K}^+ > \text{Rb}^+ > \text{Li}^+ > \text{Cs}^+.$$

However, for a different basic solute, benzylamine, the sequence is maximal for K^+ rather than Na^+ . Therefore, for solutes with no net charge, the larger the ion is generally, the smaller the salting-out effect is in both cases of cation and anion. In other words, the cation series is similar to that for positively charged solutes, while the anion series is similar to that for negatively charged solutes. However, the salting-out effect of Li^+ for neutral and basic solutes is exceptionally small. As shown in this section, ionic series for the solubility of solutes with various properties are presented, while it is remarkable that those ionic series are consistent with those of the interfacial tension for interfaces with similar properties, as demonstrated in the earlier study[16]

We presented several rankings of ions for the physical properties of aqueous solutions. Note that not all of the ion series are in full agreement with the Hofmeister series shown in Figure 1.1, but rather are partially altered or reversed. Nevertheless, since those sequences, especially those for ion size, are similar on the whole, it is highly significant to understand the mechanism of expression of the Hofmeister series.

Around fifteen years ago, it was the most popular idea that since the Hofmeister series is maintained according to the properties of aqueous electrolyte solutions without proteins or colloids, the ionic arrangements are due to the effect of ions on the structure of the surrounding water molecules[25]: ions making the structure of water (kosmotropes), i.e., ordering the hydrogen bonding network in water through strong hydration, decrease the solubility of proteins, while ions breaking the structure of water (chaotropes), i.e., disordering the hydrogen bonding network in water, increase the solubility of proteins. However, it has been revealed that the ions, in terms of hydrogen bond configurations, affect only water molecules in the first hydration sphere of the ions even the strongly hydrated ion[48, 49]. Hence, ions do not affect the hydrogen bond network in the bulk water and there is no direct correlation between the effect of ions on the water structure and the effect of ions on the protein stability[50]. On the other

hand, ions specifically affect direct interactions with hydrophilic/hydrophobic groups of proteins and configurations of the hydrated water molecules on the protein surface[51, 52]. Therefore, the current opinion is that the properties of proteins in aqueous electrolyte solutions, e.g., the stability and the conformational change, are determined by complex interplays of ion-specific interactions among ions, water, and proteins[53, 54].

III THE KIRKWOOD-BUFF INTEGRAL OF SOLUTIONS

In thermodynamics, thermodynamic quantities such as temperature T , volume V , entropy S , and chemical potential μ are constant in equilibrium, independent of time. However, for finite systems or for focusing on a part of infinite systems, each thermodynamic quantity fluctuates around the mean value. For homogeneous and isotropic fluids, it is well-known that the quantitative relationship between the Kirkwood-Buff integral (KBI), G_{ij} , and the fluctuations of the particle number N_i of species i in the $T, V, \{\mu_i\}$ ensemble, that is, in the open system is provided as[55, 56]

$$G_{ij} = \int [g_{ij}(r) - 1] d\mathbf{r} = \frac{V \langle \delta\rho_i \delta\rho_j \rangle}{\rho_i \rho_j} - \frac{\delta_{ij}}{\rho_i}, \quad (1.2)$$

where the symbol $\langle \rangle$ stands for an average in the grand canonical ensemble, δ_{ij} is the Kronecker's delta, and $g_{ij}(r)$ is the radial distribution function. In eq. 1.2, $\rho_i = \langle N_i \rangle / V$ is the average number density of particles of species i , and $\delta\rho_i = N_i/V - \langle N_i \rangle / V$. The Kirkwood-Buff (KB) theory of solutions, published in 1951[57] derived that a variety of thermodynamic quantities are expressed using KBIs. This implies a coupling between the microscopic (the radial distribution function) and macroscopic (the thermodynamic quantity) properties of solutions. The KB theory is the most general and most powerful theory of solutions since the radial distribution function is not only experimentally observed from X-ray and neutron scattering but also calculated from molecular dynamics (MD) simulations.

Consider a subsystem of a massive homogeneous thermodynamic system isolated from its surroundings. The subsystem is in thermodynamic equilibrium with the rest of the system. The probability distribution function P of the fluctuation is given by[56]

$$P \propto \exp[\delta S_t / k_B], \quad (1.3)$$

where δS_t is the entropy change of the total system due to the fluctuation and k_B is the Boltzmann constant. In an m -component system, given the particle numbers $\{N_i\}$, volume V , and energy E in the total system remain constant, then

$$\delta S_t = \delta S + \frac{1}{T} \left(-\delta U - p\delta V + \sum_i \mu_i \delta N_i \right), \quad (1.4)$$

where δS , δV , δN_i , and δU are the changes of the entropy, volume, particle number of species i , and thermodynamic internal energy in the subsystem, respectively. The second term on the right-hand side corresponds to the entropy change of the system without the subsystem. Since the fluctuations are very small, replacing δU by an expansion in powers of δS and δN_i truncated at the second order yields

$$\delta U \sim T\delta S - p\delta V + \sum_i \mu \delta N_i + \frac{1}{2} \left(\delta T \delta S - \delta p \delta V + \sum_i \delta \mu \delta N_i \right). \quad (1.5)$$

Substituting eqs. 1.4 and 1.5 into eq. 1.3, and further considering the subsystem as a constant domain, i.e., $\delta V = 0$, we obtain

$$P \propto \exp \left[-\frac{1}{2k_B T} \left(\delta S \delta T + \sum_i \delta N_i \delta \mu_i \right) \right]. \quad (1.6)$$

Only $m+1$ of the remaining $2m+2$ variables S , T , $\{\mu_i\}$, and $\{N_i\}$ are independent. Choosing T and $\{N_i\}$ as independent variables and expressing S and $\{\mu_i\}$ in terms of T and $\{N_i\}$, eq. 1.6 is written as

$$\begin{aligned} P &\propto \exp \left[-\frac{1}{2} \left\{ \frac{C_V}{k_B T^2} \delta T^2 + V^{-1} \sum_i \sum_j I^{ij} \delta N_i \delta N_j \right\} \right] \\ &= \exp \left[-\frac{1}{2} \left\{ \frac{C_V}{k_B T^2} \delta T^2 + V \sum_i \sum_j I^{ij} \delta \rho_i \delta \rho_j \right\} \right], \end{aligned} \quad (1.7)$$

where C_V is the heat capacity at constant volume, ρ_i is the number density of species i in the subsystem, and

$$I^{ij} = \frac{1}{k_B T} \left(\frac{\partial \mu_i}{\partial \rho_j} \right)_{T, \{\rho_k\}_{k \neq j}}. \quad (1.8)$$

From eq. 1.7, we obtain the mean-square fluctuations of the density as

$$\langle \delta \rho_i \delta \rho_j \rangle = V^{-1} I_{ij}, \quad (1.9)$$

where I_{ij} is the inverse matrix of I^{ij} and is given by

$$I_{ij} \equiv k_B T \left(\frac{\partial \rho_i}{\partial \mu_j} \right)_{T, \{\mu_k\}_{k \neq j}}. \quad (1.10)$$

Therefore, from eqs. 1.2 and 1.9, the KBI is written as

$$I_{ij} = \rho_i \rho_j G_{ij} + \rho_i \delta_{ij}. \quad (1.11)$$

Using eq. 1.11, several physical properties of solutions can be expressed in terms of the KBIs. Then, we shall specifically present the relationship between several physical properties and the KBIs.

Two-component Systems.

Consider two-component systems of solvent w + solute A. Then, the matrix of I_{ij} is

$$(I_{ij}) = \begin{pmatrix} \rho_w^2 G_{ww} + \rho_w & \rho_w \rho_A G_{wA} \\ \rho_w \rho_A G_{wA} & \rho_A^2 G_{AA} + \rho_A \end{pmatrix}, \quad (1.12)$$

where ρ_w is the water density and ρ_A is the solute density. Thus, computing the inverse matrix yields

$$(I^{ij}) = \frac{1}{(\rho_w^2 G_{ww} + \rho_w)(\rho_A^2 G_{AA} + \rho_A) - \rho_w^2 \rho_A^2 G_{wA}^2} \begin{pmatrix} \rho_A^2 G_{AA} + \rho_A & -\rho_w \rho_A G_{wA} \\ -\rho_w \rho_A G_{wA} & \rho_w^2 G_{ww} + \rho_w \end{pmatrix}. \quad (1.13)$$

Using eq. 1.13, the isothermal compressibility $\chi_T \equiv -V^{-1} (\partial V / \partial p)_{T, \{N_i\}}$, in combination with $\chi_T^{-1} = k_B T \sum_{i,j=w,A} \rho_i \rho_j I^{ij}$, whose relationship corresponds to eq. 4.10 in the two-component system, is given as

$$k_B T \chi_T = \frac{1 + \rho_w G_{ww} + \rho_A G_{AA} + \rho_w \rho_A (G_{ww} G_{AA} - G_{wA}^2)}{\rho_w + \rho_A + \rho_w \rho_A (G_{ww} + G_{AA} - 2G_{wA})}. \quad (1.14)$$

Similarly, the partial molecular volume $\bar{v}_A = (\partial V / \partial N_A)_{T,p,N_w}$ of solute, in combination with eqs. 1.13, 1.14, and $\bar{v}_A = k_B T \chi_T \sum_{j=w,A} I^{Aj} \rho_j$, whose relationship corresponds to eq. 4.17 in the two-component system, is given as

$$\bar{v}_A = \frac{1 + \rho_w (G_{ww} - G_{wA})}{\rho_w + \rho_A + \rho_w \rho_A (G_{ww} + G_{AA} - 2G_{wA})}. \quad (1.15)$$

Using eqs. 1.14 and 1.15, the partial molecular volume of solute at the infinite dilution limit of solute is given by

$$\bar{v}_A = -G_{wA} - k_B T \chi_w \quad (\rho_A \rightarrow 0), \quad (1.16)$$

where χ_w is the isothermal compressibility in pure water with $\chi_w = \lim_{\rho_A \rightarrow 0} \chi_T$.

Three-component Systems.

We consider a three-component system of water (w) + ions (I) + hydrophobic solute (A), which is the simplest system for expressing the solubility of solute at the infinite dilution in dilute electrolyte aqueous solutions; for salt species $X_{\nu_+} Y_{\nu_-}$ dissociates into $\nu_+ X^{z_+}$ and $\nu_- Y^{z_-}$ (z_i is the ion valence), the total ion density $\rho_I = \rho_+ + \rho_- = (\nu_+ + \nu_-) \rho_s$ with ρ_+ , ρ_- , and ρ_s the densities of cation, anion, and salt, respectively. In general, the Helmholtz free energy density of the system f expanded in powers of ρ_I and ρ_A is given by

$$\begin{aligned} f(\rho_w, \rho_I, \rho_A) &= f_w(\rho_w) + k_B T \rho_I \left\{ \ln \left(\frac{\rho_I}{\nu_+ + \nu_-} \Lambda_I^3 \right) - 1 \right\} + \mu_I^*(\rho_w) \rho_I \\ &\quad + k_B T \rho_A \left\{ \ln(\rho_A \Lambda_A^3) - 1 \right\} + \mu_A^*(\rho_w) \rho_A \\ &\quad - \frac{k_B T}{12\pi} \kappa^3 + \frac{1}{2} \sum_{i,j=I,A} U_{ij}(\rho_w) \rho_i \rho_j + \dots, \end{aligned} \quad (1.17)$$

where the logarithmic term is singular at $\rho_I = 0$ or $\rho_A = 0$, so it has not been expanded. f_0 is the Helmholtz free energy density of water without ions and solute, Λ_I and Λ_A are the thermal de Broglie lengths of ions and solute, respectively; $\Lambda_I^3 = \{(\nu_+ \Lambda_+^3)^{\nu_+} (\nu_- \Lambda_-^3)^{\nu_-}\}^{1/(\nu_+ + \nu_-)}$ with Λ_+ and Λ_- are the thermal de Broglie lengths of cation and anion. $\mu_I^*(\rho_w)$ and $\mu_A^*(\rho_w)$ are the solvation free energies of ions and solute, respectively, at the infinite dilution limit of ions and solute;

$$\mu_I^*(\rho_w) = \frac{\nu_+ \mu_+^*(\rho_w) + \nu_- \mu_-^*(\rho_w)}{\nu_+ + \nu_-} \quad (1.18)$$

with $\mu_+^*(\rho_w)$ and $\mu_-^*(\rho_w)$ the solvation free energies of cation and anion at the infinite dilution limit of ions and solute. $U_{ij}(\rho_w)$ is the coefficient of $\rho_i \rho_j$;

$$\begin{aligned} U_{AI} &= \frac{\nu_+ U_{A+} + \nu_- U_{A-}}{\nu_+ + \nu_-} \\ U_{II} &= \frac{\nu_+^2 U_{++} + 2\nu_+ \nu_- U_{+-} + \nu_-^2 U_{--}}{(\nu_+ + \nu_-)^2}, \end{aligned} \quad (1.19)$$

where A is solute, + is cation, and - is anion in the subscripts of U_{ij} . The sixth term on the right-

hand side in eq. 1.17 is the Debye-Hückel free energy in the limit of the low ion densities[58, 59], with the inverse of the Debye length

$$\kappa = \sqrt{\frac{|z_+ z_-| e^2}{\epsilon(\rho_w) k_B T} \rho_I}, \quad (1.20)$$

where $\epsilon(\rho_w)$ is the dielectric constant in pure water and e is the elementary charge. Then, the solvation free energy $\mu_A^*(\rho_w, \rho_I)$ of solute at the infinite dilution limit only of solute is given using eq. 1.17 as

$$\begin{aligned} \mu_A^*(\rho_w, \rho_I) &= \mu_A - k_B T \ln(\rho_A \Lambda_A^3) \\ &= \left(\frac{\partial f}{\partial \rho_A} \right)_{T, \{\rho_k\}_{k \neq A}} - k_B T \ln(\rho_A \Lambda_A^3) \\ &= \mu_A^*(\rho_w) + U_{IA} \rho_I + \mathcal{O}(\rho_A). \end{aligned} \quad (1.21)$$

Under the constant pressure condition, the addition of salt changes the density of the solvent, whereby ρ_w is written as

$$\begin{aligned} \rho_w &= \rho_{w,0} + \left(\frac{\partial \rho_w}{\partial \rho_I} \right)_{T, p, N_w} \Big|_{\rho_w = \rho_{w,0}} \rho_I + \mathcal{O}(\rho_I^2) \\ &= \rho_{w,0} - \bar{v}_I \rho_{w,0} \rho_I + \mathcal{O}(\rho_I^2), \end{aligned} \quad (1.22)$$

where $\rho_{w,0}$ is the number density of water in pure water. Using eq. 1.22, we obtain

$$\mu_A^*(\rho_w) = \mu_A^*(\rho_{w,0}) - \mu_A^{*'}(\rho_{w,0}) \bar{v}_I \rho_{w,0} \rho_I + \dots \quad (1.23)$$

with $\mu_i^{*'}(\rho_{w,0}) = (\partial \mu_i^*(\rho_w) / \partial \rho_w)_{T, \{\rho_j\}_{j \neq w}} \Big|_{\rho_w = \rho_{w,0}}$.

From $\chi_T^{-1} = k_B T \sum_{i,j=w,I,A} \rho_i \rho_j I^{ij}$ (in eq. 4.10), the isothermal compressibility χ_w in pure water is given as

$$\chi_w^{-1} = k_B T \lim_{\rho_I, \rho_A \rightarrow 0} \rho_w^2 I^{ww} = \rho_{w,0}^2 f_0'' \quad (1.24)$$

with $f_0'' = (\partial^2 f_0(\rho_w) / \partial \rho_w^2)_T$. At the infinite dilution limit of ions and solute, substituting $\bar{v}_i = k_B T \chi_T \sum_{j=w,I,A} I^{ij} \rho_j$ for $i = w, I, A$ (in eq. 4.17) into eq. 1.8 and using eq. 1.17, the excess partial molecular volume $\bar{v}_i^* \equiv \bar{v}_i - k_B T \chi_T$ for $i = I, A$ is written as

$$\bar{v}_i^* = \chi_w \rho_{w,0} \mu_i^{*'}(\rho_{w,0}) \quad (i = I, A), \quad (\rho_I \rightarrow 0, \rho_A \rightarrow 0). \quad (1.25)$$

Then, substituting eq. 1.23 into eq. 1.21, we obtain

$$\begin{aligned}\mu_{\text{A}}^*(\rho_{\text{w}}, \rho_{\text{I}}) &= \mu_{\text{A}}^*(\rho_{\text{w},0}) + \left[U_{\text{IA}} - \mu_{\text{A}}^{*\prime}(\rho_{\text{w},0}) \bar{v}_{\text{I}} \rho_{\text{w},0} \right] \rho_{\text{I}} + \dots \\ &= \mu_{\text{A}}^*(\rho_{\text{w},0}) + \left[U_{\text{IA}} - \frac{\bar{v}_{\text{I}}^* \bar{v}_{\text{A}}^*}{\chi_{\text{w}}} - k_{\text{B}} T \bar{v}_{\text{A}}^* \right] \rho_{\text{I}} + \dots \quad (\rho_{\text{A}} \rightarrow 0),\end{aligned}\quad (1.26)$$

where eq. 1.25 is used to derive the last equality.

At a low salt concentration, the salt addition effect on the solubility of a hydrophobic solute is measured by the Setschenow coefficient K_{s} . In the present notation, it is given by

$$K_{\text{s}} = \lim_{\rho_{\text{s}} \rightarrow 0} \left(\frac{\partial \mu_{\text{A}}^*(\rho_{\text{w}}, \rho_{\text{I}}) / k_{\text{B}} T}{\partial \rho_{\text{s}}} \right)_{T,p}. \quad (1.27)$$

Substituting eq. 1.26 into eq. 1.27, we obtain

$$\begin{aligned}K_{\text{s}} &= (\nu_{+} + \nu_{-}) \lim_{\rho_{\text{I}} \rightarrow 0} \left(\frac{\partial \mu_{\text{A}}^*(\rho_{\text{w}}, \rho_{\text{I}}) / k_{\text{B}} T}{\partial \rho_{\text{I}}} \right)_{T,p} \\ &= (\nu_{+} + \nu_{-}) \left(\frac{U_{\text{IA}}}{k_{\text{B}} T} - \frac{\bar{v}_{\text{I}}^* \bar{v}_{\text{A}}^*}{k_{\text{B}} T \chi_{\text{w}}} - \bar{v}_{\text{A}}^* \right) \quad (\rho_{\text{I}} \rightarrow 0, \rho_{\text{A}} \rightarrow 0).\end{aligned}\quad (1.28)$$

Here, from eq. 1.11, the ions-solute KBI is written as

$$\begin{aligned}G_{\text{IA}} &= \frac{1}{\rho_{\text{I}} \rho_{\text{A}}} I_{\text{IA}} \\ &= -\frac{1}{\rho_{\text{I}} \rho_{\text{A}}} \frac{1}{\det\{I^{ij}\}} \begin{vmatrix} I^{\text{ww}} & I^{\text{wI}} \\ I^{\text{wA}} & I^{\text{IA}} \end{vmatrix}.\end{aligned}\quad (1.29)$$

where

$$\begin{vmatrix} I^{\text{ww}} & I^{\text{wI}} \\ I^{\text{wA}} & I^{\text{IA}} \end{vmatrix} = \frac{f_0'' U_{\text{IA}}}{(k_{\text{B}} T)^2} - \frac{\mu_{\text{I}}^{*\prime}(\rho_{\text{w}}) \mu_{\text{A}}^{*\prime}(\rho_{\text{w}})}{(k_{\text{B}} T)^2} + \dots \quad (1.30)$$

$$\begin{aligned}\rho_{\text{I}} \rho_{\text{A}} \det\{I^{ij}\} &= \frac{f_0''}{k_{\text{B}} T} - \frac{f_0'' \kappa^3}{16\pi k_{\text{B}} T \rho_{\text{I}}} + \frac{f_0'' U_{\text{II}} - \mu_{\text{I}}^{*\prime}(\rho_{\text{w}})^2}{(k_{\text{B}} T)^2} \rho_{\text{I}} \\ &\quad + \frac{f_0'' U_{\text{AA}} - \mu_{\text{A}}^{*\prime}(\rho_{\text{w}})^2}{(k_{\text{B}} T)^2} \rho_{\text{A}} + \dots\end{aligned}\quad (1.31)$$

Thus, substituting eqs. 1.24 and 1.25 into eq. 1.29, G_{IA} at the infinite dilution limit of ions and

solute is given by

$$\begin{aligned}
G_{\text{IA}} &= -\frac{U_{\text{IA}}}{k_{\text{B}}T} + \frac{\mu_{\text{I}}^{*\prime}(\rho_{\text{w},0})\mu_{\text{A}}^{*\prime}(\rho_{\text{w},0})}{k_{\text{B}}Tf_0''} \\
&= -\frac{U_{\text{IA}}}{k_{\text{B}}T} + \frac{\bar{v}_{\text{I}}^*\bar{v}_{\text{A}}^*}{k_{\text{B}}T\chi_{\text{w}}} \quad (\rho_{\text{I}} \rightarrow 0, \rho_{\text{A}} \rightarrow 0).
\end{aligned} \tag{1.32}$$

Using eqs. 1.16, 1.28, and 1.32, the Setschenow coefficient is expressed in the KBIs as

$$K_{\text{s}} = (\nu_{+} + \nu_{-})(G_{\text{wA}} - G_{\text{IA}}) \quad (\rho_{\text{I}} \rightarrow 0, \rho_{\text{A}} \rightarrow 0), \tag{1.33}$$

Here, substituting eqs. 1.18 and 1.19 into eq. 1.32, it is clear that

$$G_{\text{IA}} = \frac{\nu_{+}G_{\text{A}+} + \nu_{-}G_{\text{A}-}}{\nu_{+} + \nu_{-}}, \tag{1.34}$$

where + is cation and - is anion in the subscripts of the KBI.

IV OUTLINE OF THESIS

In the present study, using molecular dynamics (MD) simulations, we develop a new force field of monovalent ions and examine the partial molar volume of ions and the salt effects on the solubility of nonpolar and polar solutes and on the hydrophobic interactions between solute molecules. The present paper consists of three chapters as follows:

In Chapter 2, we shall develop a force field of ions to study the ion effect on the physical properties of aqueous solutions using MD simulations. The force field of the ions sets the ionic charge scaled by a factor of 0.75 to account for the electronic polarization effect of the solvent, and the other parameters are determined so that the density of aqueous solutions consisting of the TIP4P/2005 [60] water and the model ions is in accord with the experimental data. Furthermore, it is verified that the developed force field reproduces the solubility of methane in aqueous electrolyte solutions and the partial molar volume of salt at the infinite dilution limit.

In Chapter 3, we shall discuss the microscopic origin of ion size effects on the solubility of hydrophobic solutes in aqueous electrolyte solutions through analyses of correlation function integrals, packing fractions of solvation spheres of different radii centered at an ion, orientations of water molecules in the solvation spheres, and the solute-ion potential of mean force. In particular, we discuss the origin of the exceptionally small salting-out effect of Li^{+} (the strength of the salting-out effect: $\text{Na}^{+} > \text{K}^{+} > \text{Cs}^{+} \simeq \text{Li}^{+}$).

In Chapter 4, we examine the relationship between the ion-specific effect on the solubility of a solute and that on the effective interaction between solute molecules in aqueous solutions. The ion-specific effect on the solubility is measured by the Setschenow coefficient K_s . Recently, Okamoto and Koga proposed the salt-enhanced-association (SEA) coefficient defined by $C_I = -\lim_{\rho_s \rightarrow 0} (\partial B / \partial \rho_s)_{T,p}$, where B is the osmotic second virial coefficient and ρ_s the density of a salt in aqueous solutions of electrolytes ($X_{\nu_+} - Y_{\nu_-}$), as a measure of the ion-specific effect on the effective interaction between solute molecules and derived an approximate relation $C_I \simeq K_s^2 / 2 (\nu_+ + \nu_-)$. We calculate both C_I and K_s for various sets of ions and solutes by performing MD simulations. The numerical results of C_I and K_s are in good agreement with the approximate relation when K_s is positive (when solutes are salted out).

Chapter 2

Development and Validation of Charge Scaling Force Field of Ions: Solution Density, Solubility of Hydrophobic Solute, and Partial Molar Volume of Salt

Abstract

Model ions described by conventional nonpolarizable force fields overestimate the solubility of solutes in aqueous electrolyte solutions. We then propose a force field of ions whose charges are scaled by a factor of 0.75 to account for the electronic polarization effects of the solvent. Since the solubility of a given solute in aqueous electrolyte solutions is strongly correlated with the density of solutions, we optimized the force field parameters of ions to be consistent with experimental data of the density of aqueous electrolyte solutions by performing molecular dynamics simulations of aqueous electrolyte solutions of TIP4P/2005 water. Furthermore, using the charge scaling force fields of ions proposed in the present study and earlier studies, the Setschenow coefficient K_s for methane in salt solutions and the partial molar volume \bar{v}_s of the electrolytes at the infinite dilution limit were calculated. It is confirmed that the calculation results for K_s and \bar{v}_s obtained from using those force fields are in good agreement with the experimental values. Thus, it is now established that the ionic charge scaling method, despite being

very simple, highly improves the nonpolarizable force field in terms of the ability to reproduce both the density of solutions and the salt effect on the solubility of solutes.

I INTRODUCTION

Water is the most abundant substance in living organisms, accounting for 70 ~ 80%, most of which contains electrolytes. It is then one of the most significant fields for clarifying organism phenomena to study the physical properties of aqueous electrolyte solutions. In particular, the pH, the concentration of H_3O^+ and OH^- in an aqueous electrolyte solution, is an essential element for biochemistry study to closely relate to proton transfer in the chemical reaction and the structural change and precipitation of protein[61, 62]. Therefore, experimental and computer simulation studies are actively conducted about the ion addition effect on the physical properties of aqueous solutions[63, 64, 65, 66, 67, 68, 69].

Computer simulation, especially molecular dynamics (MD) simulation, is an effective tool for analyzing the microscopic structure around ions in an aqueous electrolyte solution or investigating a wide range of pressure, temperature, and salt concentration. Here, it is necessary for studying aqueous electrolyte solutions using MD simulations to set a force field of water molecules and ions that can accurately reproduce experimental results for some physical quantities, such as the solute solubility, the interface tension, the solution density, and the radial distribution function. Nonpolarizable force fields, such as AMBER[70], CHARMM[71, 72, 73], GROMOS[74, 75], and OPLS[76, 77] are used in the majority of MD simulations, especially for large systems and long computation times. For conventional nonpolarizable force fields, the electrostatic interactions of ions are described by their original integer charges[70, 72, 75, 78, 79, 80, 81, 82, 83, 84, 85, 86, 87]. These force fields of ions directly apply ionic charges in vacuum, which overestimate the electrostatic interaction of ions because of ignoring the screening effect of solvent electronic polarization. It is known that the salt addition effect on the solubility of a hydrophobic solute in aqueous electrolyte solutions of the nonpolarizable model ions is overestimated[88, 89, 19]. Leontyev and Stuchebrukhov[90, 91, 92, 93, 94, 95] proposed scaling the ionic charge in an aqueous electrolyte solution by $q_{\text{scaled}} = q/\sqrt{\epsilon_{\text{el}}}$ instead of the integer value as one solution to this problem (ϵ_{el} is the electronic dielectric of water, $\epsilon_{\text{el}} \sim 1.78$). They argued that the nonpolarizable force fields of ions take into account the electronic screening of the solvent by the simple charge scaling, the so-called electronic continuum correction (ECC) or molecular dynamics in an electronic continuum

(MDEC). Although it is clear that polarizable force fields can improve the above problems, in practice they are both difficult and computationally expensive to fully reproduce electronic polarization of the solvent[96, 97, 98, 99]. Therefore, it is very interesting to try to develop charge scaling force fields of ions that take into account the polarization effect in aqueous solutions.

Leontyev and Stuchebrukhov result in the scaled charges for monovalent ions of about ± 0.75 . The force field of Li^+ , Na^+ , and Cl^- with $q_{\text{scaled}} = \pm 0.75$ was proposed by Jungwirth et al. and is called the ECCR (Electronic Continuum Correction with Rescaling) force field[100, 101, 102, 103]. This force field represents a readjustment of the LJ parameter to match the experimental results of neutron scattering and viscosity after scaling the charge. Since then, charge scaling force fields of a variety of ions have been developed[99, 104, 105, 106, 107]. It has been pointed out in earlier computational studies[19, 108, 109] that charge scaling force fields of ions are much improved over nonpolarizable force fields employing integer ionic charges for many structural and dynamic properties of aqueous solution, such as gas solubility, solution density, and radial distribution functions. Similarly, Carlos Vega et al.[110, 111, 112, 113, 114] developed force fields of NaCl using $|q_{\text{scaled}}| = 0.75$ (Madrid-Transport model), 0.80, 0.85 (Madrid-2019 model), and 0.92 (Madrid-Interfacial model), especially in the Madrid-2019 model, developed that of a variety of monovalent and divalent ions. The Madrid-2019 force field reproduces well the salt concentration and temperature dependences of the experimental solution density, including the temperature of maximum density[115, 116].

In the present study, we develop a new force field of five ions, Cs^+ , F^- , I^- , H_3O^+ , and OH^- with each total charge scaled to ± 0.75 . In the development of a proton force field, it is inevitable to consider the properties of a proton in aqueous solution. Protons do not exist on their own in aqueous solution, and form chemical bonds with surrounding water molecules, such as the hydronium ion, H_3O^+ , and the Zundel cation, H_5O_2^+ (the proton shared by two water molecules)[117]. Furthermore, it is known that the proton forms a variety of protonated water clusters, and it has been debated to date whether the simplest hydrated cluster, H_9O_4^+ is the Eigen form $[\text{H}_3\text{O}^+(\text{H}_2\text{O})_3]$ [118, 119], the Zundel form $[\text{H}_5\text{O}_2^+(\text{H}_2\text{O})_2]$ or a mixture of the two[120, 121, 122, 123]. It is impossible to describe such complex properties of the proton in water by the classical MD, and quantum mechanical ideas are required. We assume that the physical properties of aqueous solution are described by treating the protons in the solution only with H_3O^+ , i.e., by neglecting other multi-body effects. In other words, it is not necessary that the properties of our proposed force field of H_3O^+ , such as the polarizability, be in perfect

agreement with the results of quantum chemical calculations of the hydronium[124, 125].

We develop a charge scaling force field of Cs^+ , F^- , and I^- using the ion model proposed by Joung and Cheatham[83] as a starting point. We also propose a charge scaling force field of H_3O^+ and OH^- , starting from the force field of those developed by Bonthuis, Mamatkukov, and Netz[87] with each total charge of ± 1 . The target property used to develop the new force field of ions is solution density. In addition, in the ionic force field developed in this work, that of the ECCR, and that of the Madrid-2019, the reproducibilities of the experimental data for the solubility of hydrophobic solutes in aqueous electrolyte solutions and the partial molar volume of electrolyte at the infinite dilution limit of electrolyte are verified.

II THEORETICAL BACKGROUND

The force field of the ions proposed in the present study is denoted as the Koga model. We assume a pairwise approximation where the total energy of the system is given by the sum of the potential energies between the molecules/ions in the system. The interaction between any pair of atoms i, j in the system is given by the sum of the Coulomb potential and the Lennard-Jones (LJ) potential;

$$V(r_{ij}) = \frac{1}{4\pi\epsilon_0} \frac{q_i q_j}{r_{ij}} + 4\epsilon_{ij} \left[\left(\frac{\sigma_{ij}}{r_{ij}} \right)^{12} - \left(\frac{\sigma_{ij}}{r_{ij}} \right)^6 \right], \quad (2.1)$$

where ϵ_0 is the dielectric constant in vacuum, q_i is the charge of atom species i , and ϵ_{ij} and σ_{ij} are the depth of the potential well and the LJ diameter between atoms i, j , respectively. We abbreviate $\sigma_{ii} = \sigma_i$ for homogeneous atoms.

A Charge Scaling Force Field of Point Charge Ions

Jungwirth et al. developed the force field of several point charge ions with charges scaled to 0.75 times their original integer values to describe the behavior of ions in aqueous electrolyte solutions, with the electronic polarization effect of the solvent taken into account.[100, 101, 102, 103, 107]. We also developed a force field of Cs^+ , F^- , and I^- with charge scaling to ± 0.75 which straightly followed the suggestion of Leontyev and Stuchebrukhov, introducing the idea of Jungwirth et al. However, we set the solution density as the target property and our objective is to reproduce

the experimental data up to high salt concentration. The force field of point charge ions was developed by the following procedure.

(1) The nonpolarizable force field parameters (JC model) with charge ± 1.0 proposed by Joung and Cheatham[83] were used as a reference, scaling the charge to ± 0.75 .

(2) We performed NpT -ensemble MD simulations of six aqueous solutions, LiI, NaF, NaI, CsF, CsCl, and CsI for several salt concentrations at 1 bar and 298 K. The ECCR model was used for Li^+ , Na^+ , and Cl^- . The LJ size parameters σ of Cs^+ , F^- , and I^- were determined so that the salt concentration dependence of the density d of each aqueous salt solution is in good agreement with the experimental data. The experimental density d kg/m^3 of an aqueous electrolyte solution is expressed as a function of temperature T (≥ 273 K) and salt molarity c mol/L [12];

$$d = d_w + Ac + BcT + CcT^2 + Dc^{3/2} + Ec^{3/2}T + Fc^{3/2}T^2$$

$$d_w = 999.65 + 2.0438 \times 10^{-1}T - 6.174 \times 10^{-2}T^{3/2} \quad (2.2)$$

where d_w is the density of pure water, and A, B, C, D, E, and F are the coefficients given for each salt type. The force field parameters determined in the above procedures are listed in Table 2.1.

Table 2.1: LJ parameters σ , ϵ of ions, and scaled charge q . The ECCR force field is proposed by Jungwirth et al.

Model	Sites	σ (nm)	ϵ (kJ/mol)	q
ECCR[100]	Li^+	0.180000	0.0764700	+0.75
ECCR[103]	Na^+	0.211500	0.5442840	+0.75
ECCR[102]	Cl^-	0.410000	0.4928000	-0.75
This work	Cs^+	0.360101	0.3759584	+0.75
This work	F^-	0.361937	0.0309636	-0.75
This work	I^-	0.468096	0.1790101	-0.75
This work	O (H_3O^+)	0.265	0.8	-1.05
This work	H (H_3O^+)	0	0	+0.60
This work	O (OH^-)	0.36	0.05	-0.75
This work	H (OH^-)	0	0	0

(3) We calculated the Setschenow coefficient K_s , which represents a measure of the salt addition effect on the solubility of the solute, and the partial molar volume \bar{V}_s of salt at the infinite dilution limit using the ionic parameters determined in this work, and compared them with experimental values.

B Charge Scaling Force Field of Hydronium Ion And Hydroxide Ion

We developed force fields of H_3O^+ and OH^- that effectively account for the electronic polarization effect of the solvent by a simple scaling of the charges. In particular, the charge scaling force field of H_3O^+ has not been developed before and is very interesting to develop and verify. The force field of those was developed by the following procedure.

(1) The nonpolarizable force field parameters with the total charge ± 1 proposed by Bonthuis, Mamatkukov, and Netz were used as a reference[87], scaling the total charge to ± 0.75 by multiplying the charge of each site in the model molecule by 0.75. The hydronium ion model is triangular pyramidal as shown in Figure 2.1, with the H-O-H angle θ_{HOH} being 111.4° and the O-H bond length b_{OH} being 0.98 \AA . The hydroxide ion model is linear, and the O-H bond length b_{OH} is 1.0 \AA .

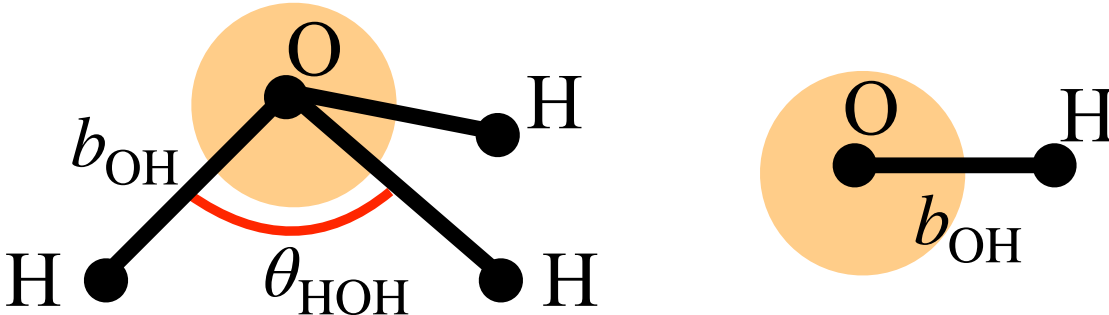


Figure 2.1: Definition of bond lengths b_{OH} and angle θ_{HOH} .

(2) We performed NpT -ensemble MD simulations of HCl and NaOH aqueous solutions for several temperature and salt concentrations at 1 bar. The LJ size parameter σ_{O} of the oxygen atom in each model molecule was determined so that the temperature and salt concentration dependences of the solution density d fit the experimental data. The force field parameters determined in the above procedures are listed in Table 2.1.

(3) As in the case of point charge ions, we verified the Setschenow coefficient K_s and the partial molar volume \bar{V}_s of salt for agreement with experimental values.

C Setschenow Coefficient K_s

The salt addition to water decreases the solubility of solutes, the so-called salting-out effect, and is applied to the separation of proteins, low molecular weight organic compounds, metal complexes, and ion pairs that cannot be separated by filtration or centrifugation. However, there are ion species that denote the opposite salt addition effect and are called the salting-in. At a low salt concentration, the salt addition effect on the solubility of a hydrophobic solute is measured by the Setschenow coefficient K_s ;

$$\begin{aligned} K_s &= - \lim_{\rho_s \rightarrow 0} \left(\frac{\partial \ln \lambda_A}{\partial \rho_s} \right)_{T,p} \\ &\simeq - \frac{1}{\rho_s} \ln \left(\frac{\lambda_A}{\lambda_A^0} \right) \quad (\rho_s \rightarrow 0), \end{aligned} \quad (2.3)$$

where λ_A and λ_A^0 are the Ostwald absorption coefficients of the gas in aqueous solution and in pure water, respectively, and ρ_s is the number density of the electrolyte. The second line in eq. 2.3 was derived by a linear approximation. The Ostwald absorption coefficient λ_A is the ratio of the solute density ρ_A in solution to that ρ_A^{gas} in the gas phase when the solution is in equilibrium with the gas phase. The value of λ_A denotes the the solute solubility and is written using the solvation free energy (SFE) μ_A^* of a solute in an aqueous electrolyte solution at the infinite dilution limit of solute as

$$\lambda_A = \lim_{\rho_A \rightarrow 0} \frac{\rho_A}{\rho_A^{\text{gas}}} = e^{-\mu_A^*/k_B T}. \quad (2.4)$$

Using eq. 2.4, eq. 2.3 is written as

$$\begin{aligned} K_s &= \lim_{\rho_s \rightarrow 0} \left(\frac{\partial \mu_A^*/k_B T}{\partial \rho_s} \right)_{T,p} \\ &\simeq \frac{\mu_A^* - \mu_{A,0}^*}{\rho_s k_B T}, \end{aligned} \quad (2.5)$$

where $\mu_{A,0}^*$ is the solvation free energy of a solute in pure water at the infinite dilution limit of solute, and the second line was derived by a linear approximation. The Setschenow coefficient K_s obtained from eq. 2.3 depends on the solute and the salt species. The Setschenow coefficients for many combinations of ion and solute species have been obtained from experimental data[42, 45, 126, 46, 127, 128], and $K_s > 0$ indicates salting-out, and $K_s < 0$ indicates

salting-in. In other words, the larger the K_s , the stronger the salting-out effect. Therefore, we performed MD simulations to calculate K_s for methane in a variety of aqueous electrolyte solutions using the ionic force field developed in the present study and compared them with experimental values. In the earlier references, the Setschenow coefficient is often defined with $k_{\text{scc}} = -\lim_{\rho_s \rightarrow 0} (\partial \log_{10} \lambda_A / \partial \rho_s)_{T,p} = K_s / \ln 10$, so we use the ordinary logarithm in the calculation result of this paper.

As explained in Chapter 1, when salt species $X_{\nu_+} Y_{\nu_-}$ dissociates into $\nu_+ X^{z_+}$ and $\nu_- Y^{z_-}$ (z_i is the ion valence), the Setschenow coefficient is also written as

$$K_s = (\nu_+ + \nu_-) (G_{Aw} - G_{As}) \quad (\rho_s \rightarrow 0) \quad (2.6)$$

with

$$G_{As} = \frac{\nu_+ G_{A+} + \nu_- G_{A-}}{\nu_+ + \nu_-}, \quad (2.7)$$

where the Kirkwood-Buff integral (KBI) G_{ij} is a measure of the fluctuation in the molecular number of species i and j , and the subscripts A, w, s, +, and - denote the solute, the solvent, the salt, and the positively and negatively charged ionic species. Using the radial distribution function $g_{ij}(r)$, the KBI is defined as

$$G_{ij} = \int [g_{ij}(r) - 1] d\boldsymbol{\tau}, \quad (2.8)$$

where $d\boldsymbol{\tau}$ is the volume prime. Thus, it is found that K_s is obtained from two routes, the SFE and the KBI. Then, we performed MD simulations of aqueous solutions using the ionic force field developed in this chapter and compared the Setschenow coefficients obtained from eqs. 2.5 and 2.6, respectively, with the experimental values and those obtained using conventional nonpolarizable force fields.

D Partial Molar Volume of Electrolytes

The partial molecule volume \bar{v}_i of species i is defined as the volume change of a solution when one molecule of species i is added to the solution, i.e., $\bar{v}_i = (\partial V / \partial N_i)_{T,p,\{N_j\}_{j \neq i}}$ with the solution volume V and the particle number N_i . The partial molecule volume is expressed as $\bar{V}_i = N_A \bar{v}_i$ by the partial molar volume \bar{V}_i and the Avogadro constant N_A , which the former is defined as the volume change of a solution when one mole of molecule species i is added to

the solution and is often used in earlier studies. As shown in eqs. 1.14 and 1.15 in Chapter 1, the partial molecular volume and the isothermal compressibility $\chi_T \equiv -V^{-1}(\partial V/\partial p)_{T,\{N_i\}}$ in a two-component system are expressed using the KBIs as

$$\bar{v}_2 = \frac{1 + \rho_1 (G_{11} - G_{12})}{\rho_1 + \rho_2 + \rho_1 \rho_2 (G_{11} + G_{22} - 2G_{12})} \quad (2.9)$$

$$k_B T \chi_T = \frac{1 + \rho_1 G_{11} + \rho_2 G_{22} + \rho_1 \rho_2 (G_{11} G_{22} - G_{12}^2)}{\rho_1 + \rho_2 + \rho_1 \rho_2 (G_{11} + G_{22} - 2G_{12})}. \quad (2.10)$$

Using eqs. 2.9 and 2.10 in the limit $\rho_2 \rightarrow 0$, we obtain

$$\bar{v}_2 = -G_{12} + k_B T \chi_w \quad (\rho_2 \rightarrow 0), \quad (2.11)$$

where $\chi_w = \lim_{\rho_2 \rightarrow 0} \chi_T$ is the isothermal compressibility for pure water.

It is known that the partial molecular volume of electrolyte at the infinite dilution is additive, i.e., $\bar{v}_s = \nu_+ \bar{v}_+ + \nu_- \bar{v}_-$ due to the disappearance of ion-ion interactions[26, 27]; \bar{v}_+ and \bar{v}_- are the partial molecular volume of a cation and an anion, respectively. In other words, the partial molar volume of an electrolyte is relatively easy to obtain experimentally and is very useful in understanding the ion-solvent interaction. Therefore, it has been carried out in earlier experimental studies[28, 29, 30, 31] that partial molar volumes \bar{V}_s of many electrolytes are measured, and partial molar volumes \bar{V}_\pm of individual ions (cation or anion) are estimated. However, the serious problem is difficult to directly determine the magnitude of individual \bar{V}_\pm although the relative values of those is easily obtained. As an example, formally based on the partial molar volume \bar{V}_{H^+} of proton, the differences $\bar{V}_\pm - \bar{V}_{H^+}$ for a variety of ions have been determined in Refs. [29, 26]. Therefore, it is essential to obtain an exact partial molar volume of a proton for determining individual \bar{V}_\pm , but many different values have been estimated experimentally in the range from -7.6 to -2.7 cm³/mol in water at 298 K[129, 130, 131, 132, 133, 134, 135, 136, 33, 34, 137, 138, 139], making it difficult to exactly obtain partial molar volumes \bar{V}_\pm of ions from the experimental data. Only the method proposed by Zana and Yeager[33, 34] has directly and experimentally determined \bar{V}_\pm of a variety of simple monovalent ions, including a proton, from ionic vibration potential measurements and density data. Furthermore, Takenaka and Arakata[32] succeeded in determining individual partial molar volumes of ions at infinite dilution with greater precision using their method.

The partial molecular volume of electrolyte in solution of water + electrolyte at the infinite

dilute limit of electrolyte is given from eq. 2.11 by

$$\lim_{\rho_s \rightarrow 0} \bar{v}_s = \nu_+ \bar{v}_+ + \nu_- \bar{v}_- = (\nu_+ + \nu_-) (-G_{ws} + k_B T \chi_w) \quad (2.12)$$

with

$$G_{ws} = \frac{\nu_+ G_{w+} + \nu_- G_{w-}}{\nu_+ + \nu_-}, \quad \chi_w = \lim_{\rho_s \rightarrow 0} \chi_T = \frac{1 + \rho_w G_{ww}}{k_B T \rho_w} \quad (2.13)$$

Equation 2.12 indicates that the salt species dependence of the partial molecular volume \bar{v}_s of salt is internalized in G_{w+} and G_{w-} . Here, it is known that the relation $G_{w+} = G_{w-}$ holds for the KBI in an opened system by the charge neutrality condition[140]. However, at a salt concentration low enough that the cation and anion can be considered independent of each other, which means that there is no solvent molecule affected by both a cation or an anion in solution, the charge neutrality condition is no longer valid, $G_{w+} \neq G_{w-}$. In this case, G_{w+} and G_{w-} have unique values for individual ions, regardless of each counter-ion species. That is, individual partial molar volumes of ions at the infinite dilution of salt can be obtained from eq. 2.11 using MD simulations if we even have a force field that accurately describes the behavior of ions in aqueous solutions. Therefore, at a low salt concentration where the charge neutrality condition does not hold, we performed MD simulations of aqueous salt solutions using charge scaling force fields of ions and compared obtained partial molar volumes \bar{V}_s of salt with the experimental data.

III COMPUTATIONAL DETAILS

We performed NpT ensemble MD simulations using the program package GROMACS2018[141] to develop and validate a new charge scaling force field of several monovalent ions in the study of Chapter 2. All of the MD simulations were performed in a cubic cell system with three-dimensional periodic boundary conditions at 1 bar and a time step of 1 fs. The Parrinello-Rahman method and the Nosé-Hoover method were used for pressure and temperature control, respectively. The duration of the production run ranges from 10 to 450 ns depending on structural properties to be calculated, after the equilibrium run of 5 ns. Configurations in the production run are sampled every 50 steps.

First, we performed MD simulations at the temperature of 298 K and salt concentration in a range from 1 to 4 mol/kg for eight aqueous model electrolyte solutions, LiI, NaF, NaI, CsF,

CsCl, CsI, HCl, and NaOH for 10 ns to calculate each solution density d . We even performed MD simulations at the temperature in a range from 265 to 298 K and salt concentration of 1 mol/kg for HCl and NaOH solutions for 10 ns. Each solution was prepared with 36, 72, 108, and 144 pairs of monovalent cations and anions added to 2000 water molecules. However, since a hydronium ion, which is the most common form of H^+ in the aqueous solution, consists of one water molecule and one proton, the total number of hydronium ions and water molecules was set to 2000 instead of setting 2000 water molecules in HCl solutions. Second, we performed MD simulations for four kinds of model systems to obtain the Setschenow coefficient K_s for methane: pure water, aqueous solutions of salt, those of methane, and those of salt + methane. Each system contains 4000 water molecules. The aqueous salt solutions contain the additional 72 pairs of monovalent cations and anions to give a salt concentration of 1 mol/kg, and a solute solution contains 48 molecules. Each system contains 4000 water molecules. The aqueous salt solutions contain the additional 72 pairs of monovalent cations and anions to give a salt concentration of 1 mol/kg, and even a solution adding 48 methane molecules is prepared. For the solutions of salt and methane, the same number of ions and methane as above are added. Finally, we prepared 8000 water molecules, added one cation and anion 3 nm apart, fixed their positions, and performed MD simulations for 150 ns to calculate the partial molar volumes of electrolytes at the infinite dilute limit. The model electrolyte solutions of HCl, LiCl, NaF, NaCl, NaI, NaOH, CsF, CsCl, and CsI are prepared. The box size is about 6 nm on each system, which satisfies the cation-anion distance of 3 nm even when the periodic boundary condition is taken into account.

The potential function for the intermolecular interactions of water molecules is of TIP4P/2005 [60]. The ionic force field parameters are shown in Table 2.1. The methane molecule was used the OPLS force field[142], a spherical monatomic LJ particle model; $\sigma_A=0.373$ nm, $\epsilon_{AA}=1.2301$ kJ/mol. The LJ parameters between heterogeneous particles were basically determined by

$$\sigma_{12} = \sqrt{\sigma_1\sigma_2}, \quad \epsilon_{12} = \sqrt{\epsilon_1\epsilon_2}. \quad (2.14)$$

However, the methane-water LJ parameters were used $\sigma_{Aw} = 0.34445$ nm and $\epsilon_{Aw} = 1.043$ kJ/mol[143], and the Na^+-OH^- LJ diameter parameter were used $\sigma_{Na^+OH^-} = 1.134$ nm. The methane-methane and interaction was replaced by the repulsive part of the Weeks-Anderson-Chandler (WCA) potential[144] to prevent solute aggregation. The original methane-methane radial distribution function $g_{AA}(r)$ is transformed from the methane-methane $g_{AA}^{sim}(r)$ obtained

from the MD simulations using the WCA repulsive potential[145, 146]. The LJ potential part of all of the intermolecular pair potentials was truncated at 0.9 nm, and the long-range Coulomb part of those was calculated by the Ewald sum with the same cutoff distance as the LJ part in the real space. However, the cutoff distance was changed to 1.2 nm to calculate the partial molar volume instead of 0.9nm.

The solvation free energy μ_A^* of methane was calculated from the Widom test-particle insertion (TPI) method[147] to evaluate the Setschenow coefficient K_s from the second line in eq. 2.5. We performed MD simulations of pure water and salt solutions for 150 ns and inserted test particles 2×10^5 times into the equilibrium configuration at 50 fs intervals. K_s for methane was even evaluated from eq. 2.6. The KBIs in eq. 2.6, G_{Aw} and G_{As} were obtained from numerical integration of the corresponding pair correlation function. MD simulations of methane solution and salt + methane solutions were performed for 450 ns. Any $h_{ij}(r)$ obtained from MD simulation at a closed system does not converge to zero at large distances due to the finite-size effect. We shifted the entire $h_{ij}(r)$ so that the average of $h_{ij}(r)$ in a certain range at large distances becomes zero. Furthermore, we evaluated the KBI in the thermodynamic limit by applying the following method proposed by Krüger et al.[148, 149] to the KBI obtained for the finite systems: The KBI for the molecule models with multiple interaction sites such as the hydronium ion was obtained by averaging the KBIs between all the pairs of sites on the molecules[150].

IV RESULT AND DISCUSSION

A Point Charge Ions

We obtained the density d of aqueous electrolyte solutions at several salt concentrations from MD calculations using the charge scaling force field of point charge ions developed in the present study at 1 bar and 298 K. The molality dependences of these results and the experimental data are shown in Figure 2.2. For many electrolytes, the calculated solution densities are in good agreement with the experimental data up to the high salt concentration, but for CsF and CsI solutions, the densities are overestimated at the high salt concentration. The deviations for CsF and CsI at the high salt concentration are attributed to ion-ion interactions in the used force field since the solution densities reproduce the experimental data well in the range of up to 1 mol/kg.

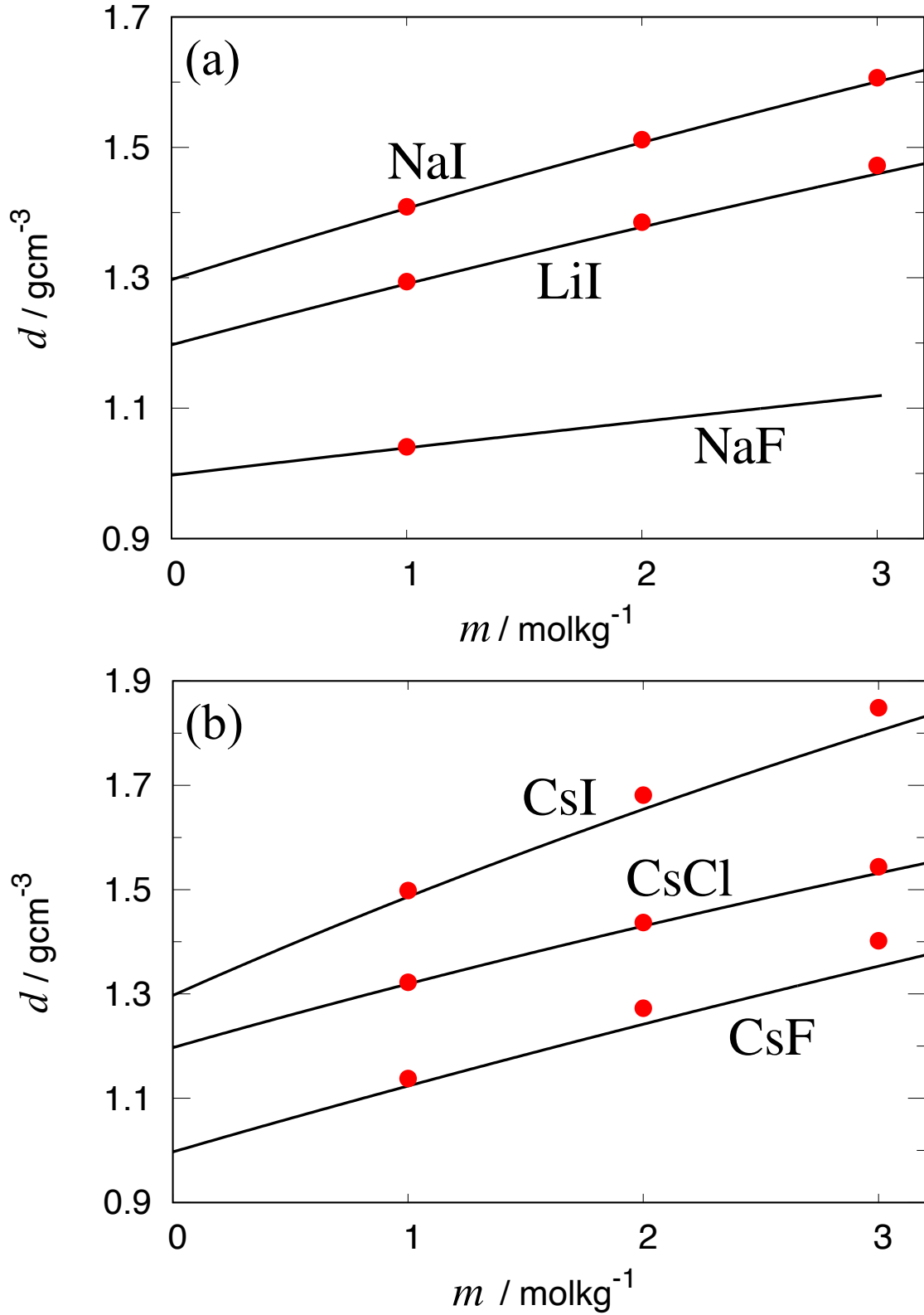


Figure 2.2: Density d vs molality for (a) LiI, NaF, NaI aqueous solutions and (b) CsF, CsCl, CsI aqueous solutions. Red circles are the result from MD simulation, and the black line are the experimental data in eq.2.2. The density for LiI and CsCl are plotted with the vertical axis shifted by +0.2 in the notation unit. Similarly, the density for NaI and CsI are plotted with the vertical axis shifted by +0.3.

B Hydronium Ion And Hydroxide Ion

Next, the molality and temperature dependences of the solution density d of HCl and NaOH solutions were verified from MD calculations using the new force field for H_3O^+ and OH^- , and compared with experimental values. Figure 2.3 shows the molality dependence of the density d of aqueous HCl and NaOH solutions calculated from MD simulations at 1 bar and 298 K. In both HCl and NaOH solutions, the densities are in very good agreement with the experimental data, from low to high salt concentration of at least 4 mol/kg.

Figure 2.4 shows the temperature dependence of the density of aqueous HCl and NaOH solutions calculated from MD simulations at 1 bar and the molality of 1 mol/kg for a total of seven temperatures, every 5 K from 260 to 285 K, plus 298 K. It is highly significant to verify the temperature dependence of the solution density to confirm the usefulness of the ionic force field since the temperature of the maximum density of an aqueous electrolyte solution depends on the salt species and it is known that TIP4P/2005 water reproduces well the temperature of the density maximum. In addition, the experimental values of density from the two routes using eq. 2.2 are plotted in Figure 2.4. The blue triangles are the solution density d obtained by substituting the salt concentration c from the numerical results at each temperature into eq. 2.2. The solid black line plots eq. 2.2 as a function only of temperature, fixed c at the molar concentration of salt at 298 K, assuming that the salt concentration change with the temperature change is very small. The values from those two routes agree well. For the aqueous HCl solution (in Figure 2.4a), the density of the numerical results (red circles) agrees well with the experimental data as a function of temperature, e.g., the density at 298 K being only 0.14% smaller than the experimental data. The temperature of the density maximum is 275 K for the MD simulation and 275.1 K for the experimental data, which are almost identical. For the aqueous NaOH solution (in Figure 2.4b), the numerical results of the density agree well with the experimental data above 273 K as a function of temperature, e.g., the density is only 0.2% larger than the experimental value at 275 K, where the difference with the experimental values is the largest. However, the temperature dependence of d from MD calculations did not show a maximum in the range of 260 to 298 K.

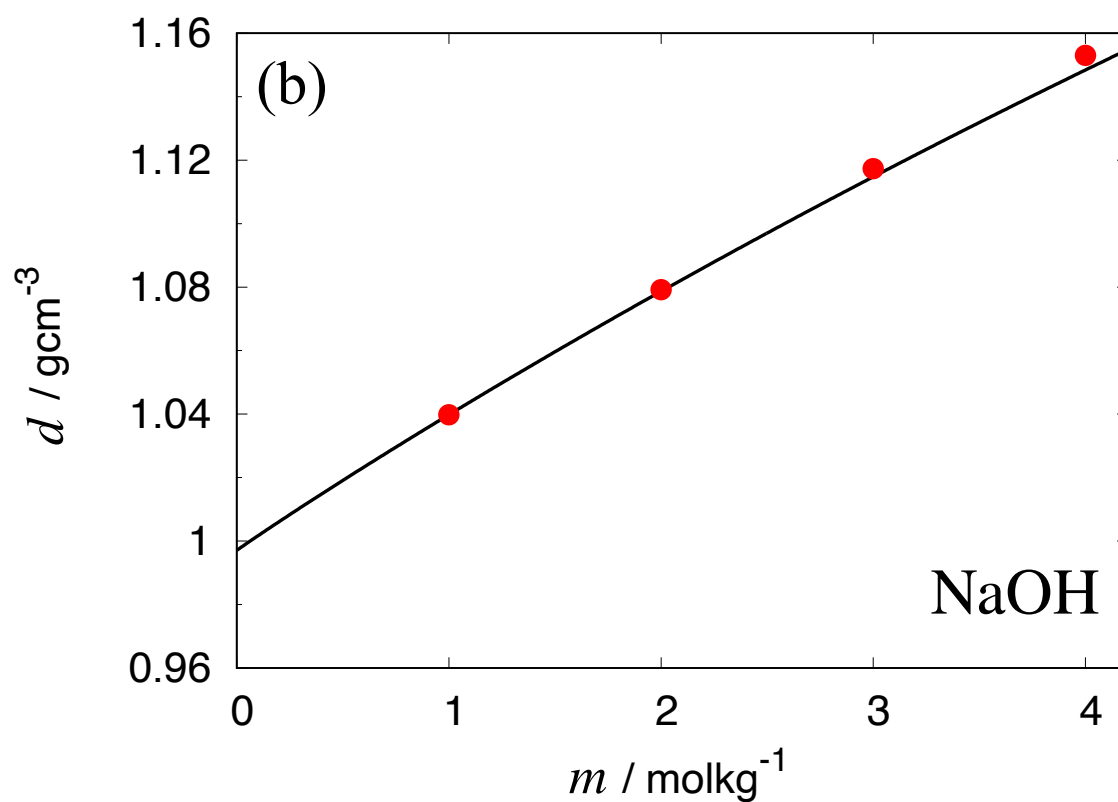
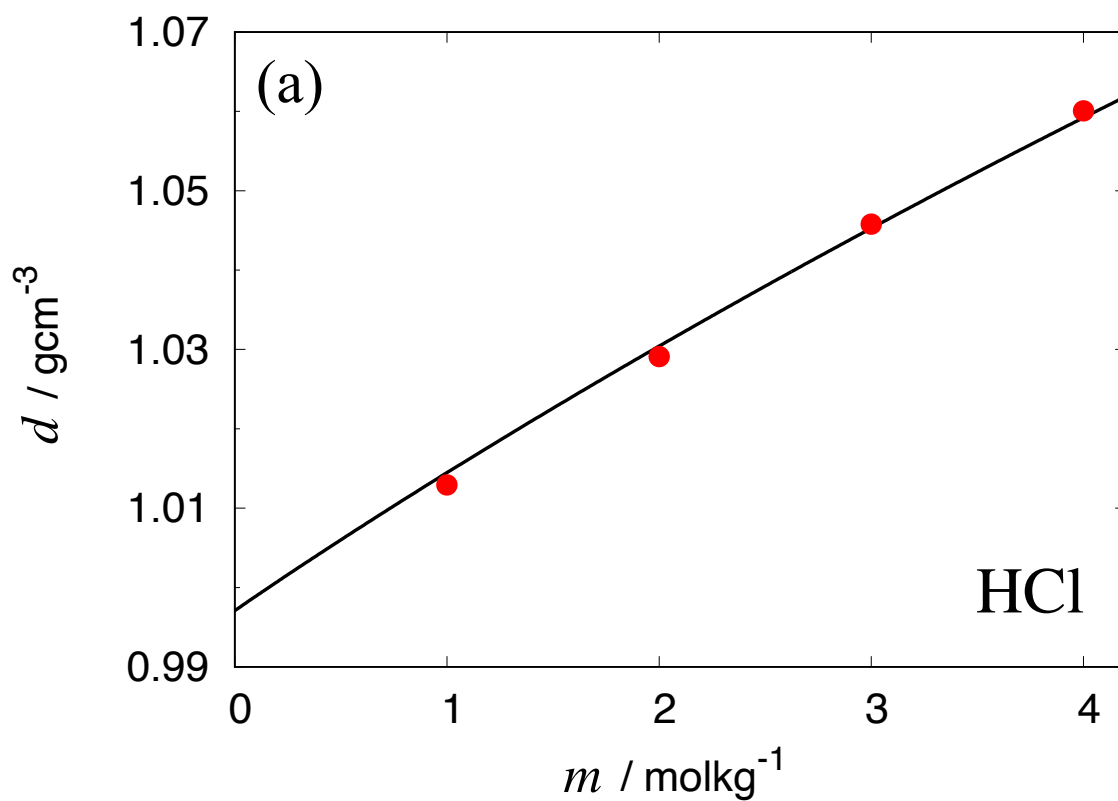


Figure 2.3: Density d vs molality for (a) HCl aqueous solution and (b) NaOH aqueous solution. Red circles are the result from MD simulations, and the black line are the experimental data in eq.2.2.

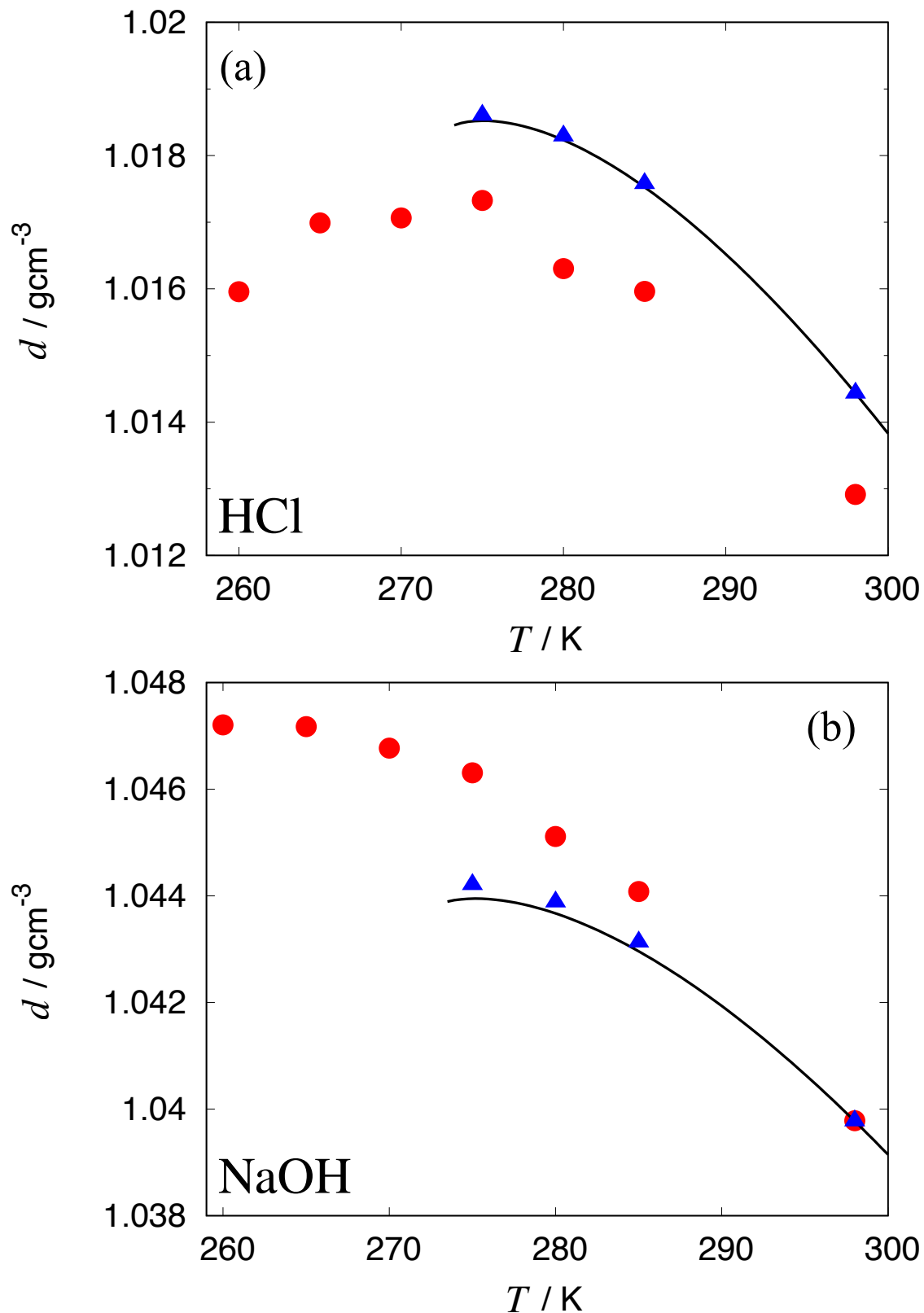


Figure 2.4: Density d vs temperature for (a) HCl aqueous solution and (b) NaOH aqueous solution. The red circles are the results from MD simulations, the blue triangles are the experimental values calculated in eq. 2.2 at each salt concentration c and temperature T , and the black line plots the experimental density d in eq. 2.2 with c fixed at 298 K.

C Setschenow Coefficient

The Setschenow coefficient k_{scc} for methane in a variety of aqueous electrolyte solutions, obtained by MD calculations using the charge scaling force field of ions, were compared with the experimental data to verify the reproducibility of the solute solubility. Figure 2.5 shows the Setschenow coefficients for methane in aqueous solutions of HCl, LiCl, NaF, NaCl, NaI, NaOH, CsF, CsCl, and CsI, calculated from force fields scaled to a charge of 0.75 (in Table 2.1) and nonpolarizable force fields with charge unscaled[83, 87], respectively, along with the experimental values. Furthermore, we calculated k_{scc} in aqueous LiCl, NaCl, and CsCl solutions using the Madrid-2019 force field with $q_{\text{scaled}} = \pm 0.85$ [111] and that in the aqueous NaCl solution using the Madrid-Transport force field with $q_{\text{scaled}} = \pm 0.75$ [114]. The Setschenow coefficients using the ECCR and Koga models in Table 2.1 were evaluated in two routes, eqs. 2.5 and 2.6. First, $\mu_{\text{A},0}^*$ and μ_{A}^* were calculated by the TPI method, in which one methane was inserted as a test particle into pure water and salt solutions that do not contain methane, respectively. It has been pointed out in the earlier study that the $\mu_{\text{A},0}^*$ calculated using the TIP4P/2005 model water and methane of a single LJ sphere model is in good agreement with the experimental value[143]. Second, we calculated G_{Aw} in a methane solution without salt and G_{As} (i.e. $G_{\text{A}+}$ and $G_{\text{A}-}$) in salt + methane solutions, respectively. G_{Aw} was calculated at low but finite solute concentrations, and G_{As} was similarly calculated at low but finite salt and solute concentrations. However, we assumed those to be G_{Aw} and G_{As} at the infinite dilution limit. Figure 2.5 shows that, for all salt solutions, the Setschenow coefficient $k_{\text{scc}}^{\text{sim}}$ calculated from the SFE route in eq. 2.5 and the KBI route in eq. 2.6 are in good agreement, and both reproduce the experimental Setschenow coefficient $k_{\text{scc}}^{\text{exp}}$ well. Focusing on NaCl as a salt, the computational Setschenow coefficients $k_{\text{scc}}^{\text{sim}}$ obtained from the ECCR force field underestimated the experimental value $k_{\text{scc}}^{\text{exp}}$ by 22% for the SFE route and 18% for the KBI route, while that from the Madrid-2019 force field is 2.7% larger than $k_{\text{scc}}^{\text{exp}}$ and that from the Madrid-Transport force field is 36% smaller than $k_{\text{scc}}^{\text{exp}}$. Those charge scaling model ions are highly improved over the JC model, which overestimates $k_{\text{scc}}^{\text{exp}}$ by 62%. The Koga model developed in this chapter expresses $k_{\text{scc}}^{\text{exp}}$ as well as or better than the ECCR model, and the Madrid-2019 model reproduces that the best. Thus, it is confirmed that the charge scaled force field of ions improves the nonpolarizable force field very well concerning the salt addition effect on the solubility of hydrophobic solutes.

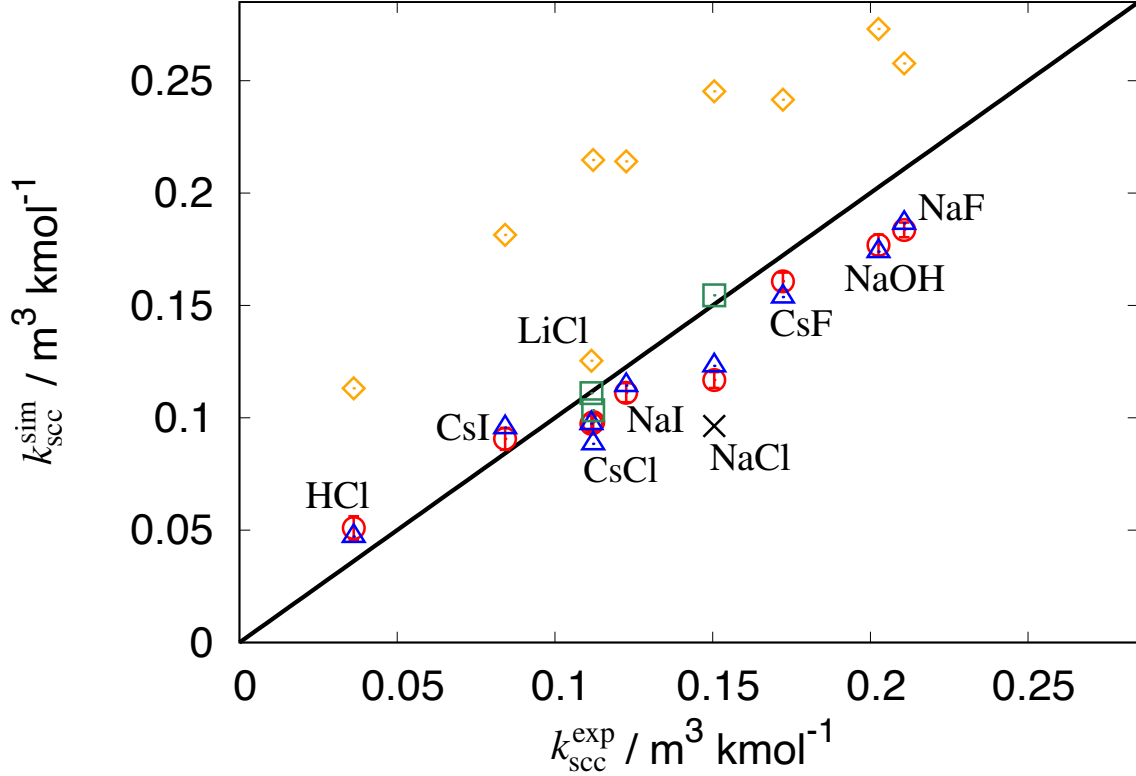


Figure 2.5: The Setschenow coefficient $k_{\text{scc}}^{\text{sim}}$ for methane from MD calculations in several ionic force fields vs the experimental $k_{\text{scc}}^{\text{exp}}$ [46]. Red circles and blue triangles are calculated from the SFE route (eq. 2.5) and KBI route (eq. 2.6), respectively, using the ionic force fields (ECCR and Koga models) with $q_{\text{scaled}} = \pm 0.75$. Green squares, black cross, and orange diamonds are the results from the SFE routes using the Madrid-2019 force field with $q_{\text{scaled}} = \pm 0.85$, the Madrid-Transport force field with $q_{\text{scaled}} = \pm 0.75$, and nonpolarizable force fields (JC and Bonthuis et al. models) with $q = \pm 1$, respectively.

D Partial Molar Volume of Electrolytes

The partial molar volumes \bar{V}_s , \bar{V}_+ , and \bar{V}_- of electrolytes, cations, and anions at the infinite dilution limit of salt were evaluated from eqs. 2.11 and 2.12 by MD calculations. Here, since a hydronium ion molecule consists of one molecule each of H^+ and H_2O , the partial molar volume of H^+ is given by $\bar{V}_{\text{H}^+} = \bar{V}_{\text{H}_3\text{O}^+} - \bar{V}_w = \bar{V}_{\text{H}_3\text{O}^+} - N_A/\rho_w$ with \bar{V}_w the partial molar volume of water. Table 2.2 shows the \bar{V}_s^{sim} , \bar{V}_+ , and \bar{V}_- for the ECCR and Koga models in nine salt solutions and the experimental values \bar{V}_s^{exp} [29, 26]. As shown in Table 2.2, it is found that the partial molar volume of the ion has the ion-specific value independent of the counterion, i.e., $G_{w+} \neq G_{w-}$, which represents that the charge neutrality condition is not satisfied at the simulation condition in the present study. The partial molar volumes of electrolytes from the charge scaling force field of ions agrees well with the experimental values except for CsF and CsI. The computational values \bar{V}_s^{sim} underestimate the experimental values by $9.9 \text{ cm}^3/\text{mol}$ in the

aqueous CsI solution and by $11.4 \text{ cm}^3/\text{mol}$ in the aqueous CsF solution, which has the largest deviation. Here, the partial molar volume \bar{V}_s of electrolytes is related to the solution density d by

$$\left(\frac{\partial d}{\partial c}\right)_{T,p,N_w} = \sum_i \frac{\partial(N_i M_i/V)}{\partial(N_s/V)} = \frac{1 - d\bar{V}_s}{1 - \rho_s \bar{V}_s/N_A}, \quad (2.15)$$

where M_i is the molar mass of molecular species i . Then, in the limit $\rho_s \rightarrow 0$, we obtain

$$\bar{V}_s = \frac{1}{d} \left[1 - \left(\frac{\partial d}{\partial c}\right)_{T,p,N_w} \right] \quad (\rho_s \rightarrow 0). \quad (2.16)$$

Equation 2.16 indicates that the partial molar volume of the electrolyte is determined by the derivative of the solution density with respect to the molar concentration of salt, whereby the differences between \bar{V}_s^{sim} and \bar{V}_s^{exp} are attributed to the deviation of $(\partial d/\partial c)_{T,p,N_w}$ from the experiment. Given the relation $1/m = d/c - M_s$ between the salt concentration c and the molality m , the deviation of $(\partial d/\partial c)_{T,p,N_w}$ from the experiment depends on that of $(\partial d/\partial m)_{T,p,N_w}$. Therefore, the validity of the ionic force field for \bar{V}_s depends on the slope of the density-molality figure (e.g. Figures 2.2 and 2.3) in the limit $m \rightarrow 0$. As shown in those figures, it is considered that the slopes of the solution densities with respect to m for CsF and CsI aqueous solutions are not in accord with the experimental data since the densities of those solutions are overestimated with increasing m . It is the reason for the large difference between \bar{V}_s^{sim} and \bar{V}_s^{exp} for CsF and CsI solutions.

It is found that the present calculation method of the KBI obtains the partial molar volume \bar{V}_s of electrolyte at the infinite dilution limit, and also obtains the individual partial molar volume of the ions, which is difficult to directly evaluate from experiments. It is expected that the discrepancies between \bar{V}_s^{sim} and \bar{V}_s^{exp} of CsF and CsI will be improved by redeveloping ionic force fields that more accurately represent the salt concentration dependence of the solution density, whereby the individual partial molar volume of the ions will be obtained with sufficient accuracy in the future.

V CONCLUSIONS

First, we have developed and validated the force field for five monovalent ions, scaling the charge to $q_{\text{scaled}} = \pm 0.75$ to take into account the electronic polarization effect of the solvent. The solution densities d at the molality of 1 mol/kg in all aqueous electrolyte solutions consisting of

Table 2.2: Partial molar volumes \bar{V}_+ , \bar{V}_- , and \bar{V}_s of cations, anions, and electrolytes at the infinite dilution limit of electrolytes, respectively. \bar{V}_s^{sim} are the results from MD calculations and \bar{V}_s^{exp} are experimental values.

Salt	\bar{V}_+ (cm ³ mol ⁻¹)	\bar{V}_- (cm ³ mol ⁻¹)	\bar{V}_s^{sim} (cm ³ mol ⁻¹)	\bar{V}_s^{exp} (cm ³ mol ⁻¹)
HCl	-10.6129	31.7371	21.1241	17.83
LiCl	-7.8459	32.0082	24.1623	16.95
NaF	-8.3499	1.6524	-6.6975	-2.37
NaCl	-8.5143	31.5899	23.0757	16.62
NaI	-7.5493	41.2588	33.7094	35.01
NaOH	-7.9885	5.4564	-2.5321	-5.25
CsF	6.0013	2.8153	8.8167	20.18
CsCl	6.4959	31.6772	38.1730	39.14
CsI	6.0048	41.5883	47.6363	57.56

this ionic force field and the TIP4P/2005 water are in good agreement with the experimental values, and these agreements extend to high salt concentrations except for CsF and CsI solutions. The densities of CsF and CsI solutions are overestimated at high salt concentrations, which are expected to be improved by redetermining individual ion-ion interactions instead of the combining rules in eq. 2.14. We also examined the temperature dependencies of d for HCl and NaOH solutions. The HCl solution reproduced the density very well, including the temperature of the density maximum, while for the NaOH solution, d deviated significantly from the experimental values at low temperatures, and there was no density maximum. One possible reason for this deviation is that the OH⁻ model has no charge on the H-site. Then, the problem of the temperature dependence of d is expected to be improved by dividing the charges into O and H sites as well as the OH⁻ force field proposed by Habibi et al[113].

Next, the Setschenow coefficient, which represents a measure of the salt addition effect on the gas solubility, for methane in a variety of aqueous model electrolyte solutions was compared with the experimental values. The ionic charge scaling force field of Koga (this work), ECCR, Madrid-2019, and Madrid-Transport were all found to be in better agreement with experimental values than the nonpolarizable force fields (JC and Bonthuis et al. models), which overestimate those by about 60%. In other words, this result indicates that the salt addition effect on the solubility of hydrophobic solutes is quantitatively evaluated by ion charge scaling to account for

the screening effect of solvent electronic polarization, despite being highly more tractable than polarizable force fields. Furthermore, the Madrid-2019 force field was the most consistent with the experimental values among these charge scaling force fields.

Then, the partial molar volumes \bar{V}_s of the electrolyte at the infinite dilution limit of salt were compared with the experimental values. We have even succeeded in determining the absolute partial molar volumes \bar{V}_+ and \bar{V}_- of cations and anions for each ion by a simple method. Most of \bar{V}_s agreed with the experimental values except for CsF and CsI, which were about $10 \text{ cm}^3/\text{mol}$ smaller than those. It is seen from eq. 2.16 that this result, including the discrepancy in CsF and CsI, depends on the reproducibility of the salt concentration dependence of the density at low salt concentrations. Focusing on the HCl solution, \bar{V}_s agrees well with the experimental data, but the partial molar volume of H^+ is $-10.6 \text{ cm}^3/\text{mol}$, which is smaller than the about $-6 \text{ cm}^3/\text{mol}$ reported in many earlier experimental studies. In other words, the koga and ECCR models reproduce \bar{V}_s well but do not guarantee to reproduce \bar{V}_+ and \bar{V}_- , the components of \bar{V}_s according to the first equality in Equation 2.12. The difference in \bar{V}_{H^+} of proton from the experimental value is attributed to the fact that the ionic LJ parameters of the Koga force field were determined so that the solution density reproduces the experimental value concerning the NaCl of the ECCR force field.

Finally, we propose that an ionic charge scaling force field will be developed that ameliorates the above problems by determining the ionic LJ parameters using the following procedure. (1) First, the LJ parameters of the ions, including NaCl, are determined such that the partial molar volume of the ions reproduces the experimental values at the infinite dilution limit of salt. This is because, at the infinite dilution, solely ion-water interactions are taken into considerations as salt species-dependent factors while the ion-ion correlations can be ignored. (2) Determine the ion-ion LJ parameters so that the solution density d agrees with the experimental data in the high salt concentration region.

Chapter 3

Microscopic Origins of Ion Size Dependences of Gas Solubility in Aqueous Electrolyte Solutions: Reversed Order of Sodium and Lithium Ions

Abstract

It is known that the magnitude of the salting-out effect of ions on hydrophobic solutes in aqueous solution depends on the ion species, and in general the smaller the ion size, the larger the effect. At low salt concentrations, the magnitude of the salting-out effect is determined by the hydrophobic solute and the salt. The magnitude of the salting-out effect of alkali metal ions on a common hydrophobic solute (experimental Sechenov coefficients [46]) is in the order $\text{Na}^+ > \text{K}^+ > \text{Cs}^+ \simeq \text{Li}^+$, with the smallest ion, Li^+ , deviating from the general trend. To clarify the cause of the reversed order in the cation series, we considered the Lennard-Jones (LJ) parameter σ of an ion as a continuous variable and varied its value (σ_+ or σ_-) for cation or anion in the range of 0.16 nm to 0.50 nm, and then performed molecular dynamics (MD) simulations of an aqueous electrolyte solution for each ion diameter. The study in this Chapter revealed that the ion size dependence of the magnitude of the salting-out effect in aqueous solutions of relatively small hydrophobic solutes such as methane is correlated with the ion size dependence of the packing

fraction η of the aqueous solution, as observed in earlier studies, and also correlated with those of the partial molar volume of an ion. Analyses of correlation function integrals, packing fractions of solvation spheres of different radii centered at an ion, and orientations of water molecules in the solvation spheres reveal the key differences in microscopic properties between the cation and anion series, which give rise to the reversed order in the cation series of the partial molar volumes of ions and ultimately that of the Setschenow coefficients. Furthermore, for analyzing cation-methane potentials of mean force in the cation series, it is found that the exceptional behavior of Li^+ for the Setschenow coefficients is caused by the water-cation potential at the distance contacting methane with the first solvation sphere of a cation. The cation size effect on the Setschenow coefficient for the amphiphilic solute (methanol) instead of methane was similarly examined.

I INTRODUCTION

Most of the water on our planet contains electrolytes. It has been extensively studied the salt addition effect on a variety of the physical properties of aqueous solution, such as the solution density[12, 13], partial molar volume[26, 34] surface tension[14, 151], viscosity[21], and gas solubility[17]. Many of the ion species dependences on those physical properties are common, and the order of the ions is called the Hofmeister series. The Hofmeister series was originally introduced as the ordering of ions in the magnitude of ion addition effects on protein aggregation[24]. Recently, it has been understood in experimental and computational studies that the Hofmeister series results from a complex interplay of the ion-water and ion-protein interactions in aqueous solution, thereby promoting a molecular-level understanding of the Hofmeister series,[152, 153, 8, 154], whereas the detailed mechanism remains unclear.

The addition of salt to water often enhances the hydrophobic effect, thereby further decreasing the solubilities of gases and hydrocarbons in water or making otherwise perfectly miscible components partially miscible. This phenomenon is called the salting-out: some ionic species induce the opposite effect, called the salting-in. Whether or not the salting-out or salting-in effect appears and its strength depends on the ion and solute species: Experimental data are reported for combinations of common ions and relatively simple solute species[42, 45, 126, 46, 127, 128]. Molecular theory has not yet been developed to understand the laws of the salting-out effect[53]. Since the hydrophobic and hydrophilic moieties of biologi-

cal molecules are the two major determinants of their solubility, the elucidation of independently ion-specific effects on each group should also provide a necessary basis to fully understand the Hofmeister series. In this chapter, we focus on the ion size effect on the solubility of small, nonpolar molecules, e.g., methane, in aqueous solution, which has been the subject of earlier theoretical studies[88, 155, 63, 89, 156, 157, 18] but remains not fully understood. In general, it is known that for a common solute and counter ion, the smaller the ion size, the larger the salting-out effect.

In 1889, Setschenow (Sechenov)[158] proposed and verified the relationship between the salt concentration and the solubility of a gas in aqueous electrolyte solution, which

$$\frac{\lambda}{\lambda_0} = e^{-K_s \rho_s} \quad (3.1)$$

in the present notation, where λ and λ_0 are the Ostwald absorption coefficients of the gas in aqueous solution and pure water, respectively, ρ_s is the number density of the electrolyte. K_s , which is called the Setschenow coefficient, is a measure of the salting-out/salting-in effect and depends on the salt and solute species: the positive value of k_{scc} indicates salting-out and negative that indicates and salting-in. Commonly used today is $k_{\text{scc}} = -(1/c_s) \log_{10} [\lambda/\lambda_0]$ with c_s the molar concentration of salt. The experimental data of k_{scc} for methane in aqueous solutions of alkali metal chlorides (LiCl, NaCl, KCl, RbCl, and CsCl) and sodium halides (NaF, NaCl, NaBr, and NaI) against the ionic radii of cations and anions, respectively, are shown in Figure 3.1. Then, the magnitude of k_{scc} of alkali metal ions with a common anion and solute is in the order $\text{Na}^+ > \text{K}^+ > \text{Rb}^+ > \text{Cs}^+ \simeq \text{Li}^+$, where it is noted that the smallest size ion, Li^+ , is deviated from the normal ordering of ion size. There are several explanations for the origin of the exceptional behavior of Li^+ or the nonmonotonic behavior of k_{scc} in the cation series including Li^+ [17, 89, 156, 157, 18]. It has been reported in earlier computational studies[89, 157, 159] that k_{scc} of electrolyte solutions are correlated with volumetric properties of the solutions such as the packing fractions, the partial molar volumes of the ions, or the volume contraction caused by electrostriction. In particular, Docherty et al.[89] pointed out similar ion size effects of k_{scc} and η for monovalent cations and anions, with exceptionally small values at the Li^+ size only for cations not for anions. In the present study, we revisit the question of the ion size effect on k_{scc} and examine the ion size dependences of k_{scc} via an investigation of the packing fraction and the microstructure of the ionic surroundings based on the theory of liquid mixtures and computer

simulation.

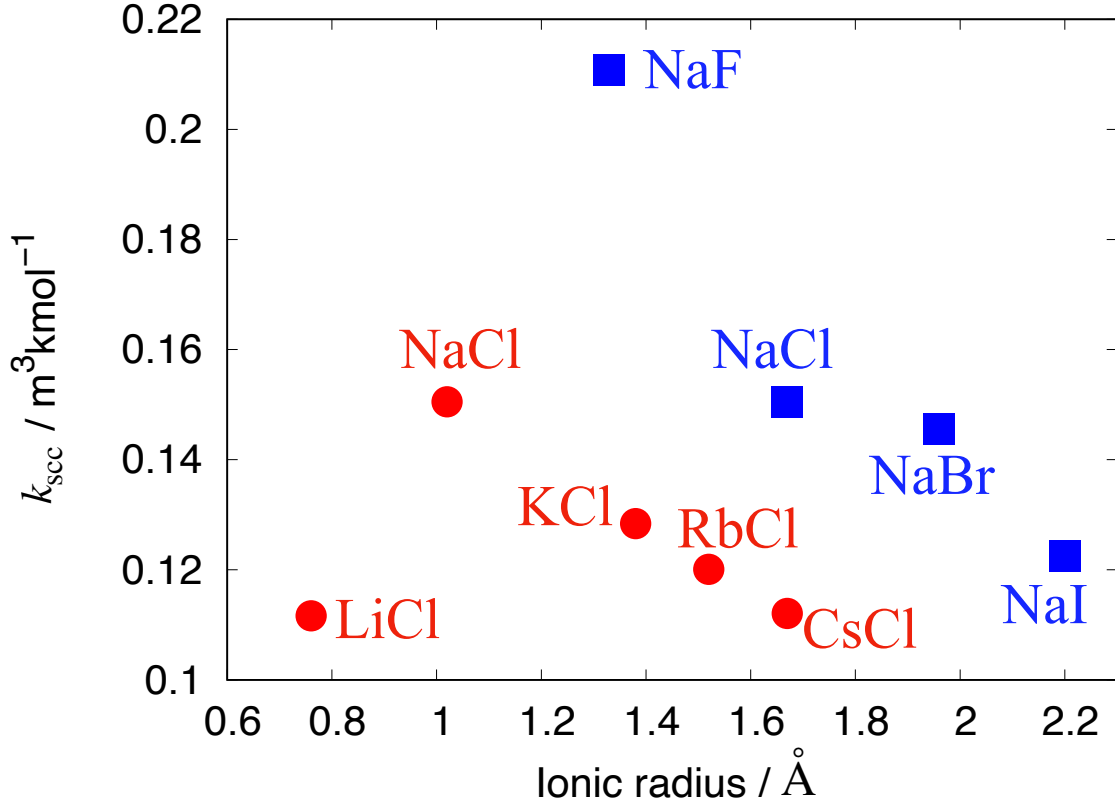


Figure 3.1: Setschenow coefficients k_{scc} for methane in aqueous solution of alkali halides. The caption in the figure indicates the electrolyte species: the experimental k_{scc} against the ionic radii of the alkali metal ions (red circles) and the halide ions (blue squares). The Setschenow coefficients and the ionic radii are taken from refs. [46] and [160], respectively.

II THEORETICAL BACKGROUND

We now consider a three-component aqueous solution consisting of w (water), s (salt $X_{\nu_+}Y_{\nu_-}$), and A (solute). Salt species $X_{\nu_+}Y_{\nu_-}$ dissociates into $\nu_+X^{z_+}$ and $\nu_-Y^{z_-}$ (z_i is the ion valence) in solution. It is discussed in Chapter 1 that the ionic effect on the solubility of a solute species in aqueous solution may be described by the theory of liquid mixtures or more specifically by fluctuation theory, and there is extensive literature on this subject[161, 55, 162]. We start with the ratio $\lambda_i = \rho_i/z_i$ of the number density to the activity z_i of species i . Here, z_i is defined as $z_i \rightarrow \rho_i$ in the ideal-gas limit for nondissociable species. For salt species $X_{\nu_+}Y_{\nu_-}$, z_i is defined such that $\rho_X^{\nu_+} \rho_Y^{\nu_-} = \nu_+^{\nu_+} \nu_-^{\nu_-} \rho^{\nu_++\nu_-}$ in the ideal gas limit. The solvation free energy μ_i^* (SFE) of a nondissociable solute in solution is then $\mu_i^* = -k_{\text{B}}T \ln \lambda_i$, with T the temperature and k_{B} the Boltzmann constant. When the solution is in equilibrium with its vapor, λ_i satisfies $\rho_i/z_i \simeq \rho_i/\rho_i^{\text{gas}}$, and corresponds to the Ostwald absorption coefficient which represents the

solubility of solute i .

The Setschenow coefficient is given by eq. 3.1 is the first-order approximation to an expansion of $\ln \lambda_A$ of solute in powers of the number density ρ_s of salt at fixed T and with some additional constraints:

$$\ln \lambda_A = \ln \lambda_A^0 - K_s \rho_s + \mathcal{O}(\rho_s) \quad (3.2)$$

with $\lambda_A^0 = \lim_{\rho_s \rightarrow 0} \lambda_A$. When the constraint is fixed p and fixed activity $z'_{w,s}$ for all species except water and salt,

$$K_s = - \lim_{\rho_s \rightarrow 0} \left(\frac{\partial \ln \lambda_A}{\partial \rho_s} \right)_{T,p,z'_{w,s}}, \quad (3.3)$$

where the constraint of fixing $z'_{w,s}$ means that the system is open for all molecular species except water and salt. We now consider solute A as a hydrophobic solute and suppose the solution is infinitely dilute in solute A, which is essentially the case for nonpolar solutes. Then the constraints on the variation in ρ_s are simply of fixed T and p , i.e.,

$$K_s = - \lim_{\rho_s \rightarrow 0} \left(\frac{\partial \ln \lambda_A}{\partial \rho_s} \right)_{T,p} = \lim_{\rho_s \rightarrow 0} \left(\frac{\partial \mu_A^*/k_B T}{\partial \rho_s} \right)_{T,p}. \quad (3.4)$$

As derived in section III of Chapter 1, the Setschenow coefficient is rewritten using the Kirkwood-Buff integral (KBI) G_{ij} as

$$K_s = (\nu_+ + \nu_-) (G_{Aw} - G_{As}) \quad (3.5)$$

$$G_{ij} = \int h_{ij}(r) d\mathbf{r}, \quad (3.6)$$

where $h_{ij}(r) = g_{ij}(r) - 1$ is the pair correlation function between molecular species i, j with $g_{ij}(r)$ the radial distribution function, and the solute-salt KBI G_{As} is given by averaging the solute-cation and solute-anion KBIs, G_{A+} and G_{A-} , respectively:

$$G_{As} = \frac{\nu_+ G_{A+} + \nu_- G_{A-}}{\nu_+ + \nu_-}. \quad (3.7)$$

Equation 3.5 implies that salting-out ($K_s > 0$) occurs when $G_{Aw} > G_{As}$, and vice versa. In the limit $\rho_A \rightarrow 0$, using 2.11, we obtain $G_{Aw} = -\bar{v}_A^*$ with the solvation volume $\bar{v}_A^* = \bar{v}_A - k_B T \chi_T$ of solute where \bar{v}_A is the partial molecular volume and χ_T is the isothermal compressibility. Then,

eq. 3.5 is rewritten by

$$K_s = -(\nu_+ + \nu_-)(\bar{v}_A^* + G_{As}). \quad (3.8)$$

\bar{v}_A^* is volume change of a solution when one molecule of solute is added at a fixed point in the system: for the solvation of hydrophobic solutes in water near room temperature, $\bar{v}_A^* \simeq \bar{v}_A > 0$. Therefore, the salting-out ($K_s > 0$) for hydrophobic solutes must be so negatively large that G_{As} makes $\bar{v}_A^* + G_{As} < 0$.

The charge neutrality condition requires $G_{w+} = G_{w-}$ in a macroscopic volume centered at a molecule of solute A[140]. In practice, however, when G_{A+} and G_{A-} are evaluated numerically from the corresponding correlation functions obtained by molecular simulation, they could be appreciably different for different ions. In particular, at the infinite dilution limit of ions, G_{A+} and G_{A-} would be ion-specific and, that is, given for each ion species.

From eq 3.8, it follows that the salt effect as measured by K_s for a common hydrophobic solute depends on G_{As} alone. So we will examine G_{As} , i.e., G_{A+} and G_{A-} , for various ions to understand the ion-specific effects of the solubility of hydrophobic solutes, especially the nonmonotonic behavior of K_s with the size of alkali metal ions. Ion-specific effects were examined through two routes as follows:

(1) It has been pointed out[17, 63, 89, 157] that the ion specificity of the Hofmeister effects for a hydrophobic solute including the salting-out or -in may be understood from how the structure of water is affected by ions, i.e., from structural properties of electrolyte aqueous solutions. This view is naturally inferred from the mean-field theory of liquid applied to hydrophobic hydration[163, 164]: the density or the packing fraction of the solution mainly determines the changes in the SFE with temperature, pressure, and salt concentration. Therefore, we shall examine the volumetric properties of salt solutions, i.e., the packing fractions and the partial molar volumes of salts (or $\bar{v}_s^* = -G_{ws}$) for model electrolyte aqueous solutions and the correlation between them and the ion specificity of the Setschenow coefficients K_s .

(2) From eqs. 3.7 and 3.8, given that the salt species dependences of K_s come only from G_{As} and the ion-specificity of G_{A+} and G_{A-} at the infinite dilution limit of salt, the ionic size effects on K_s of alkali metal ions for a common solute and anion, including the exceptional behavior of Li^+ , should be included in G_{A+} alone. Therefore, from ref. 3.5, we shall examine the cation size dependences of the solute-cation effective interaction, i.e., the potential of mean force (PMF) $w_{A+}(r)$, in aqueous solutions of electrolytes and hydrophobic solutes. The solute-cation PMF

represents the magnitude of the solute-cation potential at their distances r in aqueous solution and is given by

$$w_{A+}(r) \equiv -k_B T \ln g_{A+}(r). \quad (3.9)$$

III COMPUTATIONAL DETAILS

We performed NpT ensemble MD simulations using the program package GROMACS2018[141] to develop and validate a new charge scaling force field of several monovalent ions in the study of Chapter 3. All of the MD simulations were performed in a cubic cell system with three-dimensional periodic boundary conditions at 1 bar and a time step of 1 fs. We assumed the pairwise approximation where the total energy of the system was given by the sum of the potential energy between the particles in the system (eq. 2.1). The interaction between pairs of atoms was given by the sum of Lennard-Jones (LJ) and Coulomb potential. The Parrinello-Rahman method and the Nosé-Hoover method were used for pressure and temperature control, respectively. The duration of the production run ranges from 10 to 450 ns depending on structural properties to be calculated, after the equilibrium run of 5 ns. Configurations in the production run are sampled every 50 steps. First, we performed MD simulations for four kinds of model systems: pure water, aqueous solutions of salt, those of methane, and those of salt + solute (methane or propane). Each system contains 2000 water molecules. The aqueous salt solutions contain the additional 36 pairs of monovalent cations and anions to give a salt concentration of 1 mol/kg, and a methane solution contains 24 methane molecules. For the solutions of salt and methane, the same number of ions and methane as above are added to 2000 water molecules, while the solutions of salt and propane contain 4000 water molecules, 72 pairs of monovalent cations and anions, and 48 propane molecules. Second, we prepared 4000 water molecules and added one cation, anion, and methane. The position of the cation was fixed, the cation-methane distance was fixed to a variety of distances in the range of 0.3 nm to 1.5 nm, and the following two restrictions that prevented the anion from being close to the cation and methane: (1) the cation-anion and methane-anion LJ parameters set to $\sigma_{+-} = \sigma_{A-} = 1.5$ nm and $\epsilon_{+-} = \epsilon_{A+} = 0.517903$ kJ/mol. (2) the cation-anion Coulomb interaction is set to zero. Under similar restrictions, a solution with water + one methane molecule and solutions with water + one salt were prepared, and we performed MD simulations for 20 ns for each solution.

The potential function for the intermolecular interactions of water molecules is of TIP4P/2005[60].

The force field parameters of sodium and chloride ions (Na^+ and Cl^-), which are proposed by Jungwirth et. al., were chosen as the reference cation and anion[102, 103]: $\sigma_{\text{Na}^+} = 0.2115$ nm, $\epsilon_{\text{Na}^+} = 0.544284$ kJ/mol, $\sigma_{\text{Cl}^-} = 0.4100$ nm, and $\epsilon_{\text{Cl}^-} = 0.4928$ kJ/mol. The ion models belong to a family of recently developed force fields that effectively incorporate polarization effects of solvent by scaling ionic charges. It is suggested in Chapter 2 that the charge-scaling force fields with the TIP4P/2005 model water reproduces accurately experimental values of the solution density, and is more accurate in describing the salting-out effect of methane than the conventional nonpolarizable force field. The OPLS force field was used as a spherical monoatomic LJ particle model of methane[165, 142, 166]: $\sigma_{\text{A}}=0.373$ nm, $\epsilon_{\text{AA}}=1.2301$ kJ/mol. The monoatomic LJ particle model was also used for propane molecule; $\sigma_{\text{A}}=0.5637$ nm, $\epsilon_{\text{AA}}=2.0121$ kJ/mol[165, 167]. The LJ parameters between heterogeneous particles were basically determined by

$$\sigma_{12} = \sqrt{\sigma_1\sigma_2}, \quad \epsilon_{12} = \sqrt{\epsilon_1\epsilon_2}. \quad (3.10)$$

However, the methane-water LJ parameters were used $\sigma_{\text{Aw}} = 0.34445$ nm and $\epsilon_{\text{Aw}} = 1.043$ kJ/mol[143]. The methane-methane and interaction was replaced by the repulsive part of the Weeks-Anderson-Chandler (WCA) potential[144] to prevent solute aggregation. The original methane-methane radial distribution function $g_{\text{AA}}(r)$ is transformed from the methane-methane $g_{\text{AA}}^{\text{sim}}(r)$ obtained from the MD simulations using the WCA repulsive potential[145, 146]. The LJ potential part of all of the intermolecular pair potentials was truncated at 0.9 nm, and the long-range Coulomb part of those was calculated by the Ewald sum with the same cutoff distance as the LJ part in the real space. However, the cutoff distance was changed to 1.2 nm in the system with 4000 water molecules. The set of those model potentials reproduces accurately the density of pure water[60] and the solubility of methane in water[143] in a wide range of temperatures at 1 bar. In other words, the recently developed charge-scaled force field for Na^+ and Cl^- [102, 103] with the TIP4P/2005 water is more satisfactory in calculating the Setschenow coefficient of methane in aqueous NaCl solution than other common force fields.

We examined two series of model salts including the reference salt NaCl: one is the cation series in which only the LJ size parameters σ_+ of cations differ from each other while the anion is fixed to be Cl^- : the other is the anion series in which only anions' σ_- differ from each other while the cation is fixed to be Na^+ . All the LJ energy parameters ϵ_+ and ϵ_- for cations and anions are those of Na^+ and Cl^- , respectively. The force field parameters of the model ions are showed in Table 3.1: numbers followed by ionic species in the parentheses indicate that the

LJ size parameters are chosen to be those of the ions, and the LJ size parameters of the other model ions are hypothetical ones.

The effective hard sphere diameters d of the ions listed in Table 3.1 are as

$$d = 2r_c - \sigma_O, \quad (3.11)$$

where r_c is the smallest distance at which the ion-water radial distribution function becomes 1 and σ_O is the LJ size parameter for the oxygen site in the TIP4P/2005 model water. The effective diameters d for cations and anions will be used for the calculation of the packing fraction η of model electrolyte solutions defined by

$$\eta = \frac{\pi}{6} \sum_i \rho_i d_i^3, \quad (3.12)$$

where ρ_i is the number density of species i in the system and d_i is the effective particle diameter of that species, the sum being taken over all species.

The packing fraction η is evaluated by eq. 3.12 from MD calculations of aqueous electrolyte solutions. The solvation free energy μ_A^* of methane was calculated from the Widom test-particle insertion (TPI) method[147] to obtain the Setschenow coefficient. We performed MD simulations of pure water and aqueous salt solutions for 50 ns and inserted test particles 2×10^5 times into the equilibrium configuration at 50 fs intervals. K_s for methane was even evaluated from eq. 3.5. The KBIs G_{Aw} , G_{As} , and G_{ws} are evaluated from numerical integration of the corresponding pair correlation function. MD simulations of methane aqueous solution and salt + solute (methane or propane) aqueous solutions for 450 ns were performed to compute G_{Aw} , G_{As} and the solute-cation PMF $w_{A+}(r)$. MD simulations of salt aqueous solutions for 150ns were also performed to compute G_{ws} . Any $h_{ij}(r)$ obtained from MD simulation at a closed system does not converge to zero at large distances due to the finite-size effect. We shifted the entire $h_{ij}(r)$ so that the average of $h_{ij}(r)$ in a certain range at large distances becomes zero. Furthermore, we evaluated the KBI G_{ij} in the thermodynamic limit by applying the method proposed by Krüger et al. [148, 149] to the KBI obtained for the finite systems:

$$\begin{aligned} G_{ij}(L) &= \int_0^L 4\pi r^2 h_{ij}(r) \left[1 - \frac{3}{2} \left(\frac{r}{L} \right) + \frac{1}{2} \left(\frac{r}{L} \right)^3 \right] dr \\ G_{ij}(L) &= \frac{C}{L} + G_{ij} \quad (1/L \rightarrow 0), \end{aligned} \quad (3.13)$$

where L is the upper limit of the integral and C is a constant. Substituting corrected $h_{ij}(r)$ into the first line of eq. 3.13, $G_{ij}(L)$ are obtained as a function of L . Then, $G_{ij}(L)$ is plotted against $1/L$ and fitted linearly over the range of $1/L$ where a linear relationship holds in small $1/L$, and the intercept gives the KBI G_{ij} .

Table 3.1: Lennard-Jones size parameters σ_+ , σ_- and the effective diameters d for the cation and anion series of the model salts. Numbers followed by symbols of ionic species in the parentheses indicate that σ_+ or σ_- is of that ion species.

Cation series	1(Li ⁺)	2	3(Na ⁺)	4	5	6(K ⁺)
σ_+ (nm)	0.18	0.2	0.2115	0.225	0.24	0.28384
d (nm)	0.072	0.096	0.108	0.124	0.140	0.188
Cation series	7	8(Cs ⁺)	9			
σ_+ (nm)	0.33	0.360101	0.41			
d (nm)	0.232	0.264	0.308			
Anion series	1	2	3	4	5	6
σ_- (nm)	0.16	0.18	0.2115	0.24	0.27	0.30
d (nm)	0.0041	0.032	0.068	0.104	0.136	0.168
Anion series	7	8(F ⁻)	9(Cl ⁻)	10	11(I ⁻)	12
σ_- (nm)	0.33	0.3619368	0.41	0.44	0.468096	0.50
d (nm)	0.196	0.228	0.276	0.300	0.324	0.352

IV RESULTS AND DISCUSSION

Ion Size Dependences of K_s .

The Setschenow coefficients for methane obtained from MD calculations of model aqueous electrolyte solutions and their cation size effects were validated. Setschenow coefficients K_s are evaluated by two routes. One route is to use the linear approximation of eq. 3.4:

$$K_s = \lim_{\rho_s \rightarrow 0} \left(\frac{\partial \mu_A^*/k_B T}{\partial \rho_s} \right)_{T,p} \simeq \frac{\mu_A^* - \mu_{A,0}^*}{\rho_s k_B T}, \quad (3.14)$$

where μ_A^* and $\mu_{A,0}^*$ are the SFE of methane in salt solution and in pure water, respectively, at infinite dilution of methane: μ_A^* and $\mu_{A,0}^*$ were evaluated by applying the TPI to methane-free salt solutions and pure water. Another route is to use eq. 3.5 with G_{Aw} and G_{As} at infinite dilution of methane and salt. In this method, both G_{Aw} and G_{As} are evaluated from numerical

integrations of the pair correlation function obtained from MD simulations of aqueous solutions of methane and of methane and salt, respectively. We supposed that the KBIs obtained at low but finite concentrations of solute and salt were approximately equivalent to the KBIs in the limit of infinite dilution of those. Figure 3.2 shows the Setschenow coefficients k_{scc} (converted from K_{s}) for the cation series: plotted are two sets of numerical results, KBI and SFE routes, together with experimental data[46] for LiCl, NaCl, KCl, and CsCl aqueous solutions. It follows that the cation size dependences of k_{scc} calculated in two routes are in good agreement with each other, both giving the largest k_{scc} at σ_+ of Na^+ . The values of k_{scc} for NaCl (0.121 and 0.114 m^3/kmol) computed via eqs. 3.5 and 3.14 underestimate by 20 and 24%, respectively, the experimental value (0.1505 m^3/kmol). This result, as similarly reported in Chapter 2 and the earlier studies[88, 89], suggests that the charge-scaling force field of NaCl with the TIP4P/2005 model water is more accurate than conventional nonpolarizable force fields[96, 83] of NaCl in describing the salting-out effect for methane molecules in aqueous solutions. Here, we must consider the problem that the computed Setschenow coefficients in Figure 3.2 are systematically smaller than the experimental data in spite of the fact that the TIP4P/2005 water with the LJ methane accurately reproduces the solvation free energy of methane in an aqueous solution without ions[143]. herefore, the deviations would be attributed to the model potentials for the ion-water interactions, more specifically, the chloride ion-water interaction. It is however sufficient for the present models to investigate the reversed order of sodium and lithium ions in the salting-out effect.

From eqs. 3.5 and 3.8, the order $K_{\text{s}}(\text{LiCl}) < K_{\text{s}}(\text{NaCl})$ depends only on G_{As} and comes from the order $G_{\text{As}}(\text{NaCl}) < G_{\text{As}}(\text{LiCl})$. In other words, the order of G_{As} indicates the obvious fact that the more repulsive the solute-ion effective interactions are, the more strongly the solubility of the solute is reduced by the salt. The problem through this Chapter is then synonymous with why the methane-lithium effective interaction is less repulsive than the methane-sodium effective interaction.

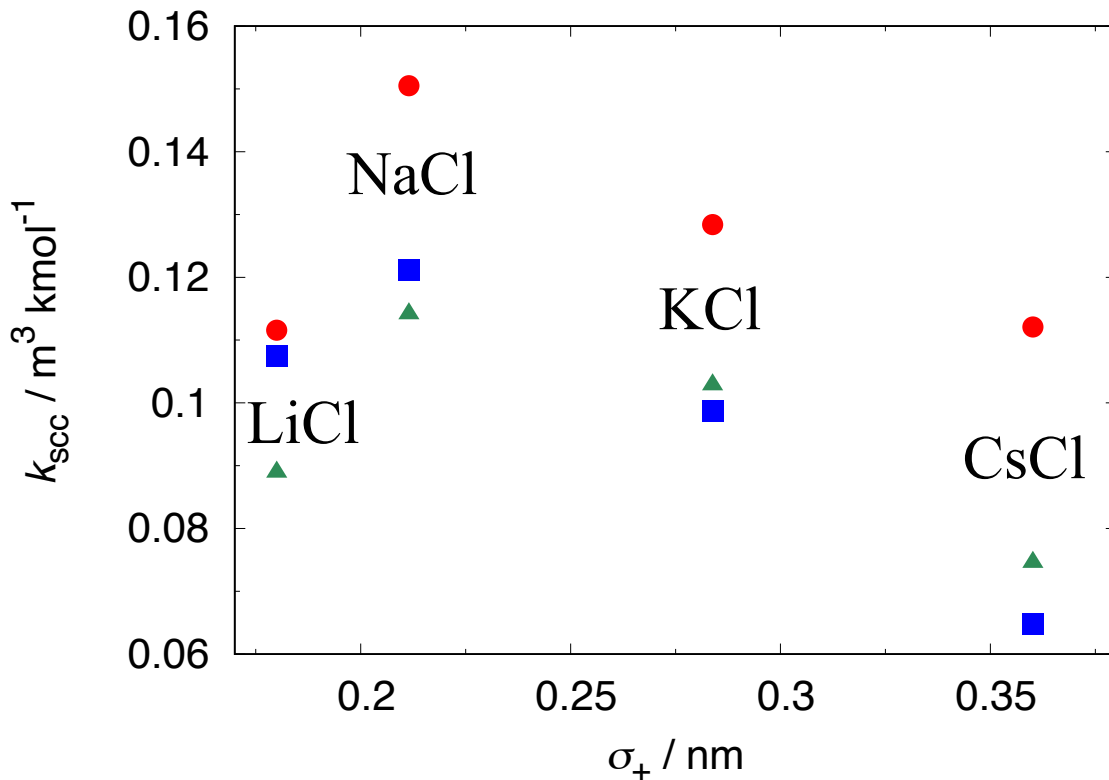


Figure 3.2: Setschenow coefficients k_{scc} calculated from two routes of the SFE in eq. 3.14 (green triangles) and the KBI in eq. 3.5 (blue squares) for aqueous solutions of four cation sizes. Experimental data for LiCl, NaCl, KCl, and CsCl aqueous solutions of methane are also plotted as a reference (red circles)

Correlation of the Setschenow Coefficient and the Packing Fraction of Solution with respect to Ion Size.

Docherty et al.[89] reported that the monovalent ion size dependence of K_s , including Li^+ , is similar to that of the packing fraction η defined in eq. 3.12. We examined the cation and anion size dependences of two properties, the SFE μ_A^* of methane in model electrolyte aqueous solutions and the packing fraction η of solutions without solute, over a wider range than they did. Figure 3.3 shows the cation size σ_+ dependences of μ_A^* and η in model electrolyte aqueous solutions, Figure 3.4 shows the anion size σ_- dependences of those in model electrolyte aqueous solutions. In the cation series, both μ_A^* and η are maximal at around the ion size of Na^+ and rather sharply decrease as σ_+ decreases to 0.18 nm, the value of Li^+ . In the anion series, μ_A^* monotonically increases with decreasing σ_- up to $\sigma_- \simeq 0.25$ nm and plateaus out at smaller σ_- , while η increases monotonically with a decrease in σ_- over the whole range. Note that σ_- of the smallest F^- is 0.36 nm so that both μ_A^* and η by halogen anions with the common cation Na^+ decrease monotonically with the anion size. The above results for the cation and anion series

are in agreement with those reported by Docherty et al[89].

It is known that the ion specificity in packing fractions η of electrolyte solutions is closely related to that in partial molar volumes of electrolytes since both reflect the degree of electrostriction. Mazzini et al.[27] thoroughly discussed the relation between ion-specific electrostriction and partial molar volumes of electrolytes in solvents. In the limit $\rho_s \rightarrow 0$, the partial molecular volume \bar{v}_s of an electrolyte in water is directly related to the water-salt KBI G_{ws} via eqs. 2.12 and 2.13: $\lim_{\rho_s \rightarrow 0} \bar{v}_s = (\nu_+ + \nu_-) (-G_{ws} + k_B T \chi_T^0)$ with χ_T^0 the isothermal compressibility of water. Here, $\lim_{\rho_s \rightarrow 0} \bar{v}_s \simeq -(\nu_+ + \nu_-) G_{ws}$ for most cases, e.g., $\bar{v}_s \simeq 17$ mol for NaCl and $k_B T \chi_T^0 \simeq 1.1$ mol for pure water at 298 K and 1 bar[26]. Furthermore, from eq. 2.12, the ion specificity of \bar{v}_s depends only on G_{ws} . Thus, the correlation between η and \bar{v}_s is synonymous with that between η and G_{ws} , especially for the ion species dependence. Figure 3.5 shows the correlation between η and G_{ws} for solutions of six model electrolyte (LiCl, NaF, NaCl, NaI, KCl, and CsCl). It is seen that a near-linear correlation between η and G_{ws} . Based on the above results, we attempt to elucidate the ion size effect on the salting-out by analyzing the microscopic structure around ions for the volumetric properties of solutions without solute, more specifically η and G_{ws} .

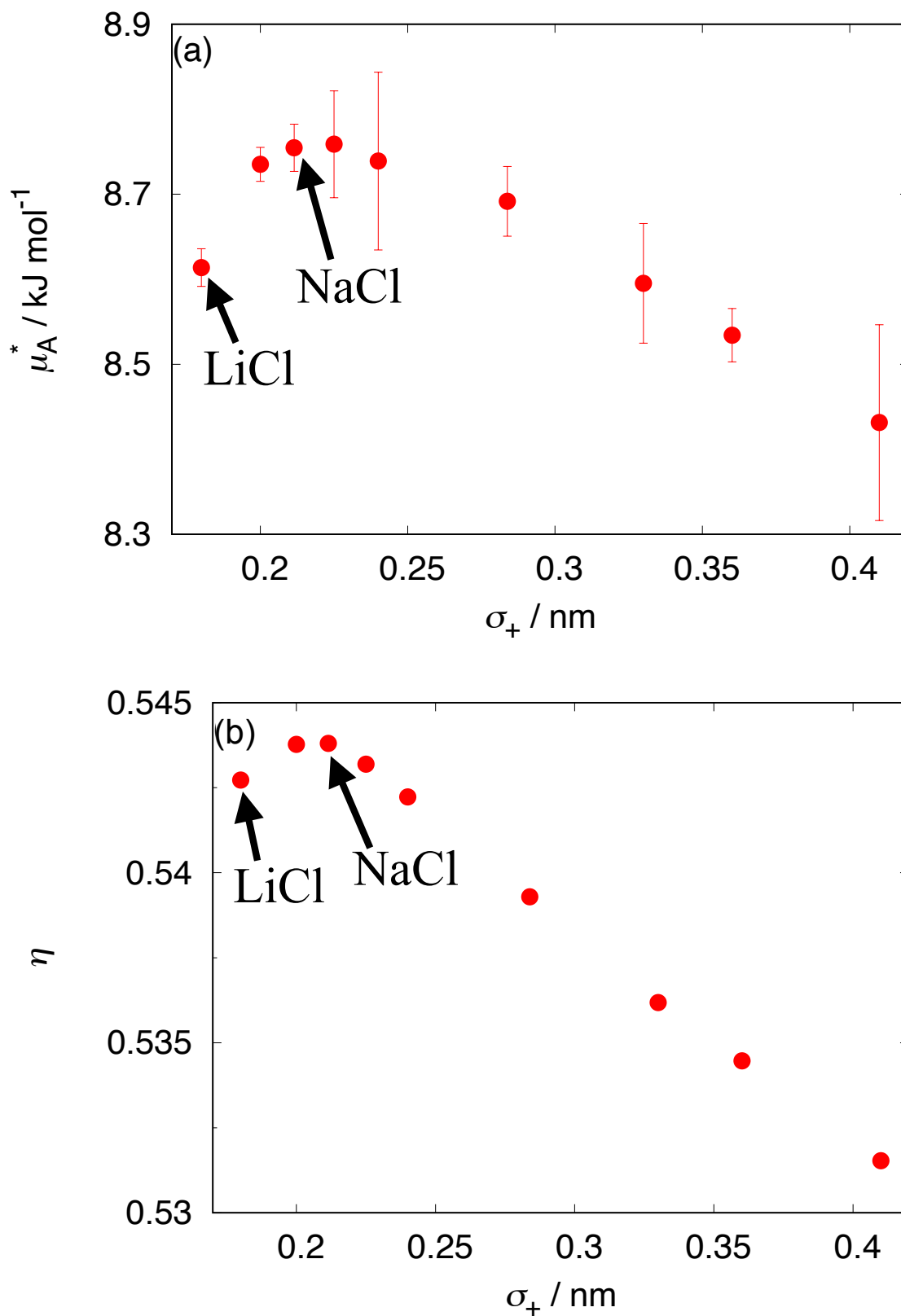


Figure 3.3: Cation size σ_+ dependences on (a) the solvation free energy μ_A^* of methane and (b) the packing fraction η in electrolyte solutions: cation series in Table 3.1 with the common anion Cl^- .

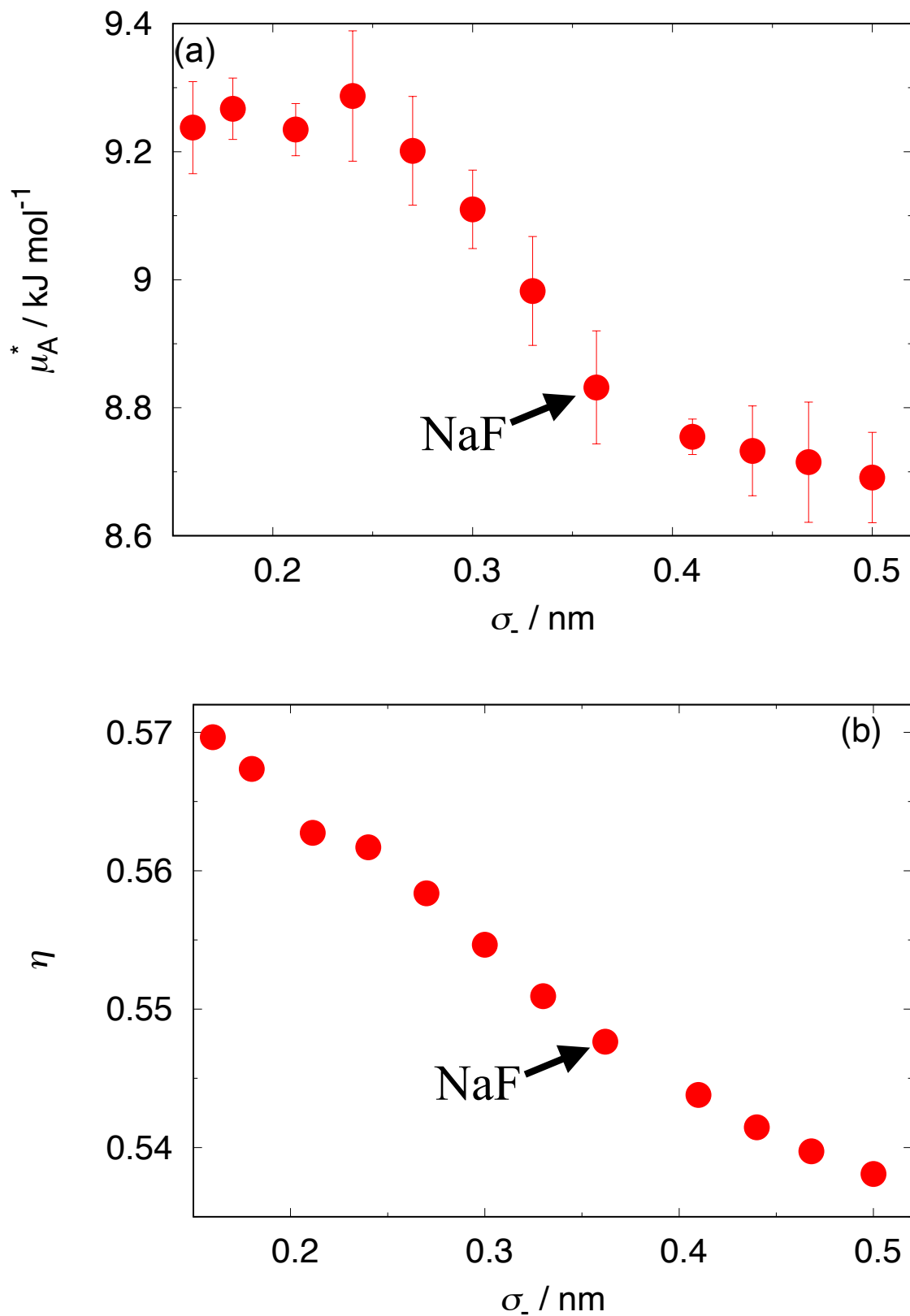


Figure 3.4: Anion size σ_- dependences on (a) the solvation free energy μ_A^* of methane and (b) the packing fraction η in electrolyte solutions: anion series in Table 3.1 with the common anion Na^+ .

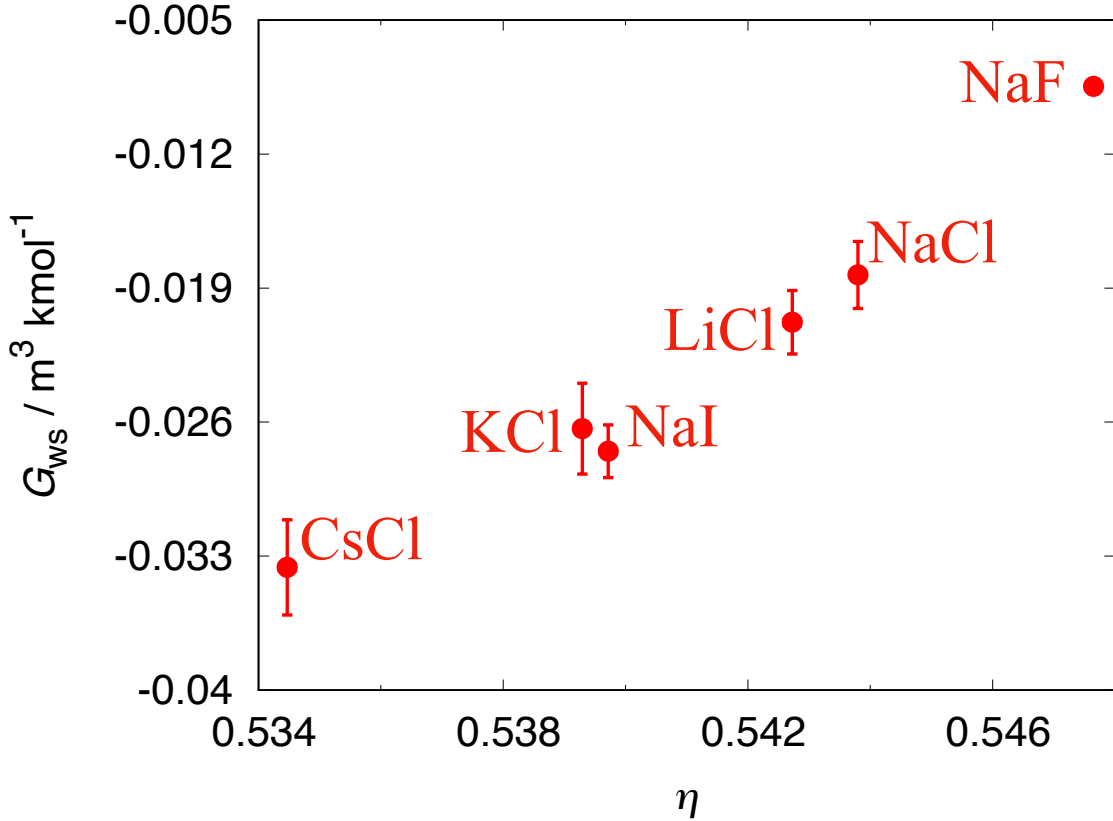


Figure 3.5: η vs G_{ws} computed in six model electrolyte solutions from the ion series in Table 3.1.

Microscopic Origins of the Ion Size Dependences of η and \bar{v}_s .

Ion pairings and cluster formation of ions in some aqueous solutions have been directly investigated in computer simulations[168, 169, 170, 100] and have been studied by experiment[171, 172]. Thomas and Elcock[156] stated that the formation of ion strings in simulated LiCl aqueous solutions may cause the exceptional behavior of lithium salts. In other words, a possible microscopic mechanism of the nonmonotonic cation size dependences of η and \bar{v}_s in cation series with a common anion species is that as the cation size decreases, the tendency to form clusters or strings of ions increases, thereby reducing the degree of electrostriction. In the snapshots of our MD simulations, we observe some associations of ions in the case of cation of the lithium-ion size. To investigate the effect of ion association on the ion size dependence of properties of aqueous solution, we performed additional MD simulations in which the cation-anion LJ size parameters are deliberately set as large as 0.6 nm to fully hydrate each ion and prevent formations of ion clusters. This setting is similar, in practice, to the constraint used by Thomas and Elcock[156].

Figure 3.6 shows the results for the system with ion associations suppressed together with

original results in Figure 3.3. It follows in Figure 3.6a that the cation size dependence of η for the system with no ion associations is virtually the same as that for the original system. Thus, the fact of decreasing η and increasing \bar{v}_s with decreasing cation size from that of Na+ is not due to ionic association. As shown in Figure 3.6b, the solvation free energy μ_A^* of methane in the model electrolyte solutions with no ion association is maximal at a cation size close to sodium ion as it is in the solutions with no constraint, which is the same result as for η . Therefore, we argue that the anomalous behavior of lithium salts regarding the salting-out effect should be explained not regarding to formation of ion clusters.

On the other method, we examine the following integrals of following the ion–water pair correlation functions $h_{w\pm}(r)$ as a function of the upper limit R of the integral to reveal the microscopic mechanisms of the anomalous ion size dependences of the packing fraction η of the solution and the partial molecular volume \bar{v}_s of salt for the cation series:

$$G_{w\pm}(R) = 4\pi \int_0^R h_{w\pm}(r) r^2 dr, \quad (3.15)$$

where w is water, + is cation, and – is anion in the subscripts. From eqs. 2.12 and 3.15, for solutions with infinitely dilute ions, $-G_{w\pm}(R)$ is the contribution to the partial molecular volume \bar{v}_s of salt via the solvation volume $\bar{v}_{\pm}^* = \bar{v}_{\pm} - k_B T \chi_T$ of cation or anion from the sphere of radius R , centered at a cation or an anion.

Figure 3.7a shows $G_{w+}(R)$ for selected four cation sizes with $h_{w+}(r)$ the pair correlation functions between oxygen and ion species. It can be seen that the orders of $G_{w+}(R)$ at the second maxima, at the third minima, and at the following extrema are the same as the order of G_{w+} , i.e., $G_{w+}(R)$ in the limit $R \rightarrow \infty$. This result indicates that the origin of the exceptional behaviors of \bar{v}_s and η for the cation series should be included in the spherical solvation volume of that radius ~ 0.5 nm around each cation. Figure 3.7b shows the first maximum and the second minimum of $G_{w+}(R)$ against the cation size σ_+ . The decrease of the first maximum and the increase of the second minimum are seen with respect to the increase of σ_+ . This means that cation size has two opposing effects on the density of water: the water density in the first hydration shell increases as σ_+ decreases, whereas that in the volume of a spherical shell adjacent to the first shell decreases with decreasing σ_+ . These opposing behaviors of the two regions cause the minimum for partial molecular volume and the maximum for packing fraction at the cation size close to that of Na⁺. Figure 3.8 shows $G_{w-}(R)$ for selected anion sizes and the first maximum and the second minimum of $G_{w-}(R)$ against the anion size σ_- . In

Figure 3.8a, the order of $G_{w-}(R)$ at any common extremum is the same as the order of \bar{v}_s for the three anions whose size is F^- , Cl^- , and I^- , and actually that is true for all of the anions in the anion series. Figure 3.8b shows that both the first maximum and the second minimum decrease monotonically with decreasing σ_- , which explains the regular behaviors of \bar{v}_s and η for the anion series.

We have found that the spherical solvation volume of radius ~ 0.5 nm around each cation basically determines the exceptional behavior of \bar{v}_s for the cation series. As with \bar{v}_s , for the packing fraction η of electrolyte solutions, we consider the packing fraction around each cation that contributes to \bar{v}_s . To confirm this, we define the solvation packing fraction $\eta(R)$ to be the packing fraction in the spherical region of radius R centered at a solvated ion. We calculate $\eta(R)$ using the radial distribution functions $g_{ci}(r)$ between pairs of the central ion c and molecular species i ($= w, +$, and $-$):

$$\eta(R) = \frac{\pi}{2R^3} \sum_i \rho_i d_i^3 \int_0^\infty f(r; R, d_i/2) g_{ci}(r) r^2 dr + \left(\frac{d_c}{2R}\right), \quad (R > d_c/2) \quad (3.16)$$

where $\eta(R)$ is the fraction of the volume of intersection of two spheres of radii R and $d_i/2$ with the center-center distance r to the volume of the sphere of radius $d_i/2$: $d_c/2$ is the effective hard-sphere diameter of the central ion. We have calculated $\eta(R_1)$, $\eta(R_2)$, and $\eta(R_3)$ for the first, second, and third solvation spheres of radii R_n ($n = 1, 2, 3$), respectively. Here, R_n is taken to be the distance of the n th local minimum of the ion-water (oxygen) radial distribution function.

Figure 3.9 shows the packing fractions of the system and the solvation packing fractions around each cation against the cation sizes σ_+ and those around each anion against the anion sizes σ_- . In the cation series (Figure 3.9a), $\eta(R_1)$ increases monotonically with decreasing σ_+ , so that for the first solvation shell, the smaller the cation, the larger the degree of electrostriction. However, both $\eta(R_2)$ and $\eta(R_3)$ for the second and third solvation spheres exhibit a maximum around the size of Na^+ , indicating that the exceptional behavior of η of the electrolyte solutions in the cation series is manifested in the cation-centered second solvation sphere. In the anion series (Figure 3.9b), all solvation packing fractions of $\eta(R_1)$, $\eta(R_2)$, and $\eta(R_3)$ increase with decreasing σ_- as does η , and the smaller the solvation sphere, the larger the rate of change in $\eta(R_n)$ with σ_- . There is no exceptional behavior in any solvation spheres in the anion series. We have found that the spherical solvation packing fraction in the second hydration shell around each cation or each anion determines the order of ion size effect on η for both the cation series,

including the exceptional behavior Li^+ size, and anion series.

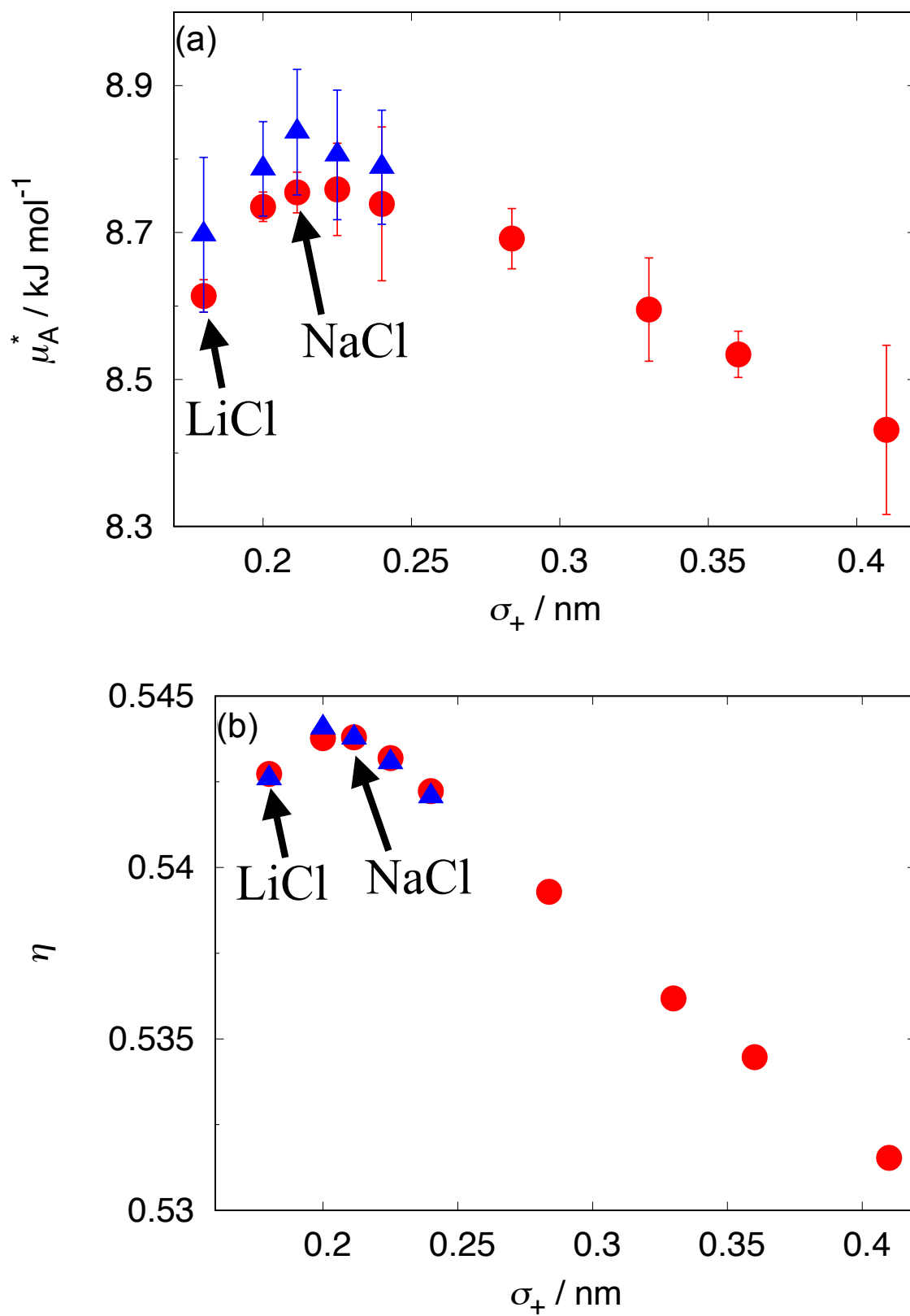


Figure 3.6: Cation size dependences on (a) the solvation free energy μ_A^* of methane and (b) the packing fraction η in electrolyte solutions with ion associations suppressed (blue triangles) and those with no constraint (red circles).

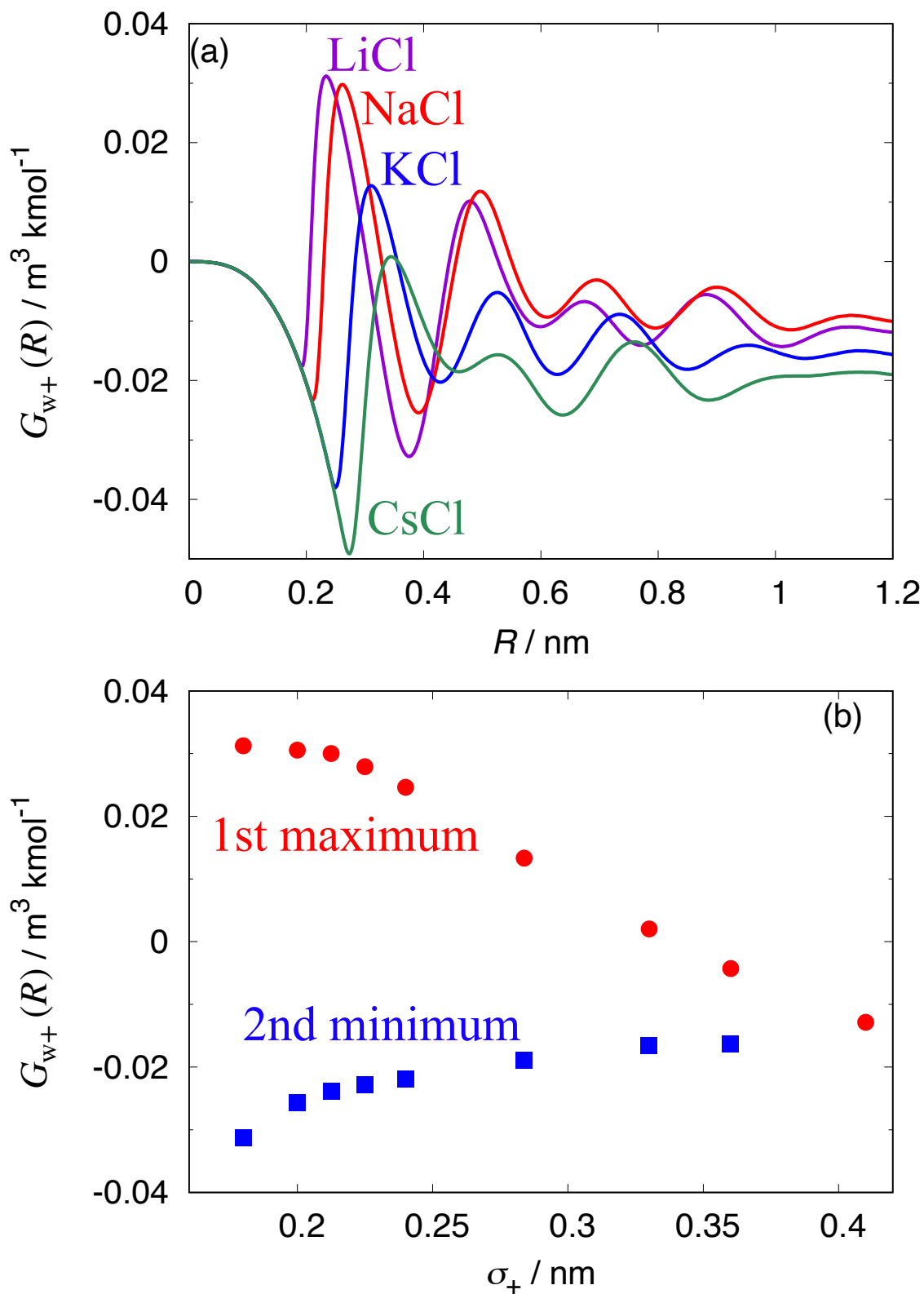


Figure 3.7: (a) The water-cation $G_{w+}(R)$ for four cation sizes, Li^+ , Na^+ , K^+ , and Cs^+ in the cation series. (b) Cation size σ_+ dependences on the first maximum (red circles) and second minimum (blue squares) of $G_{w+}(R)$ in the cation series.

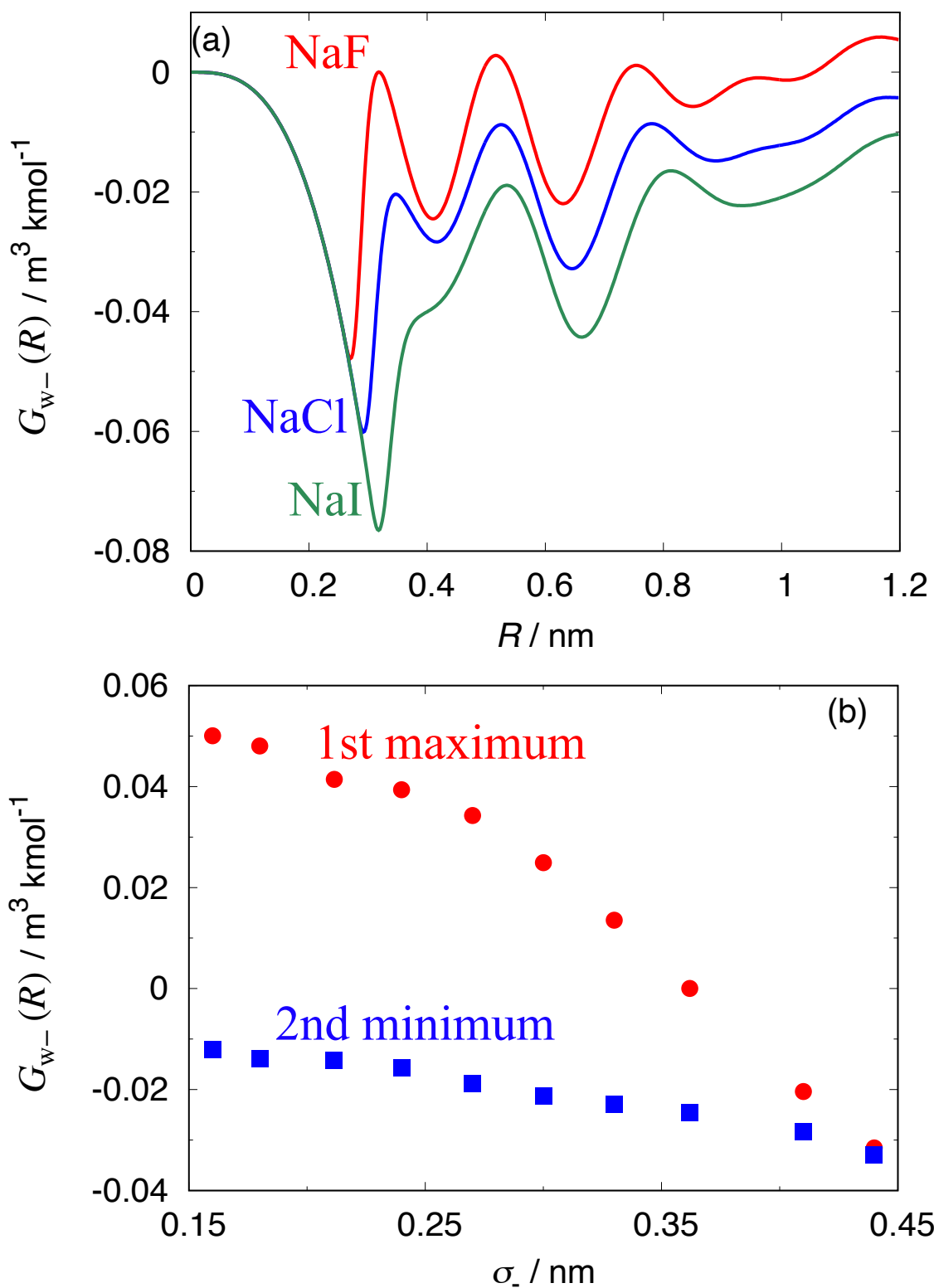


Figure 3.8: (a) The water-anion $G_{w-}(R)$ for three anion sizes, F^- , Cl^- , and I^- in the anion series. (b) Anion size σ_- dependences on the first maximum (red circles) and second minimum (blue squares) of $G_{w-}(R)$ in the anion series.

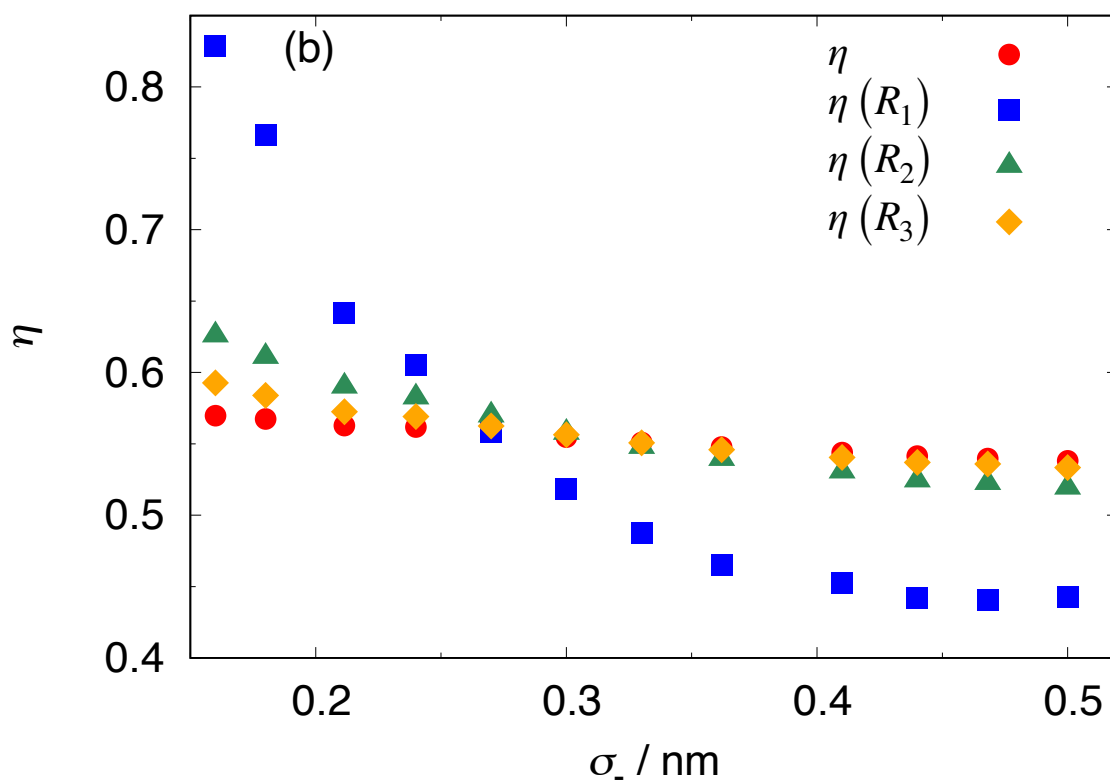
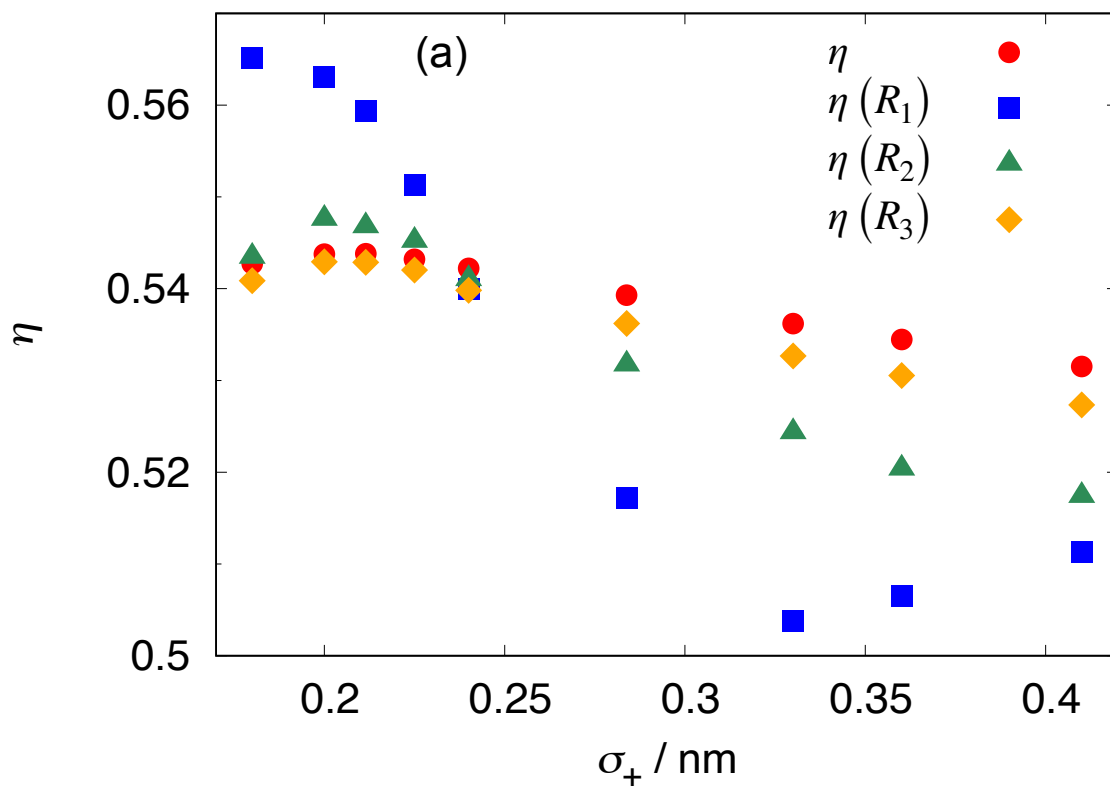


Figure 3.9: (a) Cation size σ_+ dependences in the cation series and (b) anion size σ_- dependences in the anion series of the solvation packing fractions $\eta(R_n)$ for the first, second, and third solvation spheres of radii R_n ($n = 1, 2, 3$) and the bulk packing fraction η .

Molecular Orientation and Packing in Solvation Spheres around an Ion.

Considering the fact that the ion size dependences of \bar{v}_s and η are monotonic in the anion series and nonmonotonic in the cation series, microscopic origins of that difference must be sought for in the molecular orientations of water relative to a central cation and anion. Here, we define the angle θ between the dipole moment of H_2O and the vector from the oxygen atom to a central ion as shown in Figure 3.10, and the orientations $\cos\theta$ of water molecular dipoles around ions are examined.

Figure 3.11 displays distributions of the average orientation $\langle\cos\theta\rangle$ of water molecules in the first solvation shells of cations in the selected cation series and of anions in the selected anion series. In the cation series (Figure 3.11a), the peak position of the distribution shifts significantly toward more negative values as the cation size decreases, whereas in the anion series (Figure 3.11b), the peak position shifts only slightly toward more positive values as σ_- decreases. The difference between the cation size dependence of the distributions of $\langle\cos\theta\rangle$ and the anion size dependence of those may be explained as follows: Water molecules in the first solvation shell around cations tend to orient to face their oxygen atoms toward cations, and this tendency increases continuously as the cation size decreases to Li^+ . By contrast, one OH group from each H_2O around an anion is more or less fixed in a state where the O–H and the anion are aligned straight, thereby the peak position of the $\langle\cos\theta\rangle$ distribution is only weakly dependent on the anion size.

We next calculated the conditional solvation packing fraction $\eta_{R_2}(\langle\cos\theta\rangle)$ in the second solvation shells, which is the packing fraction around each ion averaged over the simulated configurations giving a prescribed value of $\langle\cos\theta\rangle$. Figure 3.12 shows $\eta_{R_2}(\langle\cos\theta\rangle)$ of the selected cation sizes (Figure 3.12a) and the selected anion sizes (Figure 3.12b). The function $\eta_{R_2}(\langle\cos\theta\rangle)$ for each cation in the cation series depends significantly on $\langle\cos\theta\rangle$ with a maximum at some value of $\langle\cos\theta\rangle < 0$. In particular, $\eta_{R_2}(\langle\cos\theta\rangle)$ for cation sizes of Li^+ and Na^+ are very similar to each other and both decrease sharply as $\langle\cos\theta\rangle$ approach -1 , i.e., as all of the water molecules in the first solvation shell tend to orient their oxygen atoms toward a central cation. Considering this result together with the results obtained in Figure 3.11, the peak position of the distribution of $\langle\cos\theta\rangle$ of Li^+ is closer to -1 than that of Na^+ so that the solvation packing fraction $\eta(R_2)$ is lower around Li^+ than around Na^+ . Since the order of η for the cation series is determined by that of $\eta(R_2)$ according to Figure 3.9, the above result concerning Figures 3.11a and 3.12a

seems to be the microscopic origin of the nonmonotonic ion size dependences of η and \bar{v}_s for the cation series. On the other hand, $\eta_{R_2}(\langle \cos \theta \rangle)$ for each anion in the anion series has no strong dependence on $\langle \cos \theta \rangle$, and the smaller the ion size, the larger $\eta_{R_2}(\langle \cos \theta \rangle)$ (Figure 3.12b), so that one observes simple, monotonic ion size dependences of η and \bar{v}_s for the anion series.

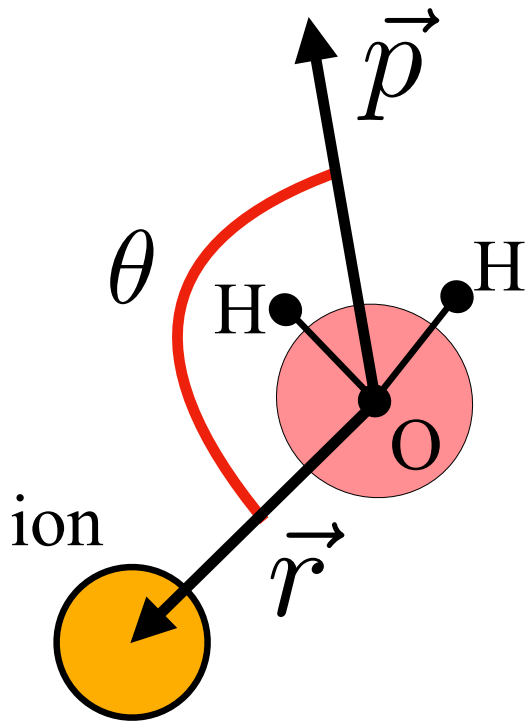


Figure 3.10: Definition of angle θ between the dipole vector \vec{p} of a water molecule and the vector \vec{r} from water to ion.

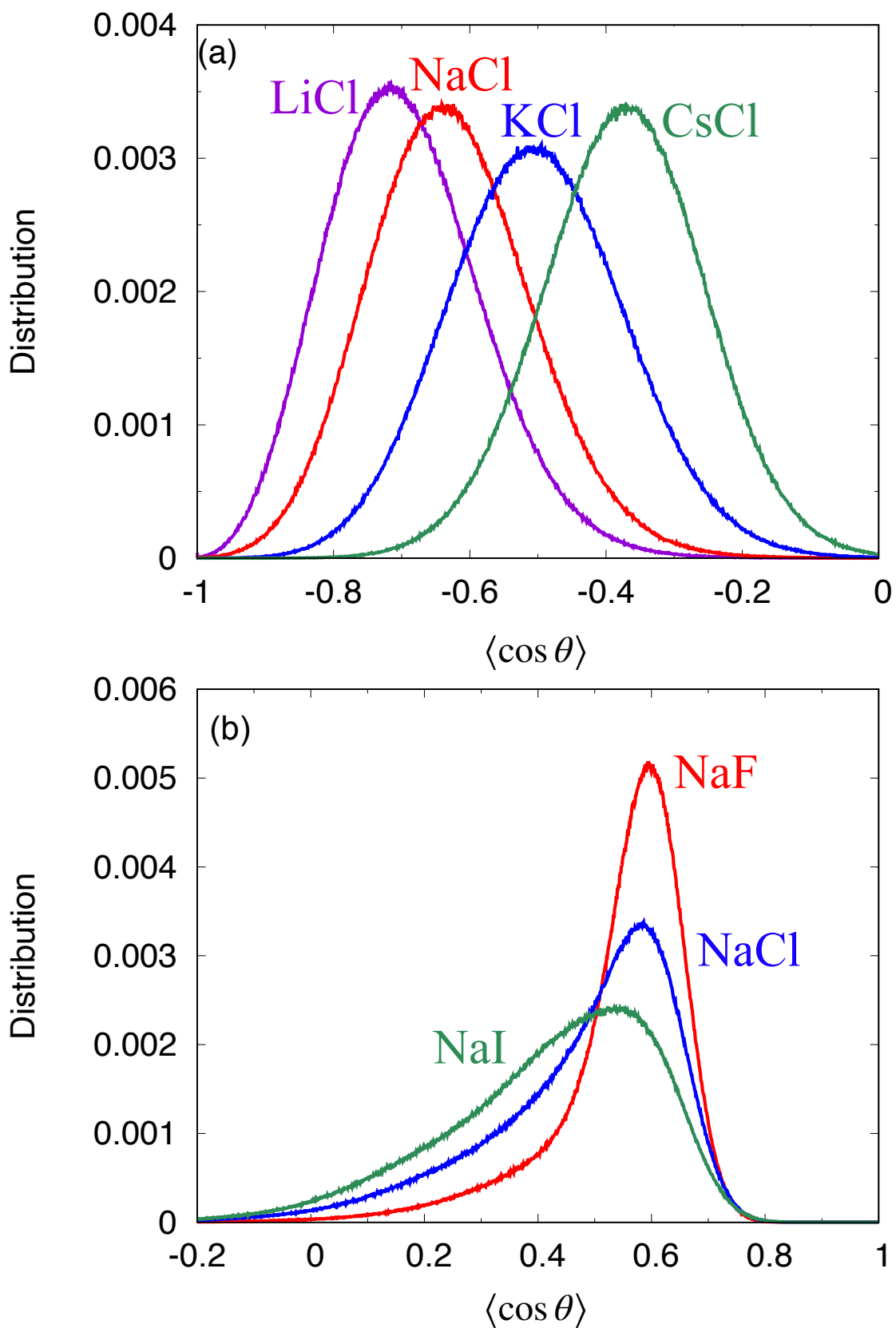


Figure 3.11: Distributions of $\langle \cos \theta \rangle$ for water molecules in the first solvation shell around each (a) cation and (b) anion.

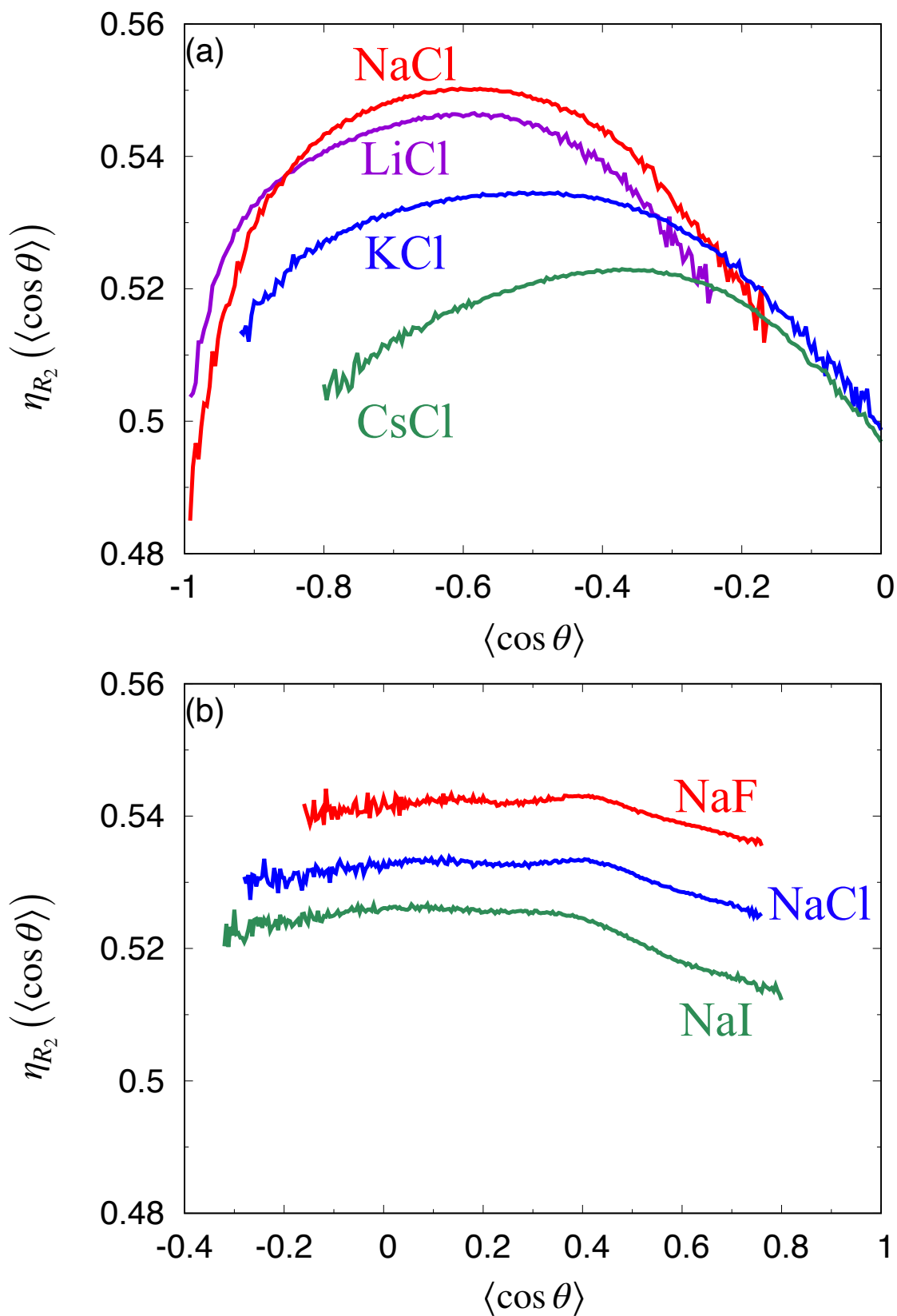


Figure 3.12: Conditional solvation packing fractions $\eta_{R_2}(\langle \cos \theta \rangle)$ in the second solvation shells around the cations and anions, as a functions of $\langle \cos \theta \rangle$.

Relation between G_{As} and G_{ws} .

As observed in earlier studies[89, 157] and shown in the present work for the cation and anion series (Figures 3.3 and 3.4), the Setschenow coefficients K_s or the solvation free energies μ_A^* of a hydrophobic solute such as methane molecule in electrolyte aqueous solutions are correlated with the packing fractions η or the partial molecular volumes \bar{v}_s of salts in those solutions. It is by no means trivial since it is a correlation observed between a property of aqueous solutions of salts alone (η and \bar{v}_s) and the one concerning both salts and solutes (the Setschenow coefficient K_s). Therefore, in terms of the Kirkwood–Buff integrals, from eqs. 3.5 and 2.12, there must be some correlation between G_{As} and G_{ws} because the ordering of ions in K_s is due to that of G_{As} and the ordering in η (or \bar{v}_s) comes from G_{ws} . Figure 3.13 shows the correlation G_{As} and G_{ws} for the selected salt aqueous solutions in the cation and anion series. As expected, there is a strong correlation between G_{As} and G_{ws} : a linear fit to the data gives $G_{As} = -6.4G_{ws} - 0.45$.

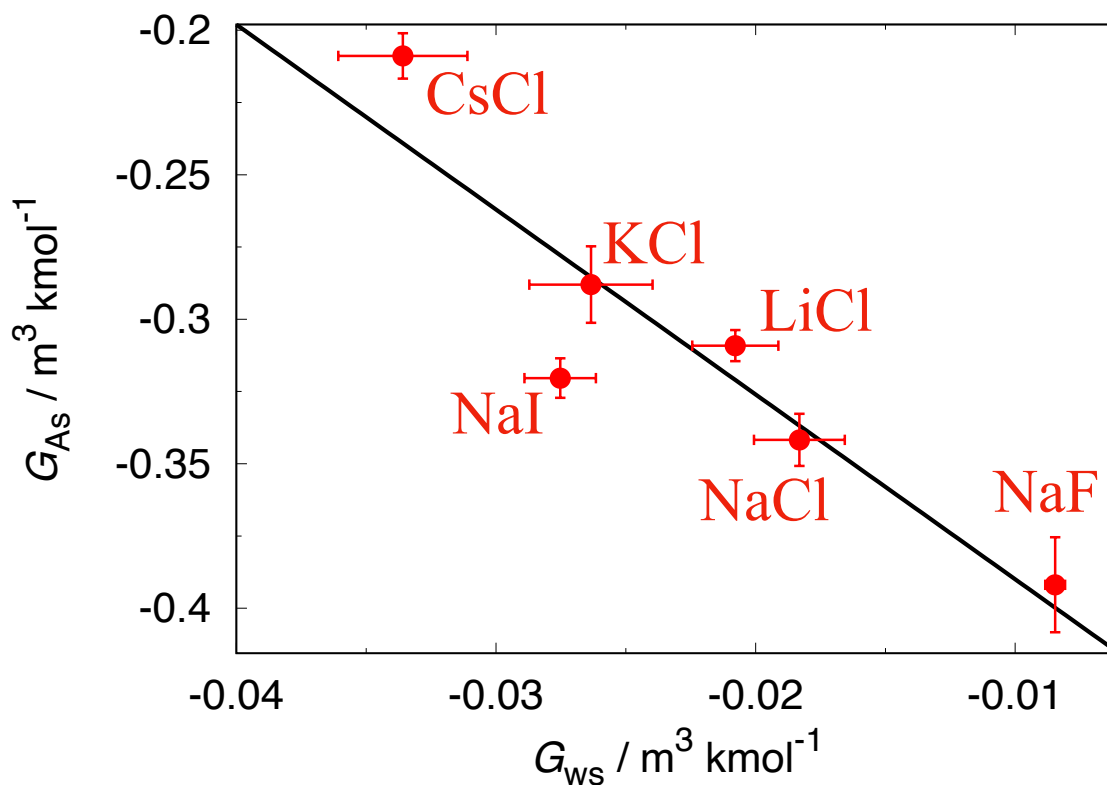


Figure 3.13: Correlation between G_{As} and G_{ws} for model salts in Table 3.1, and their linear fitting (black line).

Cation Size Effect on $w_{A+}(r)$.

In the present work, we have connected the ion size effect on the salting-out for hydrophobic solutes, including the exceptional behavior of Li^+ , with that on the volumetric properties of

aqueous salt solutions (the packing fraction η and the partial molecular volume \bar{v}_s of salt), and by observing η and \bar{v}_s , we have found that the microscopic origin for the exceptional ion size effect on the Setschenow coefficients K_s of Li^+ lies in the orientation of water molecules solvated to ions. However, the mechanism has not yet been clarified. Then, we now focus on G_{As} , which essentially determines the ionic specificity of K_s in eq. 3.5. At the infinite dilution of solute and salt, $G_{\text{A}+}$ and $G_{\text{A}-}$ are given independently of each other, which means the cation specificity of G_{As} is contained in $G_{\text{A}+}$ alone. Therefore, to understand the cation size effect of $G_{\text{A}+}$, the solute-cation potentials of mean force $w_{\text{A}+}(r)$ defined in eq. 3.9 are examined.

Figure 3.14 shows the methane-cation and propane-cation PMFs $w_{\text{A}+}(r)$ for salt aqueous solutions in the selected cation series. As shown in Figure 3.14(a), in the case of K^+ and Cs^+ , $w_{\text{A}+}(r)$ has the minimum at the contact distance between methane and cation, and the minimum for Cs^+ is lower than that for K^+ , which has a smaller cation. In the case of Na^+ , however, the minimum does not appear at the distance where the cation is in contact with the methane, and a shoulder appears slightly to the outside of it. For even smaller Li^+ , $w_{\text{A}+}(r)$ has a low minimum at a similar distance to the shoulder for Na^+ . As shown in Figure 3.14(b), the distances r at which a maximum and minimum appear in the propane-cation PMFs are in good agreement with those in the methane-cation PMFs which are shifted by +0.095 nm. The difference of 0.095 nm corresponds to that between the radii of methane ($\sigma_{\text{AA}}/2 = 0.1865$ nm) and propane ($\sigma_{\text{AA}}/2 = 0.2819$ nm). Therefore, the first minimum for Li^+ appears at the distance that a solute molecule is adjacent to water in close proximity to cations, indicating that the solute is relatively stable at that distance, e.g., $r = 0.45$ nm for methane. It is due to that minimum that the K_s of Li^+ is smaller than that of Na^+ , i.e., the G_{As} of Li^+ is larger than that of Na^+ .

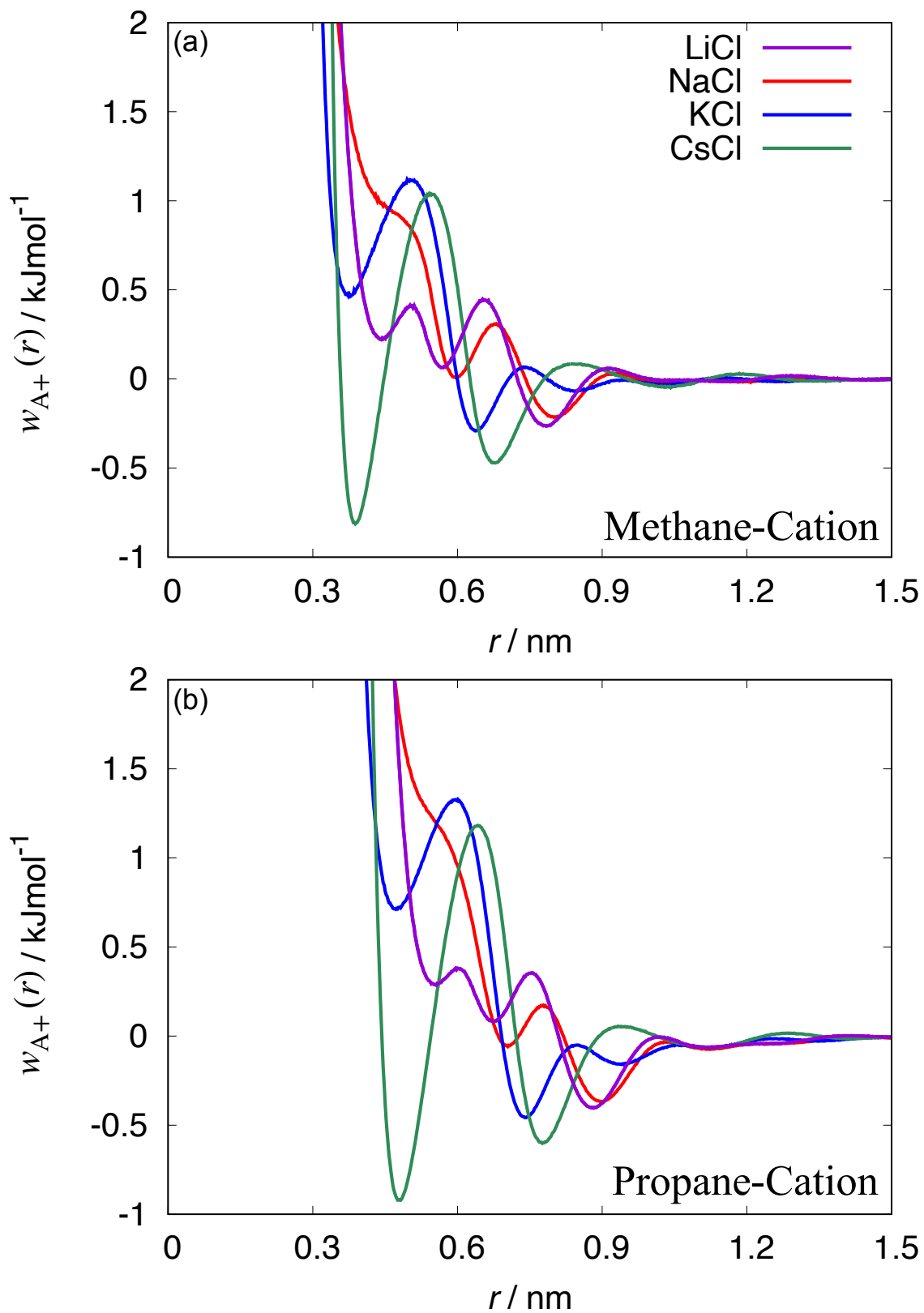


Figure 3.14: The potential of mean forces $w_{A^+}(r)$ (a) between methane and cation and (b) between propane and cation for four cation sizes, Li^+ , Na^+ , K^+ , and Cs^+ in the cation series.

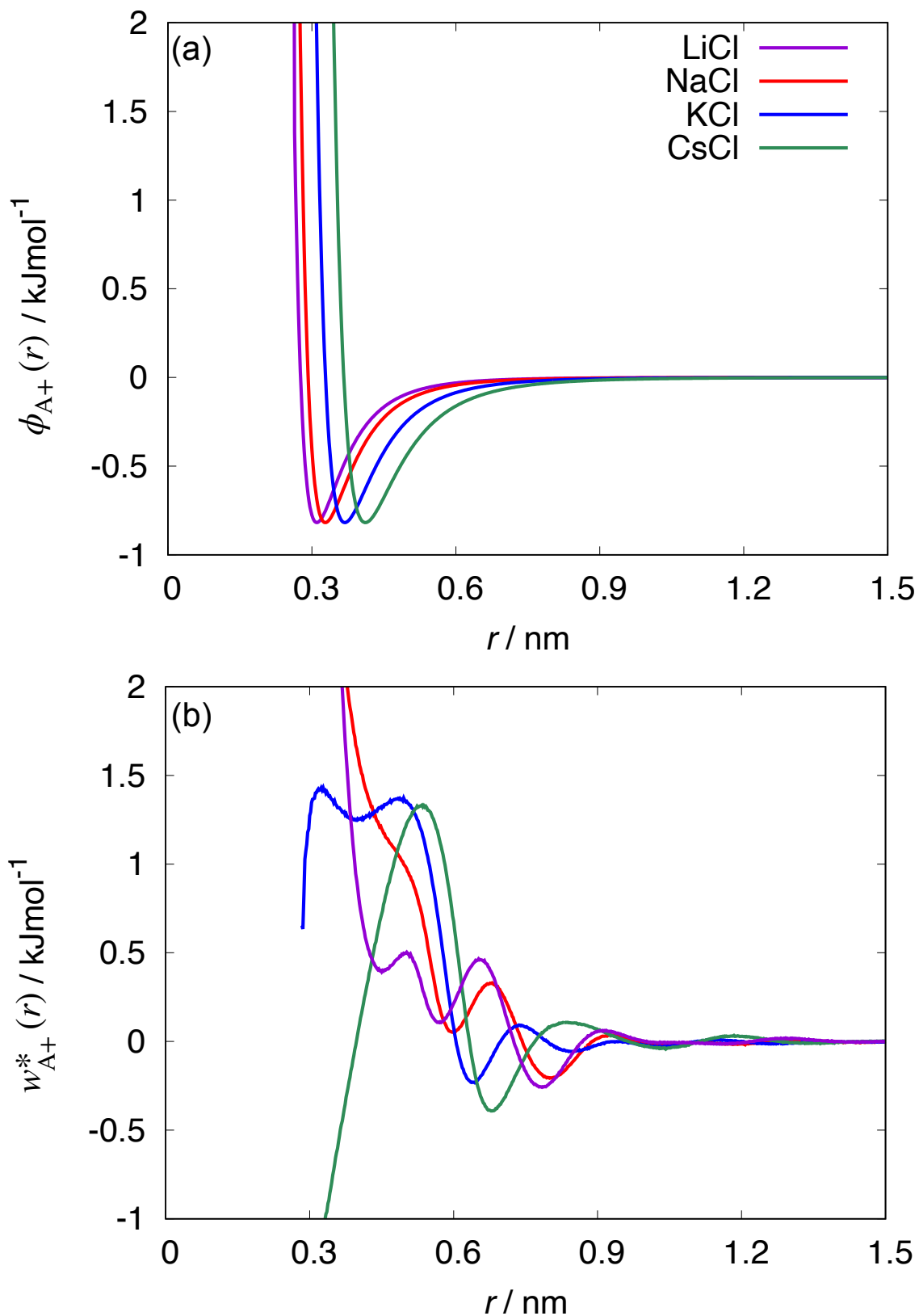


Figure 3.15: The methane-cation (a) direct interactions $\phi_{A^+}(r)$ and (b) solvent-mediated interactions $w_{A^+}^*(r)$ in aqueous solutions of methane and electrolytes for four cation sizes, Li^+ , Na^+ , K^+ , and Cs^+ in the cation series.

Origins of Exceptional Behavior of Li^+ in $w_{\text{A}+}^*(r)$.

Here, the solute-cation PMF $w_{\text{A}+}(r)$ can be divided into the direct interaction $\phi_{\text{A}+}(r)$ between methane and cation and the solvent-mediated interaction $w_{\text{A}+}^*(r)$:

$$w_{\text{A}+}(r) = \phi_{\text{A}+}(r) + w_{\text{A}+}^*(r). \quad (3.17)$$

Figure 3.15 shows that $\phi_{\text{A}+}(r)$ and $w_{\text{A}+}^*(r)$ in aqueous solutions of electrolytes and methane in the selected cation series. $\phi_{\text{A}+}(r)$ is the LJ interaction between methane and the cation, and the solvent-mediated interaction (SMI) was evaluated by the difference between $w_{\text{A}+}(r)$ obtained from the MD calculations and $\phi_{\text{A}+}(r)$: $w_{\text{A}+}^*(r) = w_{\text{A}+}(r) - \phi_{\text{A}+}(r)$. We compare with Figures 3.15a and 3.15b at the distance in which the first minimum in Figure 3.14 appears for each cation. It then follows that the minimum of $w_{\text{A}+}(r)$ is due to the direct interaction for larger cation sizes (K^+ , Cs^+), while the minimum of that is due to the solvent-mediated interaction for smaller cation sizes (Li^+ , Na^+). Therefore, the exceptional behavior of Li^+ for the salting-out effect should be included in the solvent-induced interaction.

Considering a two-component system (solvent 1 + solute 2), at the infinite dilution limit of solute, the solute-solute SMI $w_{22}^*(r)$ is given by

$$w_{22}^*(r) = \Delta E_{12}(r) + \Delta E_{11}(r) + T\Delta S(r), \quad (3.18)$$

where $\Delta E_{ij}(r)$ is defined by $\Delta E_{ij}(r) \equiv E_{ij}(r) - E_{ij}(\infty)$ with $E_{ij}(r)$ the potential energy between molecular species i and j at the solute-solute distance r , and $\Delta S(r)$ is the difference in entropy at solute-solute distances r and infinity. In the earlier studies[173, 174, 175, 176], it is known that the solvent-solvent potential is canceled out by part of the entropy terms. Then, eq. 3.18 is rewritten as

$$w_{22}^*(r) = \Delta E_{12}(r) + T\Delta S^*(r), \quad (3.19)$$

where $\Delta S^*(r)$ is the effective entropy. Therefore, at the infinite dilution limit of methane and ions, we assume that $w_{\text{A}+}^*(r)$ can be divided into the enthalpic contribution $w_{\text{H}}(r)$ and the entropic contribution $w_{\text{S}}(r)$ as follows.

$$w_{\text{A}+}^*(r) = w_{\text{H}}(r) + w_{\text{S}}(r) \quad (3.20)$$

with

$$w_{\text{H}}(r) = \Delta E_{\text{w}+}(r) + \Delta E_{\text{Aw}}(r), \quad (3.21)$$

where $E_{\text{w}+}(r)$ and $E_{\text{Aw}}(r)$ are the water-cation and water-methane potential energies at the methane-cation distance r , respectively. The question is then which contribution gives rise to the first minimum of solvent-mediated interaction in Li^+ . In a system with one salt and one methane molecule in water, we calculated $E_{\text{w}+}(r)$ and $E_{\text{Aw}}(r)$ to obtain $w_{\text{H}}(r)$ by MD simulations with fixed methane and cation positions at their distance r and restricted anion to be no closer to those. $E_{\text{w}+}(\infty)$ and $E_{\text{Aw}}(\infty)$ are calculated from systems with one salt and one methane molecule in the water, respectively, indicating that the cations and methane are independent of each other. Furthermore, $w_{\text{S}}(r)$ was obtained by the difference between $w_{\text{A}+}^*(r)$ and $w_{\text{H}}(r)$.

Figure 3.16 displays $w_{\text{H}}(r)$ and $w_{\text{S}}(r)$ at a variety of fixed methane-cation distances r in the selected cation series. As shown in Figure 3.16a, there is a minimum at $r = 0.45$ nm only for Li^+ , while for the other ion sizes, $w_{\text{H}}(r)$ is more repulsive as the methane molecule approaches the cation. The exceptional minimum of $w_{\text{H}}(r)$ for Li^+ appears at the same distance as that of the PMF for Li^+ in Figure 3.14. On the other hand, in Figure 3.16b, it follows that $w_{\text{S}}(r)$ increases with the decrease in the cation size σ_+ at the methane-cation distance r around 0.4 nm. This result means that the smaller the cation size σ_+ , the less stable methane and cation are by $w_{\text{S}}(r)$ at $r < 0.5$ nm. Therefore, it is found that the exceptional behavior of Li^+ for the salting-out effect is mainly attributed to $w_{\text{H}}(r)$.

From eq. 3.21, $w_{\text{H}}(r)$ is divided into the water-cation potential $\Delta E_{\text{w}+}(r)$ and the water-methane potential $\Delta E_{\text{Aw}}(r)$. The cation size σ_+ effects on $\Delta E_{\text{w}+}(r)$ and $\Delta E_{\text{Aw}}(r)$ are then examined separately, including the exceptional behavior of Li^+ for $w_{\text{H}}(r)$. Figure 3.17 shows $\Delta E_{\text{w}+}(r)$ and $\Delta E_{\text{Aw}}(r)$ at a variety of fixed methane-cation distances r in the selected cation series. In Figure 3.17a, $\Delta E_{\text{w}+}(r)$ has a minimum at $r = 0.45$ nm, similar to $w_{\text{H}}(r)$, while for the other cations, $\Delta E_{\text{w}+}(r)$ becomes monotonically larger as the methane-cation distance decreases. In Figure 3.17b, $\Delta E_{\text{Aw}}(r)$ becomes small around $r = 0.45$ nm as the cation size σ_+ decreases, indicating that $\Delta E_{\text{Aw}}(r)$ for Li^+ makes the methane molecule the most stable around the distance. However, the cation size dependence of $\Delta E_{\text{Aw}}(r)$ is smaller than that of $\Delta E_{\text{w}+}(r)$ and has little effect on the cation size dependence of $w_{\text{H}}(r)$. Therefore, we find that a methane molecule and Li^+ are relatively stable due to the water-cation interaction energy

around the distance of $r = 0.45$ nm, resulting in the exceptionally small salting-out effect of Li^+ . Furthermore, one of the most interesting results is that all $w_{\text{H}}(r)$, $\Delta E_{\text{w}^+}(r)$, and, albeit slightly, $\Delta E_{\text{Aw}}(r)$ for Li^+ are negative at $r = 0.45$ nm, indicating that cations along with a methane existed in the position are more stabilized than those in the solution without methane by the potential energy between cation and water.

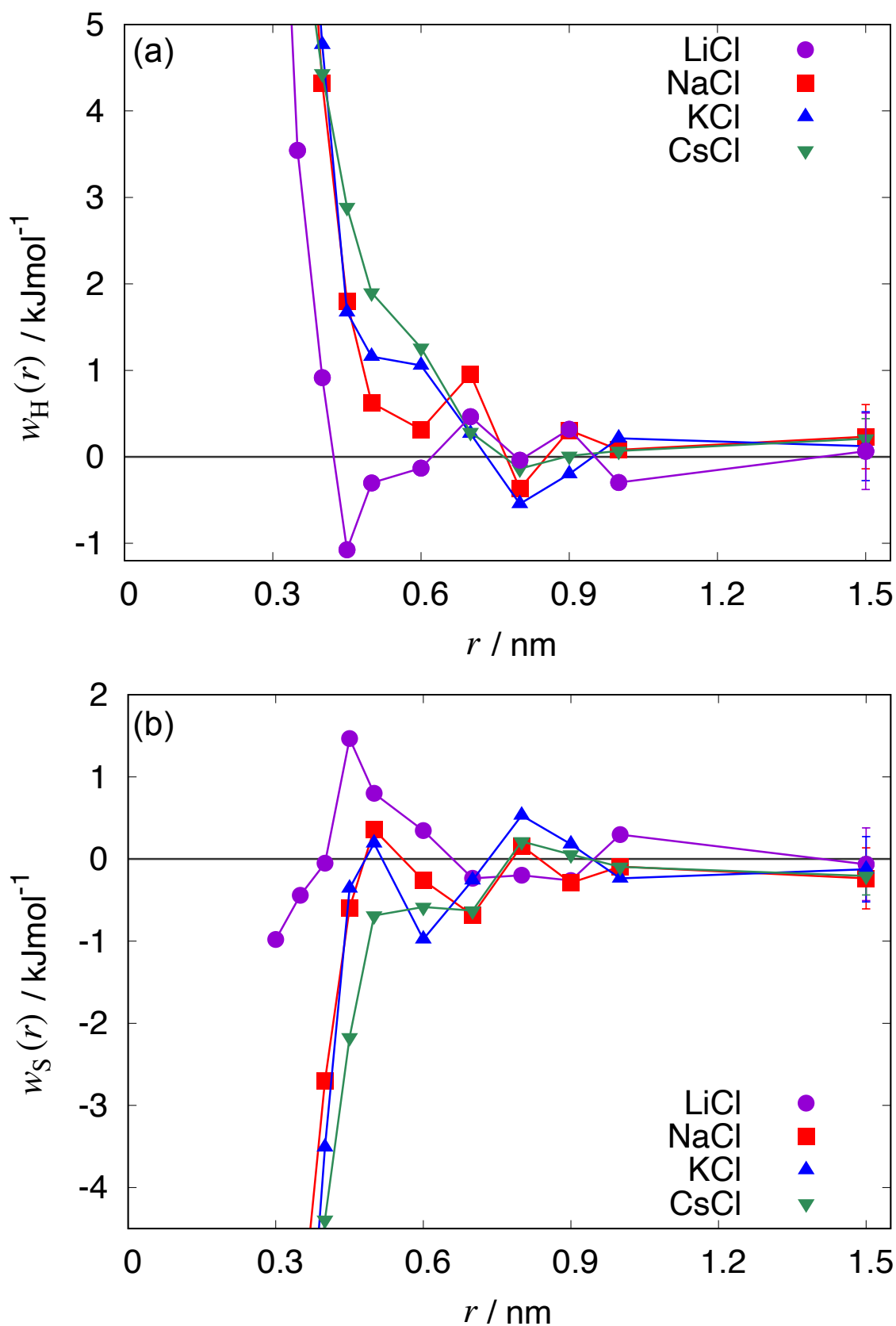


Figure 3.16: In the selected cation series, (a) the enthalpic contribution $w_H(r)$ to the solvent-mediated interaction and (b) the entropic contribution $w_S(r)$ to the solvent-mediated interaction against the methane-cation distance r . Error bars apply the standard deviation obtained from $2 \text{ nm} \times 10$ MD calculations and are displayed only at $r = 1.5 \text{ nm}$.

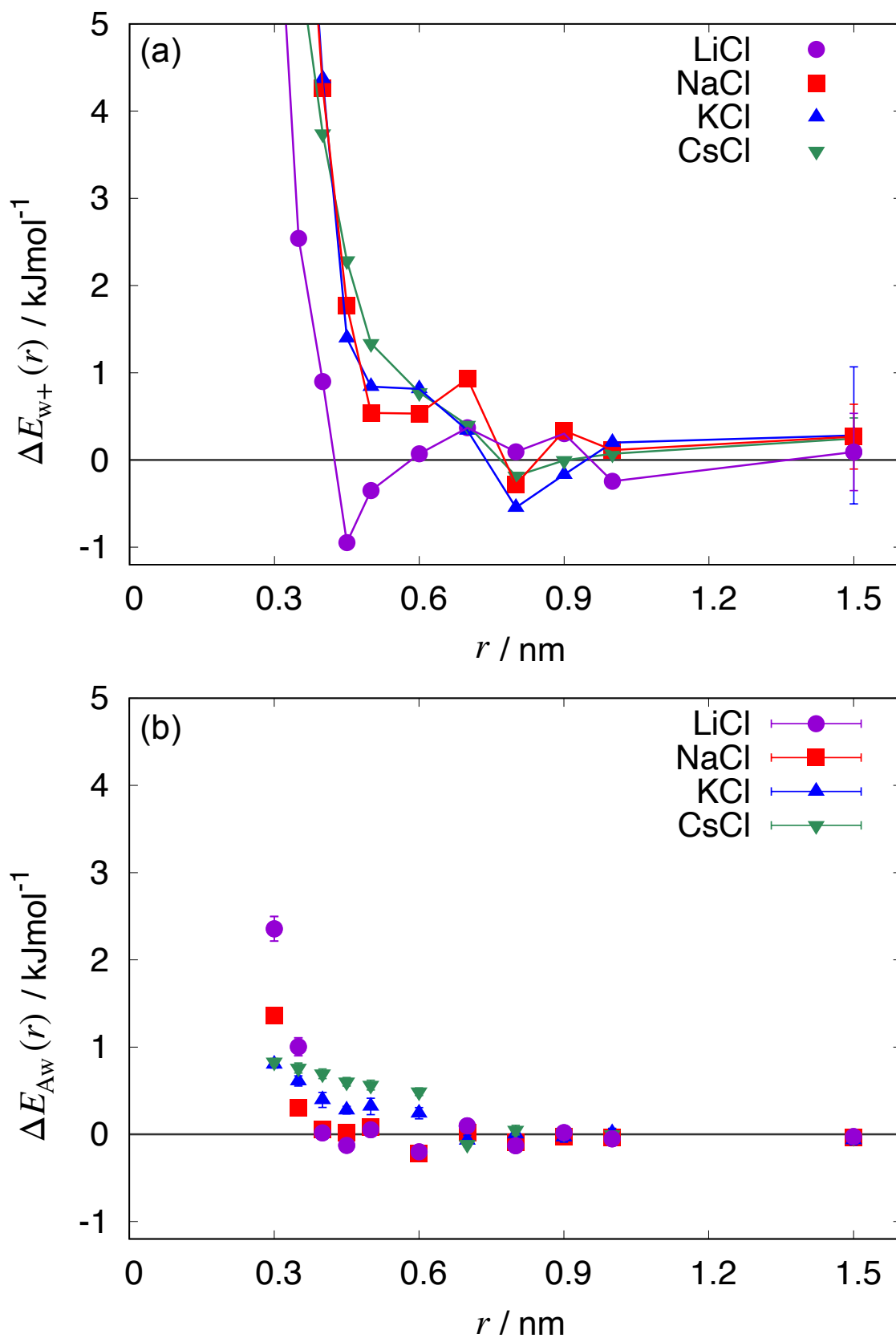


Figure 3.17: For four cation sizes, Li⁺, Na⁺, K⁺, and Cs⁺ in the cation series, (a) $\Delta E_{w+}(r)$ and (b) $\Delta E_{Aw}(r)$ at the methane-cation distance r . Error bars apply the standard deviation obtained from $2 \text{ nm} \times 10$ MD calculations and are displayed (a) only at $r = 1.5 \text{ nm}$ and (b) whole distances.

Cation Size Dependences of Setschenow Coefficient K_s for Solute with Hydrophilic Group.

The Setschenow coefficient K_s in eq. 3.4, a measure of the solubility of nonpolar solute in aqueous electrolyte solution, is derived from eq. 3.3 with considering a nonpolar solute with very small solubility in aqueous solutions in order to naturally suppose the infinite dilution of solute in eq. 3.4. However, even for polar solutes with hydrophilic groups such as methanol, there is no problem in observing K_s at infinite dilution of solute from eqs. 3.4 or 3.5, which is rather interesting. It has been reported in the earlier experimental study[177] that the magnitude of the salting-out effects for tert-butanol in a variety of aqueous electrolyte solutions: the order of cations with a common anion is $\text{Na}^+ > \text{K}^+ > \text{Li}^+$ and of anions with a common cation is $\text{F}^- > \text{Cl}^- > \text{I}^-$. Those orders are similar to the order of the ion size effects on the solubility of nonpolar solutes such as methane (Figures 3.1 and 3.2) and benzene[178]. However, there is no guarantee that the microscopic origins of the ion size dependences of the Setschenow coefficients K_s for polar and nonpolar solutes are the same. To examine the cation size effect of K_s for methanol, the simplest alcohol, we performed similar MD simulations replacing methane with methanol as the solute and obtained K_s from eq. 3.5. The TraPPE-UA force field[179] was applied to the molecule model of methanol. The KBI for the molecule models of methanol with multiple interaction sites was obtained by averaging the KBIs between all the pairs of sites on the molecules since the correlation function integral is invariant to the choice of molecular centers[150].

Figure 3.18 shows that Setschenow coefficients k_{scc} (converted from K_s) for methanol in aqueous electrolyte solutions of selected cations from the series of cations. As seen in Figure 3.18, the Setschenow coefficient for methanol is the largest at the K^+ size as varying the cation size, the order being $\text{K}^+ \simeq \text{Cs}^+ > \text{Na}^+ > \text{Li}^+$. The ion size of the salting-out maximum for methanol differs from that for tert-butanol as well as methane. Thus, it is expected that cation size dependences of K_s for alcohols, including tert-butanol, own completely different or partially common mechanism from that of the ion size effect for nonpolar solutes such as methane. Then, to understand the microscopic origins of the ion size dependences of K_s for methanol, we examined the methanol (methyl group)-cation PMFs, $w_{\text{A}^+}(r)$, in the selected cation series and compared $w_{\text{A}^+}(r)$ for methanol with those for methane. It is noted, as mentioned earlier, that the choice of molecular centers from which to measure intermolecular distances must be independent of the correlation function integral, while the shape of the correlation function

differs from the choice[150]. Therefore, we choose the methyl group as the molecular center of the methanol molecule to elucidate the differences between $w_{A^+}(r)$ for methane and those for methanol due to the hydrophilic group.

Figure 3.19 shows that the PMFs $w_{A^+}(r)$ between methanol (methyl group) and cation in the selected cation series. In Figure 3.19, it follows that the smaller the cation size, the smaller the first minimum of $w_{A^+}(r)$, that is, the first minimum for a cation of Li^+ size is the smallest at the smallest methanol (methyl group)-cation distance r . This result differs from the first minimum of the methane-cation PMFs in Figure 3.14 because of the effect of the hydrophilic group attracting smaller cations. Here, the second minimum in Figure 3.19 increases as the cation size σ_+ decreases, except for Li^+ . The $w_{A^+}(r)$ second minimum for Li^+ is smaller than that for Na^+ , and both this exceptional behavior and the distance ($0.45 \text{ nm} < r < 0.55 \text{ nm}$) at which the minimum for Li^+ appears are similar to those of $w_{A^+}(r)$ for methane. This result indicates that the hydration structure around the hydrophobic group in a solute is not broken by the presence of hydrophilic groups in that solute. Thus, considering that the ion size effect on K_s for methanol differs from that for tert-butanol, which has the larger nonpolar group than methanol, it is expected that ion size dependences of K_s for amphiphilic solutes are qualitatively estimated by a combination of a cation size effect similar to methane (the magnitude of the contribution to K_s is $\text{Na}^+ > \text{K}^+ > \text{Cs}^+ \simeq \text{Li}^+$) and an effect that the hydrophilic group attracts smaller cations (the magnitude of the contribution to K_s is $\text{Cs}^+ > \text{K}^+ > \text{Na}^+ > \text{Li}^+$).

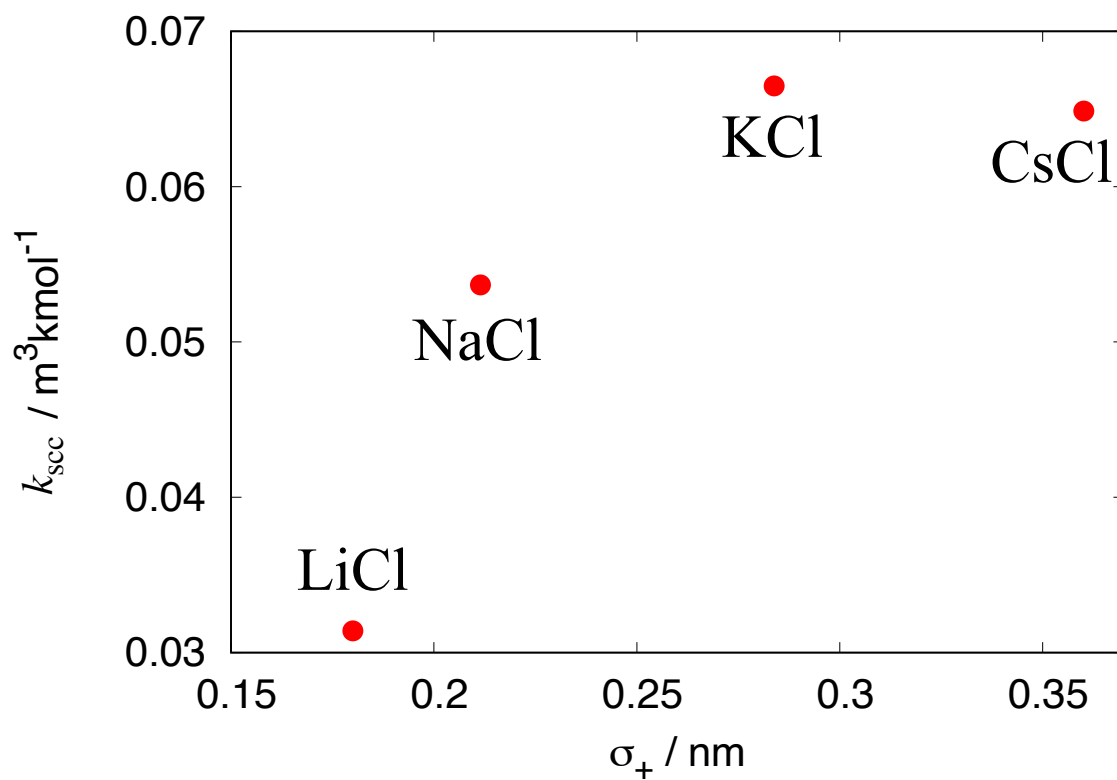


Figure 3.18: Setschenow coefficients k_{scc} for methanol calculated from eq. 3.5 in aqueous solutions of four cation sizes in the cation series.

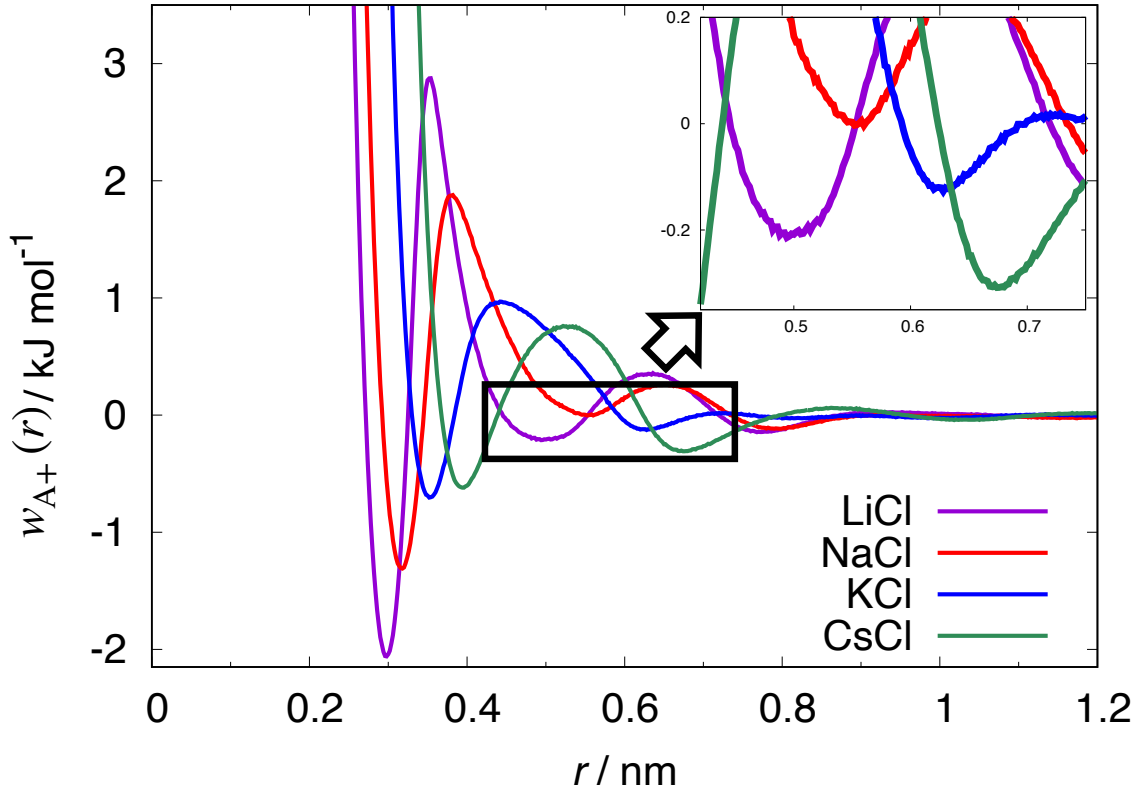


Figure 3.19: The potential of mean forces $w_{A+}(r)$ between methanol (methyl group) and cation for four cation sizes, Li^+ , Na^+ , K^+ , and Cs^+ in the cation series. The second minimum of the PMF for each cation, circled by a black square in the figure, is expanded in the upper right corner.

V CONCLUSIONS

Cation and anion size dependences of the salting-out effect were contrasted, and the origins of the differences were examined.

In the cation series, where the cation size is varied at fixed anion as Cl^- , the solvation free energy μ_A^* of methane is maximal at around the cation size σ_+ of Na^+ and decreases rather sharply as σ_+ decreases further. In the anion series where the anion size σ_- is varied at fixed cation as Na^+ , μ_A^* is a monotonic function of the σ_+ .

The Setschenow coefficients K_s in the cation series were calculated from two different routes: the SFE route in eq 3.14 with the test-particle insertion method, and the KBI route in eq 3.5 with the correlation function integrals. The results from the two routes are similar to each other and show the reversed order of Li^+ and Na^+ , in agreement with experimental data[46].

The correspondence between the salting-out effect and volumetric properties of electrolyte aqueous solutions, more specifically, the packing fraction η and the partial molar volume \bar{v}_s of

salt, was confirmed. The two properties of η and \bar{v}_s show nonmonotonic dependences on σ_+ in the cation series, while they are monotonic functions of σ_- in the anion series.

We examined the microscopic origins of the ion size dependences of μ_A^* , η , and \bar{v}_s . First, it is demonstrated that the formation of ion clusters in aqueous solutions of LiCl is not responsible for the reversed order of lithium and sodium ions in the ion size dependences of μ_A^* and η . Second, the ion–water pair correlation function integrals $G_{w\pm}(R)$, which is a function of the radius R of the spherical volume centered at each ion in the cation and anion series, were calculated. A notable conclusion derived from the computational result is that the spherical volume of radius ~ 0.5 nm, i.e., the second hydration sphere, around each cation sets the order of cations for $G_{ws} \simeq -\bar{v}_s$ including the reversed order of lithium and sodium salts. Third, we calculated the solvation packing fractions $\eta(R_1)$, $\eta(R_2)$, and $\eta(R_3)$ for the first, second, and third solvation spheres around a cation and an anion, defined by eq. 3.16. It is found that $\eta(R_1)$ increases monotonically with decreasing σ_+ , but $\eta(R_2)$ and $\eta(R_3)$ appear maxima at around σ_+ of Na^+ , thereby confirming that the tendency of the nonmonotonic behavior of η in the cation series depends on the second solvation sphere. In the anion series, all $\eta(R_1)$, $\eta(R_2)$, and $\eta(R_3)$ increase monotonically with decreasing σ_- . Fourth, we examined the distribution of the average orientation $\langle \cos \theta \rangle$ of water molecules in the first solvation shell of each ion in the cation and anion series and the conditional solvation packing fraction $\eta_{R_2}(\langle \cos \theta \rangle)$ for the second solvation spheres, and found the microscopic mechanism as follows. The peak position of the $\langle \cos \theta \rangle$ distribution shifts significantly toward -1, i.e., orients to face their oxygen atoms of water molecules toward cations, with decreasing σ_+ in the cation series: $\eta_{R_2}(\langle \cos \theta \rangle)$ for Li^+ and Na^+ are similar to each other and decrease sharply as $\langle \cos \theta \rangle$ goes to -1, and thereby $\eta(R_2)$ for Li^+ is smaller than that for Na^+ .

Next, we examined the relation between the Setschenow coefficients of methane and the volumetric properties of aqueous solutions in terms of the Kirkwood–Buff integrals G_{ws} and G_{As} . It was found that G_{As} is near-linearly correlated with G_{ws} for model electrolyte solutions containing both cation and anion series. Qualitatively, the correlation is consistent with the commonly observed results: the solubility of a hydrophobic solute is lower with the packing fraction of the aqueous solution increasing[17, 63, 89, 157, 163, 164]. The remaining question is how robust is the correlation between G_{ws} and G_{As} . In the present study, we considered the size effect of monovalent ions alone for methane. It is interesting to examine, by verifying more ion and solute species, which combinations of ion and solute form a more or less universal $G_{ws} - G_{As}$

curve and which fall off from it.

Then, the cation size dependence of G_{A_s} was examined in terms of the methane-cation potential of mean force $w_{A^+}(r)$. The exceptionally small K_s for Li^+ was found to be due to exhibiting an exceptional minimum of $w_{A^+}(r)$ for Li^+ at the methane-cation distance $r \sim 0.45$ nm. The position of this minimum is in good agreement with the region which is a smaller packing fraction at $\langle \cos \theta \rangle \simeq -1$. Furthermore, the exceptional minimum of $w_{A^+}(r)$ for Li^+ is found to be caused by the solvent-mediated interaction, specifically, the water-cation interaction energy $E_{w^+}(r)$ at the methane-cation distance r .

Finally, the cation size σ_+ dependence of the Setschenow coefficients K_s for the amphiphilic solute, methanol, was examined. No linear correlation between K_s and the volumetric properties of the aqueous solution, i.e., between G_{A_s} and G_{w_s} , was observed for methanol, unlike for methane. The cation size dependence σ_+ of K_s for methanol was examined in terms of $w_{A^+}(r)$. It was found that the cation size dependences of K_s for methanol are determined by the sum of the contributions from hydrophobic and hydrophilic groups: the former has an ion size effect similar to K_s for methane, while for the latter the smaller the salting-out effect is, the smaller the σ_+ is. This means that both hydrophobic and hydrophilic groups make the K_s for Li^+ more negative (the weaker salting-out or the stronger salting-in) than that for Na^+ . In other words, the ionic size effect on the Setschenow coefficient K_s for amphiphilic solutes including alcohols depends on the hydrophobic and hydrophilic group species and their combinations, if the effect of structural changes of solute molecules is ignored. Therefore, to quantitatively clarify the ion- and solute-specificity for K_s , it is a subject of future study to examine the hydrophobic group and hydrophilic group species dependences, e.g., size and number of each functional group, etc., of the ion-specificity for K_s , respectively.

Chapter 4

Correlation between the Salting-out/Salting-in Effect and the Osmotic Second Virial Coefficient in Aqueous Electrolyte Solutions

Abstract

Earlier simulation studies indicate that the larger the salting-out effect the ionic species has the stronger the hydrophobic interaction, i.e., the effective interaction between hydrophobic molecules, in the aqueous solution of that salt. To understand the ion-specific effects of solute-solute effective interactions, we performed molecular dynamics simulations of solutions of water + electrolytes ($X_{\nu_+}Y_{\nu_-}$) + solute at the low densities ρ_s and ρ_A of salt and solute, respectively, and calculated the osmotic second virial coefficient B and the Setschenow coefficient K_s for a variety of combinations of salt and solute. At least in the range of salting-out and small salting-in, it is confirmed that the salt-enhanced-association (SEA) coefficient $C_1 \equiv -\lim_{\rho_s \rightarrow 0} (\partial B / \partial \rho_s)_{T,p}$, which represents the magnitude of the salt effect on the solute-solute effective interaction, is correlated with the Setschenow coefficient as $C_1 \simeq K_s^2 / 2 (\nu_+ + \nu_-)$, an approximation of the analytical result derived in an earlier theoretical study.

I INTRODUCTION

The addition of salt to water decreases or increases the solubility of solutes. The former and latter are called salting-out and salting-in effect, and their strength depends on the salt and solute species. The effects are applied to the separation of proteins, low molecular weight organic compounds, metal complexes, and ion pairs that cannot be separated by filtration or centrifugation[180]. In general, the larger the ion valence and the smaller the ion size, the stronger the salting-out effect on hydrophobic solutes. The ordering of salting-out effect of ions is called the Hofmeister series. The Hofmeister series was originally introduced as the ordering of ions in the magnitude of ion addition effects on protein aggregation[24]. Since then, a lot of experimental and computer simulation studies of the ion addition effects on the physical properties of aqueous solutions have been conducted[181, 63, 27, 69, 182, 151]. This series has been found to be related to not only the structural change and precipitation of protein and colloid[61, 153, 67] but also physical properties of various aqueous electrolyte solutions[1, 8], e.g., surface tension[14, 15, 16] and solute solubility[18, 19]. Recently, it has been understood that the Hofmeister series results from a complex interplay of the ion-water and ion-protein interactions in aqueous solution[67, 8, 152], whereas the detailed mechanism remains unclear. Understanding ion species dependence on the solubility of hydrophobic solutes is the first step to revealing the molecular mechanism underlying the Hofmeister series.

Setschenow (Sechenov)[158] proposed and verified the relationship between the salt concentration and the solubility of a gas in aqueous electrolyte solution, which $k_{\text{scc}} = -(1/c_s) \log_{10} [\lambda/\lambda_0]$ in a notation commonly used today, where λ and λ_0 are the Ostwald absorption coefficients of the gas in aqueous solution and pure water, respectively, and c_s is the molar concentration of salt. The Setschenow coefficient k_{scc} represents the strength of the salting-out/salting-in effect and depends on the salt and gas species; the positive and negative value of k_{scc} indicates salting-out and salting-in, respectively. Setschenow coefficients have been experimentally measured and theoretically investigated for many solute and ion species[42, 45, 126, 46, 127, 128, 183]. Here, the magnitude of the Setschenow coefficients of alkali metal ions for a common hydrophobic solute is in the order $\text{Na}^+ > \text{K}^+ > \text{Rb}^+ > \text{Cs}^+ \simeq \text{Li}^+$, where it is noted that the smallest size ion, Li^+ , is deviated from the normal ordering of ion size. The ion size dependence of the salting-out effect, including the exceptional behavior of Li^+ , has been examined in our earlier study[19], whereas the comprehensive investigation of the Setschenow coefficients including the dependence

on the species of solute and ion has not been conducted yet except for the dependence on ion size.

In earlier studies, qualitative correlations have been found that the lower a gas solubility by varying salt concentration or changing salt species, the more attractive the solute-solute effective interaction is [184, 156, 164]. In 2021, Okamoto and Koga [185] theoretically proposed the relationship between gas solubility and the osmotic second virial coefficient B in aqueous electrolyte solutions, where the latter quantifies the strength of solute-solute effective interaction in solution at the infinite dilution limit of the solute. If a salt species $X_{\nu_+} - Y_{\nu_-}$ dissociates into $\nu_+ X^{z_+}$ and $\nu_- Y^{z_-}$, where z_i is the ion valence, we obtained the following approximate relation:

$$C_I \equiv - \lim_{\rho_s \rightarrow 0} \left(\frac{\partial B}{\partial \rho_s} \right)_{T,p} \approx \frac{K_s^2}{2(\nu_+ + \nu_-)}, \quad (4.1)$$

where C_I is called the salt-enhanced-association coefficient (SEA) coefficient, ρ_s is the salt density, and K_s is the Setschenow coefficient defined by

$$K_s = \lim_{\rho_s \rightarrow 0} \left(\frac{\partial \ln \lambda}{\partial \rho_s} \right)_{T,p}. \quad (4.2)$$

The osmotic second virial coefficient B is given by the solute-solute Kirkwood-Buff integral (KBI) G_{AA} at the infinite dilution limit of the solute;

$$B = - \lim_{\rho_A \rightarrow 0} \frac{G_{AA}}{2} = - \frac{1}{2} \lim_{\rho_A \rightarrow 0} \int h_{AA}(\mathbf{r}) d\mathbf{r}, \quad (4.3)$$

where ρ_A is the solute density and h_{AA} is the solute-solute pair correlation function. B is useful for characterizing the solute-solute interaction in solvent; in fact, the positive and negative value of B indicates a repulsive and attractive interaction, respectively. Unfortunately, it was not straightforward to obtain B from experiments for hydrophobic solutes with small solubility, such as small alkanes and inert gases. In 2013, Koga [145] proposed a scheme for directly calculating B for solutes that dissolve little in a solvent using molecular dynamics (MD) simulation, and since then there had been many studies on B for various solute species at various temperature and pressure conditions [186, 150, 187, 188, 189, 190, 191, 192, 193, 194, 146].

Equation 4.1 relates K_s to C_I , where K_s represents the ion addition effect on the solvation free energy (SFE) μ_A^* of an isolated single solute molecule and C_I represents the ion effect on the solute-solute effective interaction in a solvent. Equation 4.1 implies that the stronger the salting-

out, i.e., the more positive K_s is, the more attractive the solute-solute interaction is, while it also implies that the stronger the salting-in, i.e., the more negative K_s is, the more attractive the solute-solute interaction is, which appears to be a contradiction. Thus, it is highly significant to verify this equation. In the present study, we performed MD simulations to calculate K_s and B for a variety of ion and solute species to validate eq. 4.1. In addition, lower alcohols were employed as co-solvents instead of electrolytes to verify the prediction by eq. 4.1 for the cases of salting-in.

II THEORETICAL BACKGROUND

In the present work, we consider a three-component system (water + ions + hydrophobic solute), which is the infinitely dilute solute in a dilute electrolyte aqueous solution;

$$\rho_A \ll \rho_I \ll \rho_w. \quad (4.4)$$

where ρ_I is the total ion density and ρ_w is the water density. For salt species $X_{\nu_+}Y_{\nu_-}$, the ion densities ρ_{\pm} satisfy the charge neutrality condition,

$$\rho_s = \frac{\rho_+}{\nu_+} = \frac{\rho_-}{\nu_-} = \frac{\rho_I}{\nu_+ + \nu_-}. \quad (4.5)$$

Thus, the limit $\rho_I \rightarrow 0$ implies $\rho_A \rightarrow 0$ in this paper. Under the above conditions, we derive eq. 4.1 in this section.

A Osmotic Second Virial Coefficient B

A pressure difference occurs between two solutions of different solute concentrations separated by a semipermeable membrane in which the solute is impenetrable, and is called the osmotic pressure. In a solution of water + ions + solute and $\rho_A = 0$ in one region, the chemical potentials μ_w, μ_I of water and ions are equal in both regions, respectively, which the osmotic pressure is defined as $\Pi = p(\rho_w, \rho_I, \rho_A) - p(\rho'_w, \rho'_I, 0)$. The expansion equation for the osmotic pressure with respect to the solute density ρ_A at constant the solvent chemical potentials μ_w, μ_I and the temperature T is $\Pi = \rho_A k_B T (1 + B\rho_A + \dots)$, with B the osmotic second virial coefficient that measures the solute-solute effective interaction and k_B the Boltzmann constant. Using the

Gibbs-Duhem relation, we obtain

$$\left(\frac{d\Pi}{d\rho_A}\right)_{T,\mu_w,\mu_I} = \left(\frac{\partial p}{\partial\rho_A}\right)_{T,\mu_w,\mu_I} = k_B T \rho_A / I_{AA} \quad (i, j = w, I, A) \quad (4.6)$$

with

$$I_{ij} \equiv k_B T \left(\frac{\partial\rho_i}{\partial\mu_j}\right)_{T,\{\mu_k\}_{k\neq j}}. \quad (4.7)$$

Thus, at the infinite dilution limit of the solute, B is given by

$$B = \frac{1}{2} \lim_{\rho_A \rightarrow 0} \left(\frac{1}{I_{AA}} - \frac{1}{\rho_A} \right). \quad (4.8)$$

B Density Second Derivatives of the Free Energy Density

Let $f(\rho_w, \rho_I, \rho_A)$ be the Helmholtz free energy density of the system. Here, since we consider a constant temperature, the temperature is not shown as a variable. In general, f expanded in powers of the solute density ρ_A is given by

$$\begin{aligned} f(\rho_w, \rho_I, \rho_A) &= f_0(\rho_w, \rho_I) + \mu_A(\rho_w, \rho_I) \rho_A + \frac{1}{2} U_{AA}(\rho_w, \rho_I) \rho_A^2 + \mathcal{O}(\rho_A^3) \\ &= f_0(\rho_w, \rho_I) + k_B T \rho_A \{\ln(\rho_A \Lambda_A^3) - 1\} + \mu_A^*(\rho_w, \rho_I) \rho_A \\ &\quad + \frac{1}{2} U_{AA}(\rho_w, \rho_I) \rho_A^2 + \mathcal{O}(\rho_A^3), \end{aligned} \quad (4.9)$$

where the logarithmic term is singular at $\rho_A = 0$, so it has not been expanded. f_0 is the Helmholtz free energy density of the electrolyte solution without the solute, Λ_A is the thermal de Broglie length of the solute, μ_A and μ_A^* are the chemical potential and the solvation free energy of the solute at the infinite dilution limit of the solute, respectively, and U_{AA} is the second-order coefficient of ρ_A , related to the two-body interaction of the solute. Then, the isothermal compressibility $\chi_T \equiv \rho^{-1} (\partial\rho/\partial p)_{T,\{N_i\}}$ is given by

$$\begin{aligned} \chi_T^{-1} &= \rho \frac{\partial}{\partial\rho} \left[\sum_{i=w,I,A} \rho_i \left(\frac{\partial f}{\partial\rho_i} \right) - f \right] \\ &= k_B T \sum_{i,j=w,I,A} \rho_i \rho_j I^{ij} \end{aligned} \quad (4.10)$$

with the system density $\rho = \rho_w + \rho_I + \rho_A$, the particle number N_i of species i , and

$$I^{ij} \equiv \frac{1}{k_B T} \frac{\partial^2 f}{\partial\rho_i \partial\rho_j} = \frac{1}{k_B T} \left(\frac{\partial\mu_i}{\partial\rho_j} \right)_{T,\{\rho_k\}_{k\neq j}}. \quad (4.11)$$

From eqs. 4.7 and 4.11, the symmetric matrices $\{I^{ij}\}$ and $\{I_{ij}\}$ are inverse matrices of each other, $\sum_k I_{ik}I^{kj} = \delta_{ij}$.

In the limit $\rho_A \rightarrow 0$, eq. 4.11 is rewritten as

$$\begin{aligned} I^{iA} &= \frac{\partial \beta \mu_A^*}{\partial \rho_i} + \mathcal{O}(\rho_A) & (i = w, I) \\ I^{ij} &= I_0^{ij} + \mathcal{O}(\rho_A) & (i, j = w, I) \\ I^{AA} &= \frac{1}{\rho_A} + \beta U_{AA} + \mathcal{O}(\rho_A) \end{aligned} \quad (4.12)$$

with the inverse temperature $\beta = 1/k_B T$ and $I_0^{ij} = \lim_{\rho_A \rightarrow 0} I^{ij}$. Equation 4.7 is expanded as

$$\begin{aligned} I_{ij} &= I_{ij}^0 + \mathcal{O}(\rho_A) & (i, j = w, I) \\ I_{iA} &= A_i \rho_A + \mathcal{O}(\rho_A) & (i = w, I) \end{aligned} \quad (4.13)$$

Substituting eqs. 4.12 and 4.13 into $\sum_j I_{ij}I^{jA} = \delta_{iA}$ for $i = w, I$,

$$A_i = - \sum_{j=w, I} I_{ij}^0 \left(\frac{\partial \beta \mu_A^*}{\partial \rho_j} \right)_{T, \{\rho_k\}_{k \neq j}} \quad (i = w, I). \quad (4.14)$$

This equation is rewritten as

$$\left(\frac{\partial \beta \mu_A^*}{\partial \rho_i} \right)_{T, \{\rho_k\}_{k \neq j}} = - \sum_{j=w, I} I_0^{ij} A_j. \quad (4.15)$$

C Partial Molecular Volume

The partial molecular volume of species i is the solution volume change when a single molecule of species i is added to the solution, which is defined by $\bar{v}_i = (\partial V / \partial N_i)_{T, p, \{N_j\}_{j \neq i}}$; the partial molecular volume of the ions is $\bar{v}_s = (\nu_+ + \nu_-) \bar{v}_I$ from eq. 4.4. Since the chemical potential μ_i is the intensive variable, $\mu_i(T, V, \{N_j\}) = \mu_i(T, \lambda V, \{\lambda N_j\})$ for some positive real number λ . Differentiating both sides with respect to λ and substituting $\lambda = 1$, we obtain

$$\left(\frac{\partial \mu_i}{\partial V} \right)_{T, \{N_j\}} = -k_B T \sum_{j=w, I, A} I^{ij} \rho_j. \quad (4.16)$$

The partial molecular volume is given by

$$\bar{v}_i = \chi_T \left(\frac{\partial p}{\partial \rho_i} \right)_{T, \{\rho_j\}_{j \neq i}} = k_B T \chi_T \sum_{j=w, I, A} I^{ij} \rho_j, \quad (4.17)$$

where eq. 4.16 is used to derive the last equality. Multiplying both sides by the density ρ_i of species i and summing for $i = w, I, A$, we obtain

$$\sum_{i=w,I,A} \bar{v}_i \rho_i = 1. \quad (4.18)$$

In the limit $\rho_A \rightarrow 0$, from eqs. 4.17 and 4.18

$$k_B T \chi_T^0 = \sum_{i,j=w,I} I_{ij}^0 \bar{v}_i^0 \bar{v}_j^0 = 1 / \sum_{i,j=w,I} I_0^{ij} \rho_i \rho_j, \quad (4.19)$$

where the superscript 0 represents the infinite dilution limit of the solute, i.e., $\bar{v}_i^0 = \lim_{\rho_A \rightarrow 0} \bar{v}_i$, $\chi_T^0 = \lim_{\rho_A \rightarrow 0} \chi_T$, respectively.

The solvation partial volume is also defined as $\bar{v}_i^* \equiv \bar{v}_i - k_B T \chi_T$. In the limit $\rho_A \rightarrow 0$, substituting eq. 4.17 into eq. 4.11 and using eq. 4.9, we obtain

$$\bar{v}_A^0 = k_B T \chi_T^0 \left[1 + \sum_{i=w,I} \rho_i \left(\frac{\partial \beta \mu_A^*}{\partial \rho_i} \right)_{T, \{\rho_j\}_{j \neq i}} \right] \quad (4.20)$$

$$\begin{aligned} \bar{v}_A^{0*} &= k_B T \chi_T^0 \sum_{i=w,I} \rho_i \left(\frac{\partial \beta \mu_A^*}{\partial \rho_i} \right)_{T, \{\rho_j\}_{j \neq i}} \\ &= -(\bar{v}_w^0 A_w + \bar{v}_I^0 A_I), \end{aligned} \quad (4.21)$$

where $\bar{v}_i^{0*} = \lim_{\rho_A \rightarrow 0} \bar{v}_i^*$. Furthermore, the partial molecular volume of solute in the limit $\rho_I \rightarrow 0$ is given by

$$v_A = k_B T \chi_w \left[1 + \rho_w \left(\frac{\partial \beta \mu_A^*}{\partial \rho_w} \right) \right], \quad v_A^* = k_B T \chi_w \rho_w \left(\frac{\partial \beta \mu_A^*}{\partial \rho_w} \right) \quad (4.22)$$

with $v_i = \lim_{\rho_I \rightarrow 0} \bar{v}_i^0$, $v_i^* = \lim_{\rho_I \rightarrow 0} \bar{v}_i^{0*}$, and the isothermal compressibility for pure water $\chi_w = \lim_{\rho_I \rightarrow 0} \chi_T^0$.

D Composition Susceptibility of the Electrolyte Solvent

In this section, we consider the composition susceptibility of the electrolyte solvent $X_I \equiv k_B T \rho^{-1} (\partial x_I / \partial h)_{T,p}$ in the infinitely dilute limit of the solute, with $h = \mu_I - \mu_w$ and the ion molar fraction $x_I = \rho_I / \rho$. Composition susceptibility X_I represents a measure of fluctuations of the total ion density in the low-frequency limit[185, 193]. At first, using eq. 4.17, differentiating

the pressure with respect to the ion density can be represented as

$$\left(\frac{\partial p}{\partial \rho_{\text{I}}}\right)_T = \frac{\bar{v}_{\text{w}}^0}{\chi_T^0} \left(\frac{\partial \rho_{\text{w}}}{\partial \rho_{\text{I}}}\right)_T + \frac{\bar{v}_{\text{I}}^0}{\chi_T^0}. \quad (4.23)$$

Under isobaric condition, eq. 4.23 is written as

$$\left(\frac{\partial \rho_{\text{w}}}{\partial \rho_{\text{I}}}\right)_{T,p} = -\frac{\bar{v}_{\text{I}}^0}{\bar{v}_{\text{w}}^0}. \quad (4.24)$$

Then, differentiating the density with respect to x_{I} , we obtain

$$\left(\frac{\partial \rho_{\text{w}}}{\partial x_{\text{I}}}\right)_{T,p} = -\rho^2 \bar{v}_{\text{I}}^0, \quad \left(\frac{\partial \rho_{\text{I}}}{\partial x_{\text{I}}}\right)_{T,p} = \rho^2 \bar{v}_{\text{w}}^0. \quad (4.25)$$

Using eq. 4.25, we can rewrite X_{I} as

$$X_{\text{I}}^{-1} = \rho^3 [I_0^{\text{ww}} \bar{v}_{\text{I}}^0 + I_0^{\text{II}} \bar{v}_{\text{w}}^0 - I_0^{\text{wI}} (\bar{v}_{\text{w}}^0 + \bar{v}_{\text{I}}^0)]. \quad (4.26)$$

Furthermore, using eqs. 4.10, 4.18 and $\Delta_0 = [\det\{I_0^{ij}\}]^{-1}$, we obtain

$$X_{\text{I}} = \Delta_0 / (k_{\text{B}} T \rho^4 \chi_T^0). \quad (4.27)$$

Expanding the Helmholtz free energy density $f_0(\rho_{\text{w}}, \rho_{\text{I}})$ of the electrolyte solution in eq. 4.9 with respect to ρ_{I} , we obtain

$$\begin{aligned} f_0(\rho_{\text{w}}, \rho_{\text{I}}) &= f_{\text{w}}(\rho_{\text{w}}) + k_{\text{B}} T \rho_{\text{I}} \left[\ln \left(\Lambda_{\text{I}}^3 \frac{\rho_{\text{I}}}{\nu_+ + \nu_-} \right) - 1 \right] + \mu_{\text{I}}^*(\rho_{\text{w}}) \rho_{\text{I}} \\ &\quad - \frac{k_{\text{B}} T}{12\pi} \kappa^3 + U_{\text{II}}(\rho_{\text{w}}) \rho_{\text{I}}^2 + \mathcal{O}(\rho_{\text{I}}^3), \end{aligned} \quad (4.28)$$

where f_{w} is the Helmholtz free energy density of the pure water, Λ_{I} is the thermal de Broglie length of the ions, μ_{I}^* is the solvation free energy of the ions at the infinite dilution limit of the ions, and U_{II} is the second-order coefficient of ρ_{I} . The fourth term on the right-hand side is the Debye-Hückel free energy in the limit of the low ion densities[58, 59], with the inverse of the Debye length

$$\kappa = \sqrt{\frac{|z_+ z_-| e^2}{\epsilon(\rho_{\text{w}}) k_{\text{B}} T \rho_{\text{I}}}}, \quad (4.29)$$

where $\epsilon(\rho_{\text{w}})$ is the dielectric constant in the pure water and e is the elementary charge. Using eqs. 4.28 and 4.18 in the limit $\rho_{\text{I}} \rightarrow 0$, $I_0^{\text{II}} = 1/\rho_{\text{I}} + \mathcal{O}(\rho_{\text{I}}^{-1/2})$, $I_0^{\text{wI}} = (\partial \beta \mu_{\text{I}}^* / \partial \rho_{\text{w}})_{T, \rho_{\text{I}}} + \mathcal{O}(\rho_{\text{I}}^{1/2})$,

$\bar{v}_w^0 = 1/\rho_w + \mathcal{O}(\rho_I)$. Thus, eq. 4.27 is written as

$$X_I = \frac{\rho_I}{\rho_w^2} + \mathcal{O}(\rho_I^{3/2}). \quad (4.30)$$

E Setschenow Coefficient K_s

At the low-salt density, the Setschenow coefficient K_s , defined as eq. 4.2, represents a measure of the salting-out effect for the solute in the aqueous solution. When the solution is in equilibrium with its vapor, the Ostwald adsorption coefficient λ , which represents the ratio of the solute density in the solution to that in the gas phase, corresponds to $\lambda = e^{-\mu_A^*/k_B T}$. Then, the Setschenow coefficient K_s is written as

$$\begin{aligned} K_s &= - \lim_{\rho_s \rightarrow 0} \left(\frac{\partial \ln \lambda}{\partial \rho_s} \right)_{T,p} = (\nu_+ + \nu_-) \lim_{\rho_I \rightarrow 0} \left(\frac{\partial \beta \mu_A^*}{\partial \rho_I} \right)_{T,p} \\ &= (\nu_+ + \nu_-) \left[\lim_{\rho_I \rightarrow 0} I^{AI} - \frac{v_A^* v_I}{k_B T \chi_w} \right], \end{aligned} \quad (4.31)$$

where eqs. 4.22 and 4.24 are used to derive the last equality.

In earlier studies[162, 19], we showed that the Setschenow coefficient was given by

$$K_s = (\nu_+ + \nu_-) (G_{Aw} - G_{As}), \quad (4.32)$$

where A is solute, w is water, + is cation, and - is anion in the subscripts of the KBI. The solute-salt KBI is given by $G_{As} = (\nu_+ G_{A+} + \nu_- G_{A-}) / (\nu_+ + \nu_-)$, with

$$G_{ij} = \int h_{ij}(r) dr. \quad (4.33)$$

The Setschenow coefficient is generalized from the low to the general salt density by the solvation coefficient $g_A \equiv (\partial \beta \mu_A^* / \partial x_I)_{T,p}$. From eq. 4.25, we can rewritten as

$$\begin{aligned} g_A &= \beta \rho^2 \left[\bar{v}_w^0 \left(\frac{\partial \mu_A^*}{\partial \rho_I} \right) - \bar{v}_I^0 \left(\frac{\partial \mu_A^*}{\partial \rho_w} \right) \right] \quad (\rho_A \rightarrow 0) \\ &= \frac{A_w \rho_I - A_I \rho_w}{\rho^2 X_I}, \end{aligned} \quad (4.34)$$

where the second line follows from eqs. 4.14, 4.17, and 4.30. In the limit $\rho_I \rightarrow 0$, substituting eq. 4.22 into eq. 4.34 and using eqs. 4.18 and 4.31, g_A is reduced to K_s ;

$$\lim_{\rho_I \rightarrow 0} g_A = \rho_w \left[\lim_{\rho_I \rightarrow 0} I^{AI} - \frac{v_A^* v_I}{k_B T \chi_w} \right] = \frac{\rho_w K_s}{\nu_+ + \nu_-}. \quad (4.35)$$

Inverting eqs. 4.21 and 4.34, we obtain

$$A_w = \rho^2 X_{I g_A} \bar{v}_I^0 - \rho_w \bar{v}_A^0, \quad A_I = -\rho^2 X_{I g_A} \bar{v}_w^0 - \rho_I \bar{v}_A^0. \quad (4.36)$$

F Salt-Enhanced-Association Coefficient C_I

In the limit $\rho_A \rightarrow 0$, substituting eqs. 4.12, 4.13, and 4.15 into $\sum_i I^{Ai} I_{iA} = 1$, we obtain

$$\frac{1}{I_{AA}} = \frac{1}{\rho_A} + \beta U_{AA} - \sum_{i,j=w,I} I_0^{ij} A_i A_j. \quad (4.37)$$

Then, substituting eq. 4.36 into 4.37, and using eqs. 4.17, 4.19, and 4.27, we obtain

$$\frac{1}{I_{AA}} = \frac{1}{\rho_A} + \beta U_{AA} - \beta \frac{(\bar{v}_A^{0*})^2}{\chi_T^0} - X_{I g_A}^2. \quad (4.38)$$

Thus, we can rewrite eq. 4.8 as

$$B = \frac{1}{2} \left[\beta U_{AA} - \beta \frac{(\bar{v}_A^{0*})^2}{\chi_T^0} - X_{I g_A}^2 \right]. \quad (4.39)$$

Similarly, for a binary system of water + solute in the limit $\rho_A \rightarrow 0$, the osmotic second virial coefficient $B_0 = (U_{AA} - v_A^{*2}/\chi_w)/2k_B T$. The first two terms in eq. 4.39 are the same part as B_0 in an aqueous solution without ions and are equal to B_0 in the limit $\rho_I \rightarrow 0$. The last term in eq. 4.39 is generated by the presence of the ions and vanishes at $\rho_I \rightarrow 0$. Therefore, from eq. 4.39, the SEA coefficient C_I is rewritten as

$$\begin{aligned} C_I &= \frac{\nu_+ + \nu_-}{2} \lim_{\rho_I \rightarrow 0} \left(\frac{\partial \left[\beta U_{AA} - \beta \frac{(\bar{v}_A^{0*})^2}{\chi_T^0} - X_{I g_A}^2 \right]}{\partial \rho_I} \right)_{T,p} \\ &= C_I^{(1)} + C_I^{(2)} \end{aligned} \quad (4.40)$$

with

$$\begin{aligned} C_I^{(1)} &\equiv \frac{\nu_+ + \nu_-}{2k_B T} \lim_{\rho_I \rightarrow 0} \left(\frac{\partial \left[\frac{(\bar{v}_A^{0*})^2}{\chi_T^0} - U_{AA} \right]}{\partial \rho_I} \right)_{T,p} \\ C_I^{(2)} &\equiv \frac{\nu_+ + \nu_-}{2} \lim_{\rho_I \rightarrow 0} \left(\frac{\partial \left[X_{I g_A}^2 \right]}{\partial \rho_I} \right)_{T,p} = \frac{K_s^2}{2(\nu_+ + \nu_-)}, \end{aligned} \quad (4.41)$$

where eqs. 4.30 and 4.35 are used to derive the last equality in the second line.

eq. 4.39 is formally the same as the osmotic second virial coefficient B in a ternary solution of

a water-like solvent, an alcohol-like cosolvent, and a hydrophobic solute, proposed by Okamoto and Onuki[193]. Okamoto and Onuki[193] state that eq. 4.39 is dominated by the last term rather than the sum of the first two terms for not very small x_I ($\gtrsim 0.05$). Thus, the relation $C_I \simeq C_I^{(2)}$ was theoretically proposed and verified in various aqueous electrolyte solutions[185]. In the present work, we verified eq. 4.1 by performing MD simulations to calculate C_I and $C_I^{(2)}$ for various solute and ion (or alcohol) species, respectively.

III COMPUTATIONAL DETAILS

We performed NpT ensemble MD simulations using the program package GROMACS2018[141] to obtain the Setschenow coefficient K_s and the osmotic second virial coefficient B in various aqueous solutions in this chapter. All of the MD simulations were performed in a cubic cell system with three-dimensional periodic boundary conditions at 1 bar, 298 K, and a time step of 1 fs. The Parrinello-Rahman method and the Nosé-Hoover method were used for pressure and temperature control, respectively. Duration times of the production run were 150 and 450 ns to calculate the SFE of solute μ_A^* and the B , respectively, after equilibrium runs were carried out for 5 ns. The configurations generated by the production run simulations were sampled every 50 steps.

We performed MD simulations for four kinds of model systems: pure water, aqueous solutions of salt (or alcohol), those of solute (methane, propane or methanol), and those of the salt (or the alcohol) and solute. Each system contained 4000 water molecules. The aqueous salt solutions contained $72 \times \nu_+$ cations and $72 \times \nu_-$ anions to give a salt concentration of 1 mol/kg, and a methane or methanol solution contained 48 methane or methanol molecules as the solute molecules and a propane solution contained 24 propane solute molecules. In the solutions of salt and solute, the same number of ions and solutes as above were added. As for the model electrolyte solutions, salts of HCl, LiF, LiCl, LiI, NaF, NaCl, NaI, CsF, CsCl, CsI, NaOH, and $MgCl_2$ were prepared. Here, for solutions containing the hydronium ion, we set the number of water molecules to 3928, because a hydronium ion consisted of one water molecule and one proton. In the same manner, we prepared aqueous solutions of alcohol and those of alcohol with solute. Each aqueous alcohol solution was prepared by adding 36 molecules of methanol (MeOH), ethanol (EtOH), or 1-propanol (PrOH) in water. Furthermore, for the aqueous methanol solution, a system with 72 molecules was also prepared. For the alcohol (MeOH, EtOH, PrOH) and methane solution, the

number of alcohol and methane molecules was set to 36 and 48, respectively. We also prepared an aqueous solution containing 72 methanol and 24 propane molecules.

We assumed the pairwise approximation where the total energy of the system was given by the sum of the potential energy between the particles in the system. The interaction between pairs of atoms was given by the sum of Lennard-Jones (LJ) and Coulomb potential. The potential function for the intermolecular interactions between water molecules was of TIP4P/2005 model[60]. We adopted the model potentials with effective electric charges scaled from those vacuum values (integer values) as the force field for the ions. The parameters introduced are shown in Table 4.1. Each ion model combined with the TIP4P/2005 model of water in the present study has been known to be consistent with the experimental values of the density of aqueous salt solutions and the Setschenow coefficient for methane in those solutions[19, 111, 195, 115]. The OPLS

Table 4.1: Force field parameters of the ions; the LJ diameter σ , LJ energy parameter ϵ , and scaled charge q .

Ion Sites	Li ⁺ [100]	Na ⁺ [103]	Cs ⁺ [195]	Mg ²⁺ [111]
σ (nm)	0.18	0.2115	0.360101	0.11629
ϵ (kJ/mol)	0.07647	0.544284	0.375958	3.6519
q (e)	0.75	0.75	0.75	1.7
Ion Sites	Cl ⁻ [102]	Cl ⁻ (of MgCl ₂)[111]	F ⁻ [195]	I ⁻ [195]
σ (nm)	0.410000	0.46990563	0.3619368	0.4681
ϵ (kJ/mol)	0.4928	0.07692308	0.03096364	0.1790
q (e)	-0.75	-0.85	-0.75	-0.75
Ion Sites	O(H ₃ O ⁺)[195]	H(H ₃ O ⁺)[195]	O(OH ⁻)[195]	H(OH ⁻)[195]
σ (nm)	0.265	0	0.36	0
ϵ (kJ/mol)	0.8	0	0.05	0
q (e)	-1.05	0.6	-0.75	0

force field[142] was used as a spherical monoatomic LJ particle model of methane; $\sigma_A=0.373$ nm, $\epsilon_{AA}=1.2301$ kJ/mol. The monoatomic LJ particle model was also used for propane molecule; $\sigma_A=0.5637$ nm, $\epsilon_{AA}=2.0121$ kJ/mol[165, 167]. The TraPPE-UA force field[179] was applied to the molecule model of each alcohol. The LJ parameters between intermolecular particles were

basically determined by

$$\sigma_{12} = \sqrt{\sigma_1\sigma_2}, \quad \epsilon_{12} = \sqrt{\epsilon_1\epsilon_2}, \quad (4.42)$$

whereas $\sigma_{Aw} = 0.34445$ nm and $\epsilon_{Aw} = 1.043$ kJ/mol[143] were used as the methane-water LJ parameters, and $\sigma_{Na^+OH^-} = 1.134$ nm was used as the $Na^+ - OH^-$ LJ diameter parameter[195]. The methane-methane and propane-propane interactions were replaced by the repulsive part of the Weeks-Anderson-Chandler (WCA) potential[144] to prevent solute aggregation so that the conformation sampling of the solute molecules was enhanced. The solute-solute radial distribution function $g_{AA}(r) = h_{AA}(r) + 1$ by the original LJ potential was calculated via a transformation of the solute-solute $g_{AA}^{sim}(r)$ obtained from the MD simulations using the WCA repulsive potential[145, 146]. The ion-water and ion-ion LJ parameters for the Madrid-2019 force field were individually given by the reference [111]. The LJ and Coulomb potentials between all the intermolecular pairs were truncated at 0.9 nm, while the long-range part of the Coulomb potentials was calculated by the particle mesh Ewald method. However, the cutoff distance of these interaction potentials was changed to 1.2 nm for the alcohol solution and 1.5 nm for the propane solution.

The solvation free energy of methane was calculated using the Widom test-particle insertion (TPI) method[147]. We performed MD simulations of pure water and salt solutions for 150 ns and inserted test solute particle 2×10^5 times into the equilibrium configurations obtained every 50 fs intervals. The Setschenow coefficient K_s for the propane and methanol was calculated via eq. 4.32 because it was hard to directly use these solutes as a test particle due to the large molecular size. To determine K_s and B , the KBIs G_{Aw} , G_{As} , and G_{AA} were obtained from numerical integration of the corresponding pair correlation function. We performed MD simulations of solute solutions and salt plus solute solutions for 450 ns. $h_{ij}(r)$ obtained from MD simulation at a closed system does not converge to zero at large distances due to the finite-size effect. We scaled the entire $h_{ij}(r)$ so that the average of $h_{ij}(r)$ over a certain range at large distances becomes zero. Furthermore, we evaluated the KBI in the thermodynamic limit by applying the method proposed by Krüger et al. [148, 149] to the KBI obtained for the finite systems. The KBI for the molecule models with multiple interaction sites such as alcohol was obtained by averaging the KBIs between all the pairs of sites on the molecules[150].

IV RESULT AND DISCUSSION

In this section, the relationship between C_I and K_s in various aqueous salt (or alcohol) solutions for three solute species is verified using the results of MD simulations. First, the computational results of K_s and C_I obtained for methane in fifteen different aqueous solutions are shown in Figure 4.1. In Figure 4.1, captions represent the co-solvent species. We evaluated the Setschenow coefficient by the following linear approximation of eq. 4.31;

$$K_s = \lim_{\rho_s \rightarrow 0} \left(\frac{\partial \beta \mu_A^*}{\partial \rho_s} \right)_{T,p} \simeq \frac{\mu_A^* - \mu_{A,0}^*}{\rho_s k_B T}, \quad (4.43)$$

where $\mu_{A,0}^*$ is the SFE of solute in pure water. It has been pointed out in Chapter 2 and 3, i.e., in our earlier computational studies[19, 195], that the salt species dependence of K_s calculated in eq. 4.43 by applying the TPI method is very close to the experimental value[46]. In the same manner, C_I was evaluated by the following linear approximation of eq. 4.1;

$$C_I = - \lim_{\rho_s \rightarrow 0} \left(\frac{\partial B}{\partial \rho_s} \right)_{T,p} \simeq - \frac{B - B_0}{\rho_s}, \quad (4.44)$$

where B_0 is the osmotic second virial coefficient in pure water. Next, the results of K_s and C_I calculated for propane solutes and methanol solutes are shown in Figure 4.2. K_s was evaluated by eq. 4.32 using the KBIs instead of eq. 4.43. The numerical results obtained from these two routes are known to be in good agreement with each other for methane in Chapter 2 and 3. We supposed that the KBIs obtained at low but finite concentrations of solute and salt (or alcohol) were approximately equivalent to the KBIs in the limit of infinite dilution of those.

We find that C_I and K_s for methane solute satisfy the relationship in eq. 4.1 for all salt species (Figure 4.1). The differences between C_I and $C_I^{(2)}$ are less than 1.2×10^{-2} (L/mol)² for all salt solutions, except for 1.65×10^{-2} for MgCl₂ and 1.75×10^{-2} (L/mol)² for HCl. In the aqueous alcohol solutions, the C_I are smaller by $1.4 \sim 2.1 \times 10^{-2}$ (L/mol)². Thus, it may be difficult to fully ignore the contribution of $C_I^{(1)}$ in eq. 4.40 when $C_I^{(2)}$ is small ($|K_s|/\sqrt{\nu_+ + \nu_-} \leq 0.1$ L/mol). Most of the MD simulation results of C_I are slightly larger than $C_I^{(2)}$ in the positive K_s and smaller than $C_I^{(2)}$ in the negatively small K_s , which are consistent with the numerical results using the theoretical model by Okamoto et al[185]. The result for Li⁺ obtained from this work is consistent with the exceptional salting-out effect that has been experimentally observed for Li⁺, while this Li⁺ ion specific effect is not reproduced by the theoretical model[185].

Next, if we focus on the salting-in region, the order of K_s in alcohol co-solvents is as follows:

EtOH < MeOH < PrOH. In general, the larger the hydrophobic solute (i.e., the longer the alkane), the larger the hydrophobic interaction. Thus, the order of the salting-in effect of alcohol co-solvents on a hydrophobic solute is expected to be PrOH > EtOH > MeOH, because of the stronger hydrophobic interaction between the solute and larger hydrophobic group of alcohol and eq. 4.32. However, the computational results were opposite to the expected trend. One of the possible reasons for the exceptional trend of PrOH is the influence of finite concentration of PrOH caused by aggregation of the hydrophobic groups of PrOH. Thus, we also examined K_s for the PrOH solution model where the attractive interactions between the hydrophobic groups of PrOH molecules were removed. However, we observed the smallest salting-in effect in the PrOH solution model, too, indicating that such an aggregation behaviour does not affect K_s .

Figure 4.2 shows that C_I and K_s for propane and methanol satisfy the relationship in eq. 4.1 as well as for methane. It is not straightforward to discuss the differences between C_I and $C_I^{(2)}$ for propane because the error bars of C_I for propane are much larger than those for methane. However, the differences are less than $1.7 \times 10^{-2} \text{ (L/mol)}^2$ for the most of salt (or alcohol) solutions, exceptionally, $4.7 \times 10^{-2} \text{ (L/mol)}^2$ for NaF which has the largest salting-out effect and $-3.5 \times 10^{-2} \text{ (L/mol)}^2$ for MeOH. In the case of methanol solute, the differences between C_I and $C_I^{(2)}$ are the values ranged from 8.4×10^{-3} to $1.9 \times 10^{-2} \text{ (L/mol)}^2$, and C_I is always larger than $C_I^{(2)}$ for any salt. Thus, these results show that $C_I \simeq C_I^{(2)} = K_s^2/2(\nu_+ + \nu_-)$ is valid over the wide region of salting-out in the salt solutions, independent of the size or the property of the solute. Unfortunately, it was unable to investigate a solution indicating strong salting-in effects in the combinations of solute and co-solvent species used in this chapter. On the one side, in the weak salting-in region, C_I was found to be negative so that those results were deviated from $C_I \simeq C_I^{(2)}$. However, if eq. 4.1 holds in the negatively large K_s , C_I should give a positive value due to the effect of K_s^2 . On the other hand, in the range of K_s investigated in this work, we successfully estimated the magnitude of the salt effect on the hydrophobic interaction using eq. 4.1 from the magnitude of the salt addition effect on the gas solubility.

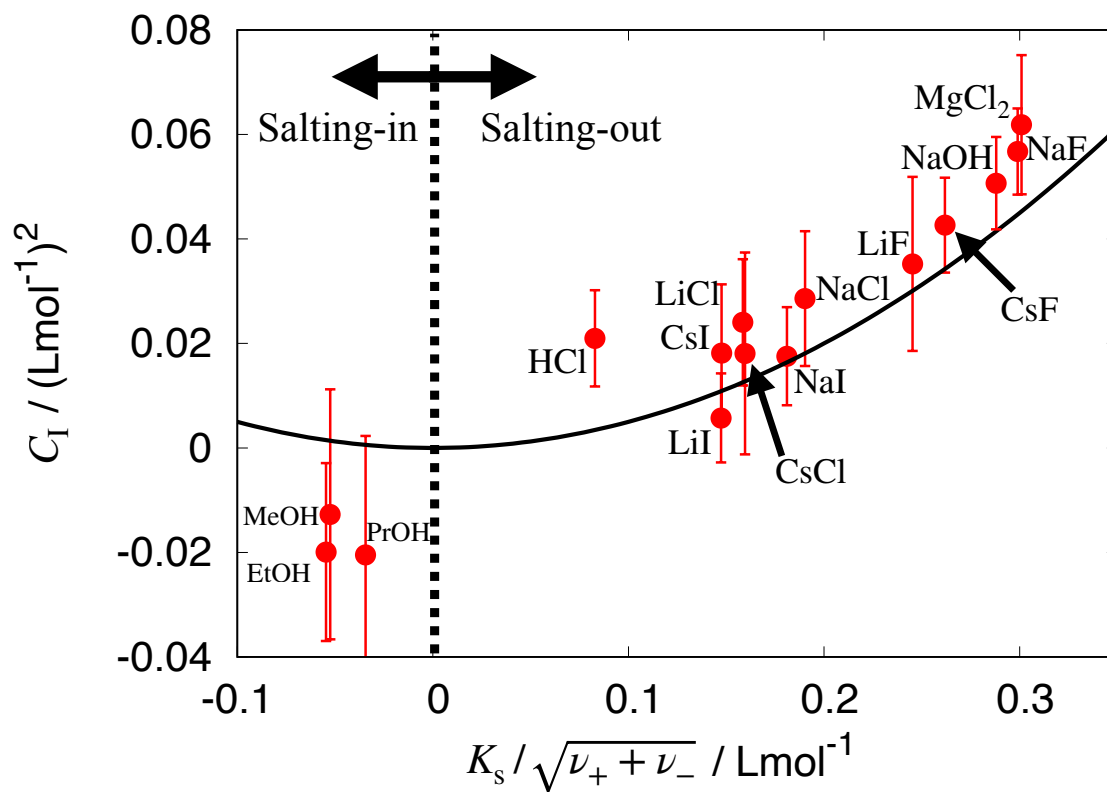


Figure 4.1: SEA coefficient C_I vs Setschenow coefficient K_s divided by $\sqrt{\nu_+ + \nu_-}$ for methane in aqueous solution of each co-solvent. However, for alcohol co-solvent, $\nu_+ + \nu_- = 1$. The solid curve indicates $C_I^{(2)} = K_s^2 / 2 (\nu_+ + \nu_-)$.

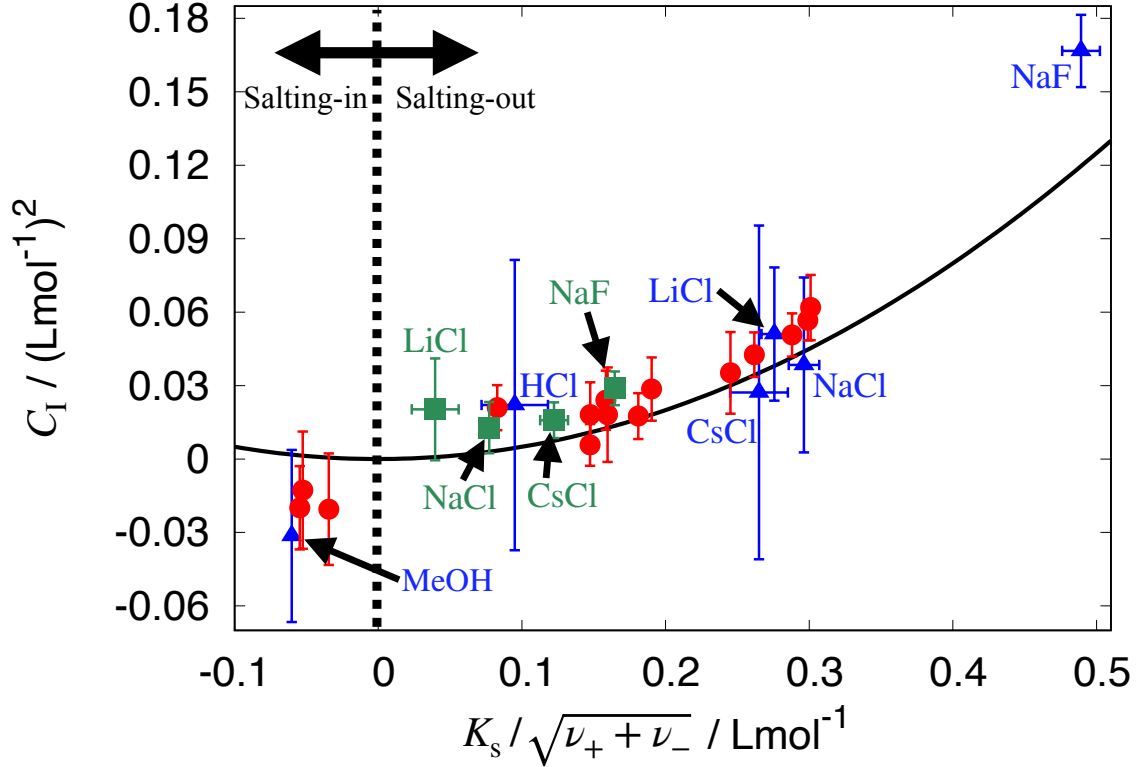


Figure 4.2: SEA coefficient C_I vs Setschenow coefficient K_s divided by $\sqrt{\nu_+ + \nu_-}$ in aqueous solution of each co-solvent; the solute species are methane (circles) and propane (triangles) and methanol (squares). However, for alcohol co-solvent, $\nu_+ + \nu_- = 1$. The solid curve indicates $C_I^{(2)} = K_s^2/2(\nu_+ + \nu_-)$. The results for methane are same as shown in Fig. 4.1.

V CONCLUSIONS

We performed MD simulations to calculate the salt addition effect on the gas solubility (Setschenow coefficient K_s) and the salt effect on the solute-solute effective interaction (osmotic second virial coefficient B), respectively, and investigated their salt (or alcohol) and solute species dependent relationships. The Setschenow coefficient was calculated through the SFE route (eq. 4.43) for a methane solute and the KBI route (eq. 4.32) for propane and methanol solutes. We evaluated a measure of the salt effect on B by the salt-enhanced-association coefficient $C_I \equiv -(\partial B/\partial \rho_s)_{T,p}$. Equations 4.40 and 4.41 provide the exact relation between C_I and K_s in the limit of infinite dilution of both salt and solute. We investigated whether the approximation $C_I \simeq K_s^2/2(\nu_+ + \nu_-)$ based on the proposal in the earlier study[193] that the third term in eq. 4.39 is dominant for B in a ternary system of water + salt (or alcohol) + solute. In addition, we examined solute and co-solvent species to which the approximations are valid.

We performed MD simulations using the force field consisting of the LJ potential and the

Coulomb potential, specifically, the single spherical LJ model for hydrophobic solutes, the charge-scaled model for ions, and the TraPPE-UA model for alcohols. The calculation results indicated that K_s and C_I are consistent with the relationship given by eq. 4.1 for all salt and solute combinations considered in the present study. This relationship is also applicable for divalent ions such as Mg^{2+} . Furthermore, we showed that this relationship was applied to not only the hydrophobic solute but also solutes with the hydrophilic group. In other words, although eq. 4.1 is derived assuming a hydrophobic solute, we clarified that this relationship was also valid for solutes with hydrophilic groups. Thus, it was demonstrated that the magnitude of the effective pair interaction between solute particles in aqueous electrolyte solutions at the infinite dilution limit of salt was estimated using the SFE of an isolated, single solute. However, we did not investigate the regime of strong salting-in. Equation 4.1 indicates that C_I should be in proportion to the square of K_s for both negatively and positively large values of K_s . In other words, it is suggested that both the salting-in and salting-out cases make the interactions between pairs of solute particles more attractive. For the salting-out, the more attractive the solute-solute interaction is, the more the aggregation of the solutes is promoted, which can be understood as a decrease in solubility of the solute. However, it remains unclear what makes B more attractive due to the salting-in effect. It is interesting to investigate the case with more negative K_s using, e.g, fullerene as the solute with a larger size and lower solubility and, e.g., tert-butyl alcohol (TBA) as the co-solvent, since a larger salting-in effect is expected.

In this chapter, $C_I^{(1)}$ was not mentioned because of the large error bars of C_I , which made it difficult to determine $C_I^{(1)} = C_I - C_I^{(2)}$. However, $C_I^{(1)}$ is a significant factor in determining the precision of eq. 4.1. Equation 4.41 indicates that $C_I^{(1)}$ depends on not only the salt species but also the solute species. It has been pointed out in the earlier theoretical study[185] that the larger the ion and solute size, the larger the contribution of $C_I^{(1)}$. In order to evaluate $C_I^{(1)}$ for various salt and solute species using MD simulations in the future, it is necessary to increase the system size and computation time. Such the approach requires an enormous computational cost. Alternative approach is to evaluate $C_I^{(1)}$ directly from eq. 4.41. It is then expected that a similar computational cost is required to obtain \bar{v}_A^{0*} and χ_T^0 in aqueous electrolyte solutions with sufficient accuracy. However, it would be informative to investigate the even larger hydrophobic solute and the solute with complex structures, such as proteins when we extend the present results and further understand the solute species dependence of the accuracy of eq. 4.1.

Publication

Hiroyuki Katsuto, Ryuichi Okamoto, Tomonari Sumi, Kenichiro Koga,

“Ion Size Dependences of the Salting-Out Effect: Reversed Order of Sodium and Lithium Ions”

The Journal of Physical Chemistry B, **125**, 6296-6305 (2021).

Acknowledgments

This work was supported by JST SPRING (Grant Number JPMJSP2126). Part of the computation was performed at the Research Center for Computational Science, Okazaki, Japan (Project: 21-IMS-C125, 22-IMS-C124, 23-IMS-C112).

I wish to acknowledge my indebtedness to Professor Kenichiro Koga for his valuable advice and sincere encouragement from the early to present stages of this work, not only on methods of conducting a study but also on the logical thought process, the skills in communicating my study, and the satisfaction of research activities.

I am grateful to Associate Professor Tomonari Sumi for his valuable help and unsparing advice, and for serving as an observer at the study meetings of electromagnetics et al.

I would like to thank Specially Appointed Lecturer at University of Hyogo Ryuichi Okamoto for giving me theoretical knowledge of liquids and, in Chapter 4, his valuable help in the study process and careful reading of the manuscript.

I wish to thank all the former and present members of the Theoretical Physical Chemistry Group, Department of Chemistry, for their help in obtaining the fundamental knowledge in mathematics, physics, and chemistry at study meetings and for their active and frank discussions among us on the study and daily life.

I also would like to express my gratitude to Sanae Furuta for his support as a staff member of our laboratory, from the application of documents to my business.

Finally, I express my most heartfelt thanks to my parents for making the environment to concentrate my research activities and protecting my health.

Okayama

January 2024

Hiroyuki Katsuto

References

- [1] Kunz, W.; Nostro, P. L.; Ninham, B. W. *Curr. Opin. Colloid Interface Sci.* **2004**, *9*(1-2), 1–18.
- [2] Ninham, B. W.; Nostro, P. L. *Molecular forces and self assembly: in colloid, nano sciences and biology*; Cambridge University Press, 2010.
- [3] Salis, A.; Ninham, B. W. *Chem. Soc. Rev.* **2014**, *43*(21), 7358–7377.
- [4] Robinson, D. R.; Jencks, W. P. *J. Am. Chem. Soc.* **1965**, *87*(11), 2470–2479.
- [5] Cacace, M.; Landau, E.; Ramsden, J. *Q. Rev. Biophys.* **1997**, *30*(3), 241–277.
- [6] Robinson, R. A.; Stokes, R. H. *Electrolyte solutions*; Courier Corporation, 2002.
- [7] Gurau, M. C.; Lim, S.-M.; Castellana, E. T.; Albertorio, F.; Kataoka, S.; Cremer, P. S. *J. Am. Chem. Soc.* **2004**, *126*(34), 10522–10523.
- [8] Lo Nostro, P.; Ninham, B. W. *Chem. Rev.* **2012**, *112*(4), 2286–2322.
- [9] Xie, W. J.; Gao, Y. Q. *J. Phys. Chem. Lett.* **2013**, *4*(24), 4247–4252.
- [10] Gregory, K. P.; Elliott, G. R.; Robertson, H.; Kumar, A.; Wanless, E. J.; Webber, G. B.; Craig, V. S.; Andersson, G. G.; Page, A. J. *Phys. Chem. Chem. Phys.* **2022**, *24*(21), 12682–12718.
- [11] Zhu, J.; Zhao, Z.; Li, X.; Wei, Y. *J. Chem. Phys.* **2023**, *159*(21).
- [12] Novotny, P.; Sohnel, O. *J. Chem. Eng. Data.* **1988**, *33*(1), 49–55.
- [13] Laliberte, M.; Cooper, W. E. *Journal of Chemical & Engineering Data* **2004**, *49*(5), 1141–1151.
- [14] Garrett, B. C. *Science* **2004**, *303*(5661), 1146–1147.

- [15] Pegram, L. M.; Record, M. T. *J. Phys. Chem. B* **2007**, *111*(19), 5411–5417.
- [16] Schwierz, N.; Horinek, D.; Netz, R. R. *Langmuir* **2013**, *29*(8), 2602–2614.
- [17] Kinoshita, M.; Hirata, F. *J. Chem. Phys.* **1997**, *106*(12), 5202–5215.
- [18] Ganguly, P.; Hajari, T.; van der Vegt, N. F. *J. Phys. Chem. B* **2014**, *118*(20), 5331–5339.
- [19] Katsuto, H.; Okamoto, R.; Sumi, T.; Koga, K. *J. Phys. Chem. B* **2021**, *125*(23), 6296–6305.
- [20] Jones, G.; Dole, M. *J. Am. Chem. Soc.* **1929**, *51*(10), 2950–2964.
- [21] Jenkins, H. D. B.; Marcus, Y. *Chem. Rev.* **1995**, *95*(8), 2695–2724.
- [22] Zhang, Y.; Cremer, P. S. *Proc. Natl. Acad. Sci. U. S. A.* **2009**, *106*(36), 15249–15253.
- [23] Lo Nostro, P.; Peruzzi, N.; Severi, M.; Ninham, B. W.; Baglioni, P. *J. Am. Chem. Soc.* **2010**, *132*(18), 6571–6577.
- [24] Hofmeister, F. *Arch. Exp. Pathol. Pharmacol* **1888**, *24*(24), 247–260.
- [25] Marcus, Y. *Chemical Rev.* **2009**, *109*(3), 1346–1370.
- [26] Millero, F. J. *Chem. Rev.* **1971**, *71*(2), 147–176.
- [27] Mazzini, V.; Craig, V. S. *Chem. Sci.* **2017**, *8*(10), 7052–7065.
- [28] Ellis, A. *J. Chem. Soc. A: Inorg. Phys. Theor.* **1966**, pages 1579–1584.
- [29] Millero, F. *Wiley, New York* **1971**, *15*, 622.
- [30] Graves Pedersen, T.; Sejersen, L.; Ifft, J. B. *Carlsberg Res. Commun.* **1977**, *42*, 211–224.
- [31] Marcus, Y.; Hefter, G. *Chem. Rev.* **2004**, *104*(7), 3405–3452.
- [32] Takenaka, N.; Arakawa, K. *Bull. Chem. Soc. Jpn.* **1989**, *62*(9), 2880–2884.
- [33] Zana, R.; Yeager, E. *J. Phys. Chem.* **1966**, *70*(3), 954–955.
- [34] Zana, R.; Yeager, E. *J. Phys. Chem.* **1967**, *71*(3), 521–536.
- [35] Robertson, T. B. *J. Biol. Chem.* **1911**, *9*(3), 303–326.
- [36] Green, A. A. *J. Biol. Chem.* **1932**, *95*(1), 47–66.

- [37] Poillon, W. N.; Bertles, J. F. *J. Biol. Chem.* **1979**, *254*(9), 3462–3467.
- [38] Ries-Kautt, M.; Ducruix, A. F. *J. Biol. Chem.* **1989**, *264*(2), 745–748.
- [39] Lyklema, J. *Mol. Phys.* **2002**, *100*(19), 3177–3185.
- [40] López-León, T.; Jódar-Reyes, A. B.; Bastos-González, D.; Ortega-Vinuesa, J. L. *J. Phys. Chem. B* **2003**, *107*(24), 5696–5708.
- [41] López-León, T.; Santander-Ortega, M. J.; Ortega-Vinuesa, J. L.; Bastos-González, D. *J. Phys. Chem. C* **2008**, *112*(41), 16060–16069.
- [42] McDevit, W.; Long, F. *J. Am. Chem. Soc.* **1952**, *74*(7), 1773–1777.
- [43] McDevit, W.; Long, F. *J. Amer. Chem. Soc.* **1952**, *74*(4), 1090–1091.
- [44] Sergeeva, V. *Russ. Chem. Rev.* **1965**, *34*(4), 309.
- [45] Clever, H. L. *J. Chem. Eng. Data* **1983**, *28*(3), 340–343.
- [46] Weisenberger, S.; Schumpe, d. A. *AIChE J.* **1996**, *42*(1), 298–300.
- [47] Bergen Jr, R.; Long, F. *J. Phys. Chem.* **1956**, *60*(8), 1131–1135.
- [48] Omta, A. W.; Kropman, M. F.; Woutersen, S.; Bakker, H. J. *Science* **2003**, *301*(5631), 347–349.
- [49] Näslund, L.-Å.; Edwards, D. C.; Wernet, P.; Bergmann, U.; Ogasawara, H.; Pettersson, L. G.; Myneni, S.; Nilsson, A. *J. Phys. Chem. A* **2005**, *109*(27), 5995–6002.
- [50] Batchelor, J. D.; Olteanu, A.; Tripathy, A.; Pielak, G. J. *J. Am. Chem. Soc.* **2004**, *126*(7), 1958–1961.
- [51] Nostro, P. L.; Ninham, B. W.; Milani, S.; Fratoni, L.; Baglioni, P. *Biopolymers* **2006**, *81*(2), 136–148.
- [52] Rossi, S.; Lo Nostro, P.; Lagi, M.; Ninham, B. W.; Baglioni, P. *J. Phys. Chem. B* **2007**, *111*(35), 10510–10519.
- [53] Jungwirth, P.; Cremer, P. S. *Nat. Chem.* **2014**, *6*(4), 261–263.
- [54] Nihonyanagi, S.; Yamaguchi, S.; Tahara, T. *J. Amer. Chem. Soc.* **2014**, *136*(17), 6155–6158.

- [55] Ben-Naim, A. *Molecular theory of solutions*; OUP Oxford, 2006.
- [56] Hansen, J.-P.; McDonald, I. R. *Theory of simple liquids: with applications to soft matter*; Academic press, 2013.
- [57] Kirkwood, J. G.; Buff, F. P. *J. Chem. Phys.* **1951**, *19*(6), 774–777.
- [58] Debye, P.; Hückel, E. *Physikalische Zeitschrift* **1923**, *24*, 185.
- [59] Okamoto, R.; Koga, K.; Onuki, A. *J. Chem. Phys.* **2020**, *153*(7).
- [60] Abascal, J. L.; Vega, C. *J. Chem. Phys.* **2005**, *123*(23).
- [61] Moreira, L.; Boström, M.; Ninham, B.; Biscaia, E. C.; Tavares, F. W. *Colloids and Surfaces A: Physicochem. Eng. Aspects* **2006**, *282*, 457–463.
- [62] Isogai, Y.; Imamura, H.; Sumi, T.; Shirai, T. *Biochemistry* **2022**, *61*(15), 1543–1547.
- [63] Hribar, B.; Southall, N. T.; Vlachy, V.; Dill, K. A. *J. Am. Chem. Soc.* **2002**, *124*(41), 12302–12311.
- [64] Thomas, A. S.; Elcock, A. H. *J. Am. Chem. Soc.* **2006**, *128*(24), 7796–7806.
- [65] Jungwirth, P.; Tobias, D. *J. Chem. Rev.* **2006**, *106*(4), 1259–1281.
- [66] Jungwirth, P.; Winter, B. *Annu. Rev. Phys. Chem.* **2008**, *59*, 343–366.
- [67] Pegram, L. M.; Record Jr, M. T. *J. Phys. Chem. B* **2008**, *112*(31), 9428–9436.
- [68] Mamatkulov, S. I.; Allolio, C.; Netz, R. R.; Bonthuis, D. J. *Angew. Chem. Int. Ed.* **2017**, *56*(50), 15846–15851.
- [69] Brecht, A. J.; Kim, Y.; Mendes de Oliveira, D.; Urbina, A. S.; Slipchenko, L. V.; Ben-Amotz, D. *J. Phys. Chem. B* **2022**, *126*(4), 869–877.
- [70] Cornell, W. D.; Cieplak, P.; Bayly, C. I.; Gould, I. R.; Merz, K. M.; Ferguson, D. M.; Spellmeyer, D. C.; Fox, T.; Caldwell, J. W.; Kollman, P. A. *J. Am. Chem. Soc.* **1995**, *117*(19), 5179–5197.
- [71] Brooks, B. R.; Bruccoleri, R. E.; Olafson, B. D.; States, D. J.; Swaminathan, S. a.; Karplus, M. *J. Comput. Chem.* **1983**, *4*(2), 187–217.

- [72] MacKerell Jr, A. D.; Bashford, D.; Bellott, M.; Dunbrack Jr, R. L.; Evanseck, J. D.; Field, M. J.; Fischer, S.; Gao, J.; Guo, H.; Ha, S.; others. *J. Phys. Chem. B* **1998**, *102*(18), 3586–3616.
- [73] MacKerell Jr, A. D.; Banavali, N.; Foloppe, N. *Biopolymers: original Research on biomolecules* **2000**, *56*(4), 257–265.
- [74] van Gunsteren, W. F.; Billeter, S.; Eising, A.; Hünenberger, P.; Krüger, P.; Mark, A.; Scott, W.; Tironi, I. *Vdf Hochschulverlag AG an der ETH Zürich, Zürich* **1996**, *86*, 1–1044.
- [75] Scott, W. R.; Hünenberger, P. H.; Tironi, I. G.; Mark, A. E.; Billeter, S. R.; Fennen, J.; Torda, A. E.; Huber, T.; Krüger, P.; Van Gunsteren, W. F. *J. Phys. Chem. A* **1999**, *103*(19), 3596–3607.
- [76] Jorgensen, W. L.; Maxwell, D. S.; Tirado-Rives, J. *J. Am. Chem. Soc.* **1996**, *118*(45), 11225–11236.
- [77] Jorgensen, W. L.; Tirado-Rives, J. *J. Am. Chem. Soc.* **1988**, *110*(6), 1657–1666.
- [78] Aqvist, J. *J. Phys. Chem.* **1990**, *94*(21), 8021–8024.
- [79] Dang, L. X. *J. Chem. Phys.* **1992**, *96*(9), 6970–6977.
- [80] Dang, L. X. *J. Am. Chem. Soc.* **1995**, *117*(26), 6954–6960.
- [81] Weerasinghe, S.; Smith, P. E. *J. Chem. Phys.* **2003**, *119*(21), 11342–11349.
- [82] Jensen, K. P.; Jorgensen, W. L. *J. Chem. Theory Comput.* **2006**, *2*(6), 1499–1509.
- [83] Joung, I. S.; Cheatham III, T. E. *J. Phys. Chem. B* **2008**, *112*(30), 9020–9041.
- [84] Klasczyk, B.; Knecht, V. *J. Chem. Phys.* **2010**, *132*(2).
- [85] Fyta, M.; Kalcher, I.; Dzubiella, J.; Vrbka, L.; Netz, R. R. *J. Chem. Phys.* **2010**, *132*(2).
- [86] Fyta, M.; Netz, R. R. *J. Chem. Phys.* **2012**, *136*(12).
- [87] Bonthuis, D. J.; Mamatkulov, S. I.; Netz, R. R. *J. Chem. Phys.* **2016**, *144*(10).
- [88] Smith, P. E. *J. Phys. Chem. B* **1999**, *103*(3), 525–534.

- [89] Docherty, H.; Galindo, A.; Sanz, E.; Vega, C. *J. Phys. Chem. B* **2007**, *111*(30), 8993–9000.
- [90] Leontyev, I.; Stuchebrukhov, A. *J. Chem. Phys.* **2009**, *130*(8).
- [91] Leontyev, I.; Stuchebrukhov, A. *J. Chem. Theory Comput.* **2010**, *6*(10), 3153–3161.
- [92] Leontyev, I. V.; Stuchebrukhov, A. *J. Chem. Theory Comput.* **2010**, *6*(5), 1498–1508.
- [93] Leontyev, I.; Stuchebrukhov, A. *Phys. Chem. Chem. Phys.* **2011**, *13*(7), 2613–2626.
- [94] Leontyev, I. V.; Stuchebrukhov, A. A. *J. Chem. Theory Comput.* **2012**, *8*(9), 3207–3216.
- [95] Leontyev, I. V.; Stuchebrukhov, A. A. *J. Chem. Phys.* **2014**, *141*(1).
- [96] Smith, D. E.; Dang, L. X. *J. Chem. Phys.* **1994**, *100*(5), 3757–3766.
- [97] Lamoureux, G.; Roux, B. *J. Phys. Chem. B* **2006**, *110*(7), 3308–3322.
- [98] Yu, H.; Whitfield, T. W.; Harder, E.; Lamoureux, G.; Vorobyov, I.; Anisimov, V. M.; MacKerell Jr, A. D.; Roux, B. *J. Chem. Theory Comput.* **2010**, *6*(3), 774–786.
- [99] Kiss, P. T.; Baranyai, A. *J. Chem. Phys.* **2014**, *141*(11).
- [100] Pluharova, E.; Mason, P. E.; Jungwirth, P. *J. Phys. Chem. A* **2013**, *117*(46), 11766–11773.
- [101] Kohagen, M.; Mason, P. E.; Jungwirth, P. *J. Phys. Chem. B* **2014**, *118*(28), 7902–7909.
- [102] Pluhařová, E.; Fischer, H. E.; Mason, P. E.; Jungwirth, P. *Mol. Phys.* **2014**, *112*(9-10), 1230–1240.
- [103] Kohagen, M.; Mason, P. E.; Jungwirth, P. *J. Phys. Chem. B* **2016**, *120*(8), 1454–1460.
- [104] Fuentes-Azcatl, R.; Barbosa, M. C. *The Journal of Physical Chemistry B* **2016**, *120*(9), 2460–2470.
- [105] Li, J.; Wang, F. *J. Chem. Phys.* **2015**, *143*(19).
- [106] Li, J.; Wang, F. *J. Phys. Chem. B* **2017**, *121*(27), 6637–6645.
- [107] Duboué-Dijon, E.; Mason, P. E.; Fischer, H. E.; Jungwirth, P. *J. Phys. Chem. B* **2017**, *122*(13), 3296–3306.
- [108] Kann, Z.; Skinner, J. *J. Chem. Phys.* **2014**, *141*(10).

- [109] Barbosa, G. D.; Liu, X.; O’Harra, K. E.; Bara, J. E.; Turner, C. H. *J. Ionic Liquids* **2022**, *2*(1), 100020.
- [110] Benavides, A.; Portillo, M.; Chamorro, V.; Espinosa, J.; Abascal, J.; Vega, C. *J. Chem. Phys.* **2017**, *147*(10).
- [111] Zeron, I.; Abascal, J.; Vega, C. *J. Chem. Phys.* **2019**, *151*(13).
- [112] Blazquez, S.; Conde, M.; Abascal, J.; Vega, C. *J. Chem. Phys.* **2022**, *156*(4).
- [113] Habibi, P.; Rahbari, A.; Blazquez, S.; Vega, C.; Dey, P.; Vlugt, T. J.; Moulton, O. A. *J. Phys. Chem. B* **2022**, *126*(45), 9376–9387.
- [114] Blazquez, S.; Conde, M.; Vega, C. *J. Chem. Phys.* **2023**, *158*(5).
- [115] Sedano, L.; Blazquez, S.; Noya, E. G.; Vega, C.; Troncoso, J. *J. Chem. Phys.* **2022**, *156*(15).
- [116] Gámez, F.; Sedano, L.; Blazquez, S.; Troncoso, J.; Vega, C. *J. Molecular Liquids* **2023**, *377*, 121433.
- [117] Zundel, G. *Adv. Chem. Phys.* **1999**, pages 1–217.
- [118] Eigen, M.; De Maeyer, L. *Proceedings of the Royal Society of London. Series A. Mathematical and Physical Sciences* **1958**, *247*(1251), 505–533.
- [119] Eigen, M. *Angewandte Chemie International Edition in English* **1964**, *3*(1), 1–19.
- [120] Kulig, W.; Agmon, N. *J. Phys. Chem. B* **2014**, *118*(1), 278–286.
- [121] Fournier, J. A.; Wolke, C. T.; Johnson, M. A.; Obadrakh, T. T.; Jordan, K. D.; Kathmann, S. M.; Xantheas, S. S. *J. Phys. Chem. A* **2015**, *119*(36), 9425–9440.
- [122] Yagi, K.; Thomsen, B. *J. Phys. Chem. A* **2017**, *121*(12), 2386–2398.
- [123] Wang, H.; Agmon, N. *J. Phys. Chem. A* **2017**, *121*(16), 3056–3070.
- [124] Park, M.; Shin, I.; Singh, N. J.; Kim, K. S. *J. Phys. Chem. A* **2007**, *111*(42), 10692–10702.
- [125] Vácha, R.; Buch, V.; Milet, A.; Devlin, J. P.; Jungwirth, P. *Phys. Chem. Chem. Phys.* **2007**, *9*(34), 4736–4747.

- [126] Schumpe, A. *Chem. Eng. Sci.* **1993**, *48*(1), 153–158.
- [127] Endo, S.; Pfennigsdorff, A.; Goss, K.-U. *Environ. Sci. Technol.* **2012**, *46*(3), 1496–1503.
- [128] Francisco, O. A.; Glor, H. M.; Khajehpour, M. *ChemPhysChem* **2020**, *21*(6), 484–493.
- [129] Couture, A.; Laidler, K. *Can. J. Chem.* **1956**, *34*(9), 1209–1216.
- [130] Couture, A.; Laidler, K. J. *Can. J. Chem.* **1957**, *35*(3), 207–210.
- [131] Stokes, R.; Robinson, R. *Trans. Faraday Soc.* **1957**, *53*, 301–304.
- [132] Mukerjee, P. *J. Phys. Chem.* **1961**, *65*(5), 740–744.
- [133] Padova, J. *J. Chem. Phys.* **1963**, *39*(6), 1552–1557.
- [134] Noyes, R. M. *J. Am. Chem. Soc.* **1964**, *86*(6), 971–979.
- [135] Conway, B.; Verrall, R.; Desnoyers, J. *Z. Phys. Chem.* **1965**, *230*(1), 157–178.
- [136] Conway, B.; Verrall, R.; Desnoyers, J. *Trans. Faraday Soc.* **1966**, *62*, 2738–2749.
- [137] Millero, F. J.; Drost-Hansen, W. *J. Phys. Chem.* **1968**, *72*(5), 1758–1763.
- [138] King, E. J. *J. Phys. Chem.* **1970**, *74*(26), 4590–4592.
- [139] Millero, F. J. *J. Phys. Chem.* **1971**, *75*(2), 280–282.
- [140] Kusalik, P. G.; Patey, G. *J. Chem. Phys.* **1987**, *86*(9), 5110–5116.
- [141] Hess, B.; Kutzner, C.; Van Der Spoel, D.; Lindahl, E. *J. Chem. Theory Comput.* **2008**, *4*(3), 435–447.
- [142] Jorgensen, W. L.; Madura, J. D.; Swenson, C. J. *J. Am. Chem. Soc.* **1984**, *106*(22), 6638–6646.
- [143] Docherty, H.; Galindo, A.; Vega, C.; Sanz, E. *J. Chem. Phys.* **2006**, *125*(7).
- [144] Weeks, J. D.; Chandler, D.; Andersen, H. C. *J. Chem. Phys.* **1971**, *54*(12), 5237–5247.
- [145] Koga, K. *J. Phys. Chem. B* **2013**, *117*(41), 12619–12624.
- [146] Naito, H.; Sumi, T.; Koga, K. *Faraday Discussions* **2024**.
- [147] Widom, B. *J. Chem. Phys.* **1963**, *39*(11), 2808–2812.

- [148] Krüger, P.; Schnell, S. K.; Bedeaux, D.; Kjelstrup, S.; Vlugt, T. J.; Simon, J.-M. *J. Phys. Chem. Lett.* **2013**, *4*(2), 235–238.
- [149] Dawass, N.; Krüger, P.; Schnell, S. K.; Moulτος, O. A.; Economou, I. G.; Vlugt, T. J.; Simon, J.-M. *Nanomaterials* **2020**, *10*(4), 771.
- [150] Koga, K.; Widom, B. *J. Chem. Phys.* **2013**, *138*(11).
- [151] Seki, T.; Yu, C.-C.; Chiang, K.-Y.; Greco, A.; Yu, X.; Matsumura, F.; Bonn, M.; Nagata, Y. *J. Am. Chem. Soc.* **2023**, *145*(19), 10622–10630.
- [152] Zhang, Y.; Cremer, P. S. *Curr. Opin. Chem. Biol.* **2006**, *10*(6), 658–663.
- [153] Shimizu, S.; McLaren, W. M.; Matubayasi, N. *J. Chem. Phys.* **2006**, *124*(23).
- [154] Okur, H. I.; Hladílková, J.; Rembert, K. B.; Cho, Y.; Heyda, J.; Dzubiella, J.; Cremer, P. S.; Jungwirth, P. *J. Phys. Chem. B* **2017**, *121*(9), 1997–2014.
- [155] Kalra, A.; Tugcu, N.; Cramer, S. M.; Garde, S. *J. Phys. Chem. B* **2001**, *105*(27), 6380–6386.
- [156] Thomas, A. S.; Elcock, A. H. *J. Am. Chem. Soc.* **2007**, *129*(48), 14887–14898.
- [157] Graziano, G. *J. Chem. Eng. Data* **2009**, *54*(2), 464–467.
- [158] Setschenow, J. *Zeitschrift für Physikalische Chemie* **1889**, *4*(1), 117–125.
- [159] Holzmann, J.; Ludwig, R.; Geiger, A.; Paschek, D. *ChemPhysChem* **2008**, *9*(18), 2722–2730.
- [160] Shannon, R. D. *Acta Crystallogr., Sect. A: Found. Adv.* **1976**, *32*(5), 751–767.
- [161] Ruckenstein, E.; Shulgin, I. *Ind. Eng. Chem. Res.* **2002**, *41*(18), 4674–4680.
- [162] Smith, P. E.; Mazo, R. M. *J. Phys. Chem. B* **2008**, *112*(26), 7875–7884.
- [163] Abe, K.; Sumi, T.; Koga, K. *J. Phys. Chem. B* **2016**, *120*(8), 2012–2019.
- [164] Koga, K.; Yamamoto, N. *J. Phys. Chem. B* **2018**, *122*(13), 3655–3665.
- [165] Hirschfelder, J. O.; Curtiss, C. F.; Bird, R. B.; others. *Molecular theory of gases and liquids*; Wiley New York, 1954.

- [166] Guillot, B.; Guissani, Y. *J. Chem. Phys.* **1993**, *99*(10), 8075–8094.
- [167] Adachi, Y.; Fijihara, I.; Takamiya, M.; Nakanishi, K. *Fluid Phase Equilibria* **1988**, *39*(1), 1–38.
- [168] Degrève, L.; Mazzé, F. M. *Mol. Phys.* **2003**, *101*(10), 1443–1453.
- [169] Hassan, S. A. *J. Phys. Chem. B* **2008**, *112*(34), 10573–10584.
- [170] Fennell, C. J.; Bizjak, A.; Vlachy, V.; Dill, K. A. *J. Phys. Chem. B* **2009**, *113*(19), 6782–6791.
- [171] Antonio, M. R.; Nyman, M.; Anderson, T. M. *Angew. Chem., Int. Ed.* **2009**, *48*(33), 6136–6140.
- [172] Bian, H.; Wen, X.; Li, J.; Chen, H.; Han, S.; Sun, X.; Song, J.; Zhuang, W.; Zheng, J. *Proc. Natl. Acad. Sci. U.S.A.* **2011**, *108*(12), 4737–4742.
- [173] Yu, H.-A.; Karplus, M. *J. Chem. Phys.* **1988**, *89*(4), 2366–2379.
- [174] Graziano, G. *J. Chem. Soc., Faraday Trans.* **1998**, *94*(22), 3345–3352.
- [175] Gallicchio, E.; Kubo, M.; Levy, R. M. *J. Phys. Chem. B* **2000**, *104*(26), 6271–6285.
- [176] Ben-Amotz, D.; Raineri, F. O.; Stell, G. *J. Phys. Chem. B* **2005**, *109*(14), 6866–6878.
- [177] Desnoyers, J. E.; Billon, M.; Léger, S.; Perron, G.; Morel, J.-P. *J. Solution Chem.* **1976**, *5*, 681–691.
- [178] Wilcox, F. L.; Schrier, E. E. *J. Phys. Chem.* **1971**, *75*(24), 3757–3764.
- [179] Chen, B.; Potoff, J. J.; Siepmann, J. I. *J. Phys. Chem. B* **2001**, *105*(15), 3093–3104.
- [180] Matsumoto, M. *Bull. Soc. Sea Water Sci., Jpn* **2016**, *70*(6), 354–357.
- [181] Collins, K. D. *Biophys. J.* **1997**, *72*(1), 65–76.
- [182] Wise, P. K.; Slipchenko, L. V.; Ben-Amotz, D. *J. Phys. Chem. B* **2023**.
- [183] Blazquez, S.; Zeron, I.; Conde, M.; Abascal, J.; Vega, C. *Fluid Phase Equilibria* **2020**, *513*, 112548.
- [184] Fujita, T.; Watanabe, H.; Tanaka, S. *Chem. Phys. Lett.* **2007**, *434*(1-3), 42–48.

- [185] Okamoto, R.; Koga, K. *J. Phys. Chem. B* **2021**, *125*(46), 12820–12831.
- [186] Widom, B.; Koga, K. *J. Phys. Chem. B* **2013**, *117*(4), 1151–1154.
- [187] Chaudhari, M. I.; Holleran, S. A.; Ashbaugh, H. S.; Pratt, L. R. *Proc. Natl. Acad. Sci. U. S. A* **2013**, *110*(51), 20557–20562.
- [188] Ashbaugh, H. S.; Weiss, K.; Williams, S. M.; Meng, B.; Surampudi, L. N. *J. Phys. Chem. B* **2015**, *119*(20), 6280–6294.
- [189] Chaudhari, M. I.; Sabo, D.; Pratt, L. R.; Rempe, S. B. *J. Phys. Chem. B* **2015**, *119*(29), 9098–9102.
- [190] Chaudhari, M. I.; Rempe, S. B.; Asthagiri, D.; Tan, L.; Pratt, L. *J. Phys. Chem. B* **2016**, *120*(8), 1864–1870.
- [191] Cerdeiriña, C. A.; Widom, B. *J. Phys. Chem. B* **2016**, *120*(51), 13144–13151.
- [192] Tang, D.; Delpo, C.; Blackmon, O.; Ashbaugh, H. S. *The Journal of Chemical Physics* **2018**, *148*(1).
- [193] Okamoto, R.; Onuki, A. *J. Chem. Phys.* **2018**, *149*(1).
- [194] Naito, H.; Okamoto, R.; Sumi, T.; Koga, K. *J. Chem. Phys.* **2022**, *156*(22).
- [195] Katsuto, H.; Sumi, T.; Koga, K. **2023**, *in preparation*.